Understanding the wettability of different surfaces for the fractionation of complex lipid mixtures using supercritical carbon dioxide

by

Eileen Vanessa Santos Hernandez

A thesis submitted in partial fulfillment of the requirements for the degree of

Doctor of Philosophy

in

Bioresource and Food Engineering

Department of Agricultural, Food and Nutritional Science
University of Alberta

Abstract

Supercritical fluid fractionation of complex lipid mixtures has emerged as a green alternative for conventional methods. Packed columns have been used to fractionate diverse lipid mixtures using supercritical carbon dioxide (SC-CO_2) under different conditions. However, there is a lack of fundamental knowledge about how the contact between the phases at the packing level is affecting process performance. Therefore, a systematic approach was taken to determine the wettability of different lipid classes on diverse surfaces in SC-CO_2 and to correlate it with the fractionation process outcomes of a model mixture.

The first study aimed to determine the effect of pressure and temperature on the interfacial tension (IFT) and equilibrium contact angle (CA_{eq}) of corn oil in air, SC-CO_2 and SC-N_2 on polished stainless steel (SS) metal sheet under unsaturated and saturated surrounding phases at 40, 60, 80 °C and 0.1, 16, 20, 24 MPa. The IFT of corn oil/N_2 and corn oil/CO_2 showed a remarkable difference depending on pressure and temperature conditions where the IFT of corn oil/CO_2 decreased dramatically with pressure. The wetting behaviour of corn oil on polished SS surface under dense N_2 and CO_2 was characterized as complete wetting, showing CA_{eq} values below 10°, mainly influenced by the saturation or unsaturation condition of the environment.

The objective of the second study was to determine the IFT and the CA_{eq} of oleic acid (OA) and canola oil (CanO) on polished glass in SC-N_2 and SC-CO_2 environments at 40, 60, 80 °C and 16, 20, 24 MPa. The IFT of OA and CanO in SC-CO_2 at 60 ºC and pressures of up to 24 MPa showed a remarkable decrease with pressure. CA_{eq} of the OA/SC-CO_2 system on glass exhibited partial to complete wettability at 40 ºC and 60 ºC, while complete wettability was obtained at 80 ºC from 16 to 24 MPa. In contrast, CanO/SC-CO_2 exhibited three different wetting patterns on glass surface with complete wettability at 40 ºC, partial wettability at 60 ºC and partial to complete

wettability at 80 ºC with an increase in pressure. Some novel surface phenomena of lipids on solid surfaces in SC-CO_2 medium were identified in both studies, including bouncing of lipid droplets on polished SS and glass surfaces, sliding of the CanO droplet on glass surface, supercritical fluid cavity formation during droplet spreading and satellite droplet formation.

The main goal of the third study was to determine the effect of process parameters (temperature, pressure, solvent-to-feed (S/F) ratio and different types of packing) on the output variables of extract yield, free fatty acid separation efficiency (FFA-SE) and dynamic hold-up (DH) amount. Continuous countercurrent fractionation of a model mixture (85% FFA and 15% triacylglycerol (TAG)) was performed using three different types of packing (stainless steel perforated and beads, and glass beads) at S/F ratios of 15 and 25, pressures of 16 and 24 MPa and temperatures of 40 °C, 60 °C and thermal gradient of 60-100 °C. The extract yield and FFA-SE at isobaric conditions were significantly affected by temperature. At isothermal conditions, the extract yield and FFA-SE were affected by S/F ratio and pressure, whereas the type of packing had an effect only on FFA-SE. At high S/F ratio, the extract yield was higher since there was a larger amount of CO_2 to solubilize lipids, specifically lighter molecular weight FFA, resulting in higher extract yield and higher FFA-SE. CO_2 density increased with pressure, resulting in higher extract yield as well as FFA-SE. DH amounts at isobaric conditions were influenced not only by temperature, but also by the type of packing. Differences in packing characteristics affected the DH amounts where lower void volume percentage corresponded to lower contact surface area, leading to higher DH amounts. More wettable packing surface by the lipids resulted in lower DH amount. In addition, CO_2 might have a lubricant effect on the holes of perforated packing, inducing disruption of the lipid film, possibly generating an easier mechanism for lipid film renewal, and thus enhancing mass transfer.

The findings of this Ph.D. thesis contribute to better understanding of the relationship between packing wettability and process performance in supercritical column fractionation of complex lipid mixtures and thus can lead to improved equipment design and enhanced process efficiency.

Preface

The research reported in this Ph.D. thesis was led by Dr. Feral Temelli, the principal investigator at the Department of Agricultural, Food and Nutritional Science (AFNS), University of Alberta and financially supported by the Discovery Grant (RGPIN-2017-04384) offered to Dr. Feral Temelli by the Natural Sciences and Engineering Research Council of Canada (NSERC). All work presented in Chapters 3, 4, and 5 was conducted at the University of Alberta.

This thesis contains original research work done by Eileen Vanessa Santos Hernandez under Prof. Feral Temelli's supervision, written according to the guidelines for the paper-based thesis format of the Faculty of Graduate Studies and Research of the University of Alberta. The thesis comprises six chapters, and the contributions made by Eileen Santos and the co-authors to the completion of this work are described here.

Chapter 1 provides the background information and research objectives, while **Chapter 2** presents the literature review based on the topics of the three research studies.

A version of **Chapter 3** is published as Eileen Santos, Prashant Waghmare, and Feral Temelli. Interfacial tension and equilibrium contact angle of corn oil on polished stainless steel in supercritical CO_2 and N_2 in the *Journal of Supercritical Fluids* (2020), 156, 104665 (https://doi.org/10.1016/j.supflu.2019.104665). As the first author, I was responsible for the investigation, methodology, validation, data collection and processing, formal analysis and writing the original manuscript draft. The experiments and data processing were completed at the *interfacial* Science and Surface Engineering Lab (iSSELab) KRÜSS Surface Science Hub, at the Department of Mechanical Engineering, supervised by Dr. Prashant Waghmare. Dr. Waghmare was the co-author of the published version of **Chapter 3** and provided guidance on results analysis and explanation of the phenomena observed. Dr. Feral Temelli was responsible for

conceptualization, project administration, supervision, reviewing and editing the manuscript and fund acquisition.

A version of **Chapter 4** is published as Eileen Santos, Prashant Waghmare, and Feral Temelli. Interfacial tension and equilibrium contact angle of lipids on polished glass in supercritical CO_2 in the *Journal of Supercritical Fluids* (2022), 181, 105486 (https://doi.org/10.1016/j.supflu.2021.105486). As the first author, I was responsible for the investigation, methodology, validation, data collection and processing, formal analysis and writing the original manuscript draft. The experiments and data processing were completed at the *interfacial* Science and Surface Engineering Lab (*i*SSELab) KRÜSS Surface Science Hub, at the Department of Mechanical Engineering, supervised by Dr. Prashant Waghmare. Dr. Waghmare was co-author of the published version of **Chapter 4** and provided guidance on results analysis and explanation of the phenomena observed. Dr. Feral Temelli was responsible for conceptualization, project administration, supervision, reviewing and editing the manuscript and fund acquisition.

A version of **Chapter 5** is in preparation for submission to the *Journal of Supercritical Fluids* for consideration for publication by Eileen Santos, Ricardo Couto, Jonathan Curtis, Rike Pfeufer, Ereddad Kharraz, and Feral Temelli. I was responsible for the investigation, methodology, validation, data collection and processing, formal analysis and writing the original manuscript draft. The state-of-art, design and modification of the operation mode of the supercritical fluid fractionation column, located at Agri-Food Discovery Place, from semi-continuous countercurrent mode was supported by Dr. Ricardo Couto and Dr. Feral Temelli and executed by Eileen Santos. Rike Pfeufer, who was a visiting student at the University of Alberta from the Technische Universität Bergakademie Freiberg, Germany in 2022, contributed to the writing of the initial draft

of introduction and experimental sections as well as performing some experiments. Additionally, in the experimental section, the modification and calibration of the fatty acid analysis method were completed by Eileen Santos under the guidance and supervision of Dr. Jonathan Curtis and Ereddad Kharraz at the Lipid Chemistry Group Laboratory. Dr. Feral Temelli was responsible for conceptualization, project administration, supervision, reviewing and editing the manuscript and fund acquisition.

Chapter 6 presents the overall conclusions with key findings and future recommendations of this Ph.D. thesis.

This thesis is dedicated to my husband, Juan, daughter Victoria, and my parents, Diana and Gustavo.

Acknowledgements

I want to express my sincere gratitude to Dr. Feral Temelli for being my role model as a woman leader in science and technology. The achievement of this critical professional goal in my career would not have been possible without her great support from the beginning to the end of my Ph.D. studies in exciting and challenging times. Thanks for your trust in my capacity and for your guidance in every step.

Thank you, Dr. Jonathan Curtis, for being my supervisory committee member; being your student has been a pleasure. Your guidance during my Ph.D. project, as well as your great disposition to collaborate with me, using your laboratory equipment and being supported by your research team members, have positively impacted the achievement of this goal, especially Ereddad Kharraz, Tolib Omonov and Vinay Patel. Thanks to Dr. Prashant Waghmare for being my supervisory committee member and teaching me about surface/material science applied to engineering as well as the use of the high-pressure equipment for interfacial tension and contact angle measurements. Also, I would like to thank Dr. Marleny Saldaña for being on my supervisory committee and for the great discussions, time and valuable feedback making this work successful. Thanks to Dr. Roopesh Syamaladevi for being my arm's length examiner and providing valuable feedback.

Thanks to Dr. Pedro Miguel Calado Simões, Universidade Nova de Lisboa, Portugal for being my external examiner for his time and valuable feedback. Also, I am grateful to NSERC (Natural Sciences and Engineering Research Council of Canada) for their financial support.

Furthermore, I would also like to give special thanks to Dr. Ricardo Couto for his continuous guidance and for teaching me all the hands-on skills in the supercritical technology field since July 2016; Rike Pfeufer for her important support in the achievement of the third study

of my thesis; Dr. Aleksey Baldygin from KRÜSS for his great assistance and the support in *interfacial* Science and Surface Engineering Lab (*iSSELab*) KRÜSS Surface Science Hub, and Ryan Baily for being my technical support during the studies reported in Chapters 3 and 4; Nathan Buzik for helping me during troubleshooting of the fractionation column at Agri-Food Discovery Place during development of experiments of Chapter 5.

Thanks to my mentor Dr. John Nychka for his unconditional support and strategical professional guidance during my Ph.D. journey. Thanks for empowering me during difficult times; I did not give up because of you; to Mr. Dinuka Guaratne for being my career advisor; and to all my lab mates and friends across campus.

Finally, I would like to thank God, my husband Juan, my daughter Victoria, my parents Diana and Gustavo, my sister Mayra, my grandparents Julio and Emilia, and uncle Lorenzo, for their emotional support, positive thoughts, and prayers during this journey. Thanks to all my Canadian family members, Dean Richardson, Brenda Bratrud, Louis and Gail Spavor, and especially my friends from Venezuela and Brazil, who have made this journey achievable during difficulties. Also, I would like to thank my former professors in Venezuela, Dr. Catheryna Aiello, Dr. Viluzka Fernandez and Dr. Jorge Ortega, for providing that feeling of curiosity and showing me the versatility of science that motivated me to start and finish my Ph.D. program.

Table of Contents

List of Tables

List of Figures

List of Abbreviations and Symbols

ANOVA	Analysis of Variance
ASTM	American Society for Testing and Materials
Bo	Bond number
CA	Contact angle
CA_{eq}	Equilibrium contact angle
CA_{stat}	Static contact angle
CA_{app}	Apparent contact angle
CanO	Canola oil
DOD	Deodorizer distillate
DHA	Docosahexaenoic acid
DH	Dynamic hold-up
EPA	Eicosapentaenoic acid
EOR	Enhanced oil recovery
FA	Fatty acid
FFA	Free fatty acid
FAEE	Free fatty ethyl ester
FFA-SE	Free fatty acid separation efficiency
GB	Glass beads
HTU	Height of a transfer unit
IFT	Interfacial tension
ID	Internal diameter
MW	Molecular weight

N	Normality
NIST	National Institute of Standards and Technology
NTU	Number of transfer units
OA	Oleic acid
OOO	Triolein
OD	Outside diameter
PTFE	Polytetrafluoroethylene or Teflon
PS	Pro-Pak perforated stainless steel packing
R_a	Roughness
SB	Stainless steel beads
SC-CO_2	Supercritical carbon dioxide
SC-N_2	Supercritical nitrogen
SS	Stainless steel
SH	Static hold-up
S/F	Solvent-to feed- ratio
TAG	Triacylglycerol

Greek symbols:

σ	Interfacial tension
μ	Viscosity
α	Tanner's law exponent
Δρ	Density difference

θ	Angle
$\sigma_{S/V}$	Solid-vapour interfacial tension
$\sigma_{L/V}$	Liquid-vapour interfacial tension

Chapter 1. Introduction and thesis objectives

According to the Food and Agriculture Organization of the United Nations report in 2021 about the future of food waste and loss with projections to 2030, around 14% of food produced is ending up as loss between harvest and retail processes, corresponding to $400 billion per year deficit in food value (FAO, 2021). It is estimated that approximately 17% of the total global food production is disposed of as waste. Moreover, such food loss and waste generate up to 10% of greenhouse gas emissions (FAO, 2021), creating an urgent need to focus on the food loss and waste management towards a sustainable practice. As a result, there is urgency for innovation in the agri-food supply chain that would lead to a noticeable enhancement in land use efficiency and water resource management, anticipating a positive impact on climate change (FAO, 2021).

The global interest in sustainable utilization of agri-food waste and by-products might positively benefit climate change and minimize waste. Research initiatives in the academia and private industries are focusing on conventional and novel processes to isolate high-value compounds with bioactivity for final incorporation into human consumption products, for example, functional foods, nutraceuticals, dietary supplements, and cosmetics, resulting in value addition and generating additional income for the industry (Saldaña et al., 2015).

One sector where more work is needed to maximize recovery of high-value compounds is the oil (vegetable and marine) processing industry. Conventional oil extraction and refining involves the use of large amounts of toxic solvents/chemicals, exposure to high temperatures and production of waste, which contributes to environmental pollution. In addition, there may be loss of some valuable bioactive compounds, for example, tocopherols and phytosterols, which can be used as supplements or incorporated into various products.

Different approaches and separation processes have been developed to minimize waste and pollution by processing it using green technologies that offer the possibility to recover thermally sensitive lipid-based bioactive compounds from various sources, for example, vegetable deodorizer distillates (DOD) or other complex lipid mixtures. One of the alternative green technologies is supercritical fluid technology using carbon dioxide. Supercritical carbon dioxide (SC-CO_2) exhibits versatility in being a non-toxic and non-polar solvent, while behaving as a liquid with high solvent power and as a gas with high diffusivity and low viscosity, resulting in a suitable option as a green solvent for this purpose. Thus, SC-CO_2 can be used to solubilize valuable non-polar lipid compounds and to separate different lipid classes from complex lipid mixtures.

The use of SC-CO_2 in the fractionation of complex lipid mixtures to deacidify oil refining mixtures or to isolate minor lipid compounds with bioactivity (tocopherols and phytosterols) has led to continued interest for further development (Fleck et al., 1998; Güçlü-Üstündağ & Temelli, 2007; Ibáñez et al., 2002; Ruivo et al., 2001; Stockfleth & Brunner, 2001). The supercritical fluid fractionation process involves the use of different types of packing inside a packed column to enhance the contact between the feed and SC-CO_2, increasing the mass transfer between phases to achieve the desired lipid separation. During the fractionation of complex lipid mixtures with SC-CO_2, several aspects have been investigated such as the effects of pressure, temperature, and solvent to feed (S/F) ratio, using different packing materials to enhance the separation efficiency of target compound(s). The key problems during the evaluation of the process performance of the countercurrent fractionation of lipid mixtures inside packed columns using SC-CO_2 are the lack of a) physicochemical property information related to lipid mixtures and their individual components while they are in contact with CO_2; and b) packing characteristics in terms of wettability and the variation in surface energy under experimental conditions. This information is critical for

designing and/or optimizing the fractionation process to achieve an effective separation of the target compound(s), since such data are important to correlate the mass transfer and hydrodynamic behaviour inside the column. As a result, there is need for further research to better understand the fundamentals related to the impact of the packing material used on the outcome process variables (separation efficiency (SE), extract yield and liquid hold-up).

Therefore, it was **hypothesized** that the type of packing has an effect on the separation efficiency and liquid hold-up during the packed column fractionation of lipid mixtures with SC-CO_2 under different processing conditions because of the different wettability behaviour of lipids on diverse materials under SC-CO_2 medium.

The **overall objective** of this Ph.D. thesis research was to investigate the wettability behaviour of different lipid classes on glass and stainless steel surfaces at different experimental conditions to understand how the wettability impacts the separation efficiency during the packed column fractionation of lipid mixtures with SC-CO_2. To accomplish this overall goal, the **specific objectives** were:

1. To determine the effect of pressure and temperature on interfacial tension (IFT) and equilibrium contact angle (CA_{eq}) of corn oil in air, SC-CO_2 and SC-N_2 on polished stainless steel metal sheet under unsaturated and saturated surrounding phases (Chapter 3),
2. To determine the effect of pressure and temperature on IFT and CA_{eq} of oleic acid and canola oil on polished glass in SC-N_2 and SC-CO_2 environments (Chapter 4), and
3. To determine the effect of the type of packing on the separation efficiency of lipid classes and liquid hold-up during the fractionation of a model lipid mixture using a countercurrent column with SC-CO_2 at different experimental conditions (Chapter 5).

Throughout the development of this Ph.D. thesis, different lipids, gases and solid surface materials were considered towards the ultimate goal of the isolation of different lipid classes using SC-CO_2 with a preference for canola lipids (canola oil and DOD), considering the importance of canola processing for the Canadian economy. Canada has great expertise in canola seed processing, with 14 crushing and refining plants across the country, crushing 11 million tonnes of canola seed each year (Canola Council of Canada, 2023). Based on the continuous growth in the global demand for canola oil and meal it is expected that the processing capacity will grow to 11.1. million metric tons by 2025, representing 60% increase of the current capacity (Canola Council of Canada, 2023).

For Objective 1, corn oil and different gases (CO_2 and N_2) were used mainly to validate the experimental protocols for the IFT determination and to be able to compare the results with the values available in the literature for corn oil and other oils at 80 ºC and up to 40 MPa. Then, canola oil and oleic acid were selected for Objective 2 to represent different lipid classes of triacyglycerols and free fatty acids, respectively, considering that oleic acid represents 61% of the fatty acids in canola oil (Przybylski et al., 2005). Even though high purity triolein (OOO) was also considered initially, it was not possible to incorporate it into the experimental design due to its high cost.

For Objective 3, the original goal was to isolate phytosterols from canola DOD using a continuous countercurrent packed column and SC-CO_2; however, despite all the efforts, unfortunately, that was not possible due to the equipment limitations and the numerous challenges encountered at the time of manipulation of this complex lipid mixture. For example, the blockage of the liquid pump occurred due to free phytosterols being still in solid form and not dissolved in the lipid mixture at 40 °C, which was the maximum operational temperature specified by the liquid pump manufacturer. Therefore, it was necessary to reformulate the lipid mixture composition

excluding the phytosterols to accomplish all the objectives using a model mixture of free fatty acids and triacyglycerols, composed of oleic acid and canola oil as an economic and appropriate alternative. Moreover, considering the lipid composition of canola oil (94.4-99.1 wt% triacyglycerols (TAG); 0.4-1.2 wt% free fatty acids (FFA)) and its TAG profile (22.4% OOO; 22.5% LOO; 10.4% LnOO) (Przybylski et al., 2005) as well as the limited availability of physicochemical properties for canola oil, OOO was selected as the representative TAG to explain the differences in the behaviour of the lipid classes in contact with SC-CO_2. The other major TAGs present in canola oil were not considered due to the limited data available, regarding their solubility, density and interfacial tension in SC-CO_2 (Chrastil, 1982; Ilieva et al., 2016a; Nilsson et al., 1991).

Regarding the selection of the different solid surfaces evaluated, polished stainless steel (SS) sheet was used in Objectives 1 and 2, polished glass sheet in Objective 2 and different packings with diverse materials and geometries (perforated Pro-Pak® SS, SS bead and glass beads) in Objective 3. To maintain consistency in the type of materials used, the stainless steel was 316 SS and glass was borosilicate for all the different solid surfaces. Furthermore, smooth and perforated geometries were considered for the sheets used in Objectives 1 and 2 to correlate them with the lipid behaviour inside the packed column when perforated packing and smooth beads were used as packings.

Chapter 2. Literature review

2.1. The major and minor compounds of lipid mixtures

Lipids are chemical molecules soluble in organic solvents and insoluble in water, ranging from simple to complex molecular structures. Based on the chemical structure, lipids can be classified as fatty acids and oxylipins, simple lipids (glycerolipids and triacylglycerols or triacyglycerols (TAG), sterols, lipoproteins, etc.), complex glycerophospho- and glyceroglyco-lipids, and sphingolipids (Christie, 2023a). Lipids are widely present in biological organism cells of plants and animals. Fats and oils are comprised of lipids and behave as solid and liquid at ambient temperature, respectively, reflective of their melting points. Fatty acids (FA) and triacyglycerols, representing different lipid classes, are the main focus of this thesis research. Whereas FFA are carboxylic acids with an aliphatic chain, the TAG have three fatty acids (could be the same or different saturated or unsaturated FAs) esterified to a glycerol backbone. TAG are present in vegetable oils, especially in oilseeds such as canola and soybean as well as other vegetable sources as corn, palm kernel, and rice bran, where olive and canola oils contain higher concentrations of oleic acid (Damodaran & Parkin, 2017). On the other hand, animal fats contain higher amounts of TAG with saturated fatty acids, for instance, fat from milk, sheep, beef, pig, chicken, and turkey (Damodaran & Parkin, 2017). Algal oil has received increasing attention over the years since this raw material is affordable and rich in nutrients, containing diverse bioactive compounds with potential health benefits (Osório et al., 2020). Moreover, fish oil contains high concentrations of long-chain polyunsaturated fatty acids, like eicosapentaenoic acid (EPA), docosahexaenoic acid (DHA) and arachidonic acid, which are in high demand due to their beneficial health effects (Health Canada's Food Directorate, 2016).

There are several minor lipid compounds contained in agri-food waste or vegetable oil refining by-products that receive high interest from the industry due to their bioactivity and health benefits, leading to their potential use as value-added ingredients in human consumption products. As an example of the agri-food waste reality, in Canada, the canola oil processors produce large amounts of deodorizer distillates (DOD) in their refining processes, which is added back into the animal feed without considering the recovery of bioactive minor lipid compounds, such as tocopherols and phytosterols (Güçlü-Üstündağ & Temelli, 2007). Those bioactive compounds are associated with health benefits; for instance, while tocopherols show vitamin E activity and are effective antioxidants, phytosterols reduce the total serum cholesterol, and reduce the risk of cardiovascular and chronic diseases (Ghazani & Marangoni, 2013; Health Canada Food Directorate, 2010).

Phytosterols or plant sterols are part of a triterpenes group with a tetracyclic cyclopenta-α-phenanthrene structure and a side chain at carbon 17. The structure exhibits *trans* ring junctions, two methyl groups at C-18 and C-19 and a hydroxyl group on C-3. Their hydroxyl group could be not linked to any other moite or conjugated to an ester bond or glucose, referred to as free or esterified or steryl glycosides, respectively. Usually, they have a double bond in position 5 and exhibit a variable stereochemistry in the side chain at C-24 with one or two carbon substituents (Christie, 2023b) They are essential in the structure and functionality of cell membranes in plants, specifically participating in the regulation of membrane fluidity as well as in cellular differentiation and proliferation, etc. (Piironen et al., 2000). Phytosterols can be found in vegetable oils and their derivates, nuts, grains and cereals. In humans, the metabolism of these compounds is similar to that of cholesterol, and they compete with cholesterol, thus, their bioactivity is related to the reduction of the total serum cholesterol through the decrease in the low-density lipoprotein-

cholesterol. Additional possible reasons for the positive effect that phytosterols have on total serum cholesterol decrease have been highlighted, such that they: a) inhibit the cholesterol absorption; b) compete during the solubilization of cholesterol in the micelles and their transportation across apical membrane of enterocytes; c) may not co-crystallize with cholesterol to a great extent, and d) prevent the intracellular re-esterification of cholesterol by acyl coenzyme cholesterol acyltransferase (Jesch & Carr, 2017). The solubility behaviour of phytosterols varies depending on their molecular structure. While free phytosterols are poorly soluble in lipid-based products, esterified phytosterols exhibit the opposite trend, making this form of phytosterols more attractive for different industrial applications and for further use as value-added ingredients in food products, such as margarine, yogurt, salad dressing and fruit juice (AbuMweis et al., 2008; Clifton et al., 2004; Cusack et al., 2013; Demonty et al., 2009). However, there is need for further research to develop green processes for the separation of minor lipid bioactive compounds from agri-food waste and oil refining by-products as well as simple, practical and applicable analytical techniques to identify their presence in complex lipid mixtures and quantification of individual lipid classes.

2.2. Extraction and fractionation of lipid mixtures

2.2.1. Conventional and modern techniques for lipid extraction

Lipids have several applications in different industries, for example, food, nutraceutical, pharmaceutical, oleochemical, leather, paint, rubber, and textile. The industry has focused their efforts to optimize their extraction towards more sustainable processes that involve the usage of environmentally friendly solvents, for example, carbon dioxide, reducing the use of toxic organic solvents and energy consumption as well as avoiding the loss and degradation of minor bioactive lipid compounds.

To extract lipids and minor compounds from biological sources (seeds, algae, plant and animal sources), there are several challenges mainly because they can be bound to other components like proteins and carbohydrates, resulting in the need for material pretreatment to facilitate their extraction. The main goal of the pretreatment step is to break the cell wall to facilitate the release of intracellular lipids for their extraction, which could involve moisture conditioning of the starting material. Some of the steps related to this pretreatment process of the starting material (for example, oilseeds like canola seed) are cracking, dehulling and crushing/flaking the seeds. Then, based on the targeted lipid extraction process, the crushed or flaked seeds are subjected to mechanical processing, like cold pressing. Usually, the pre-conditioned material subjected to mechanical pressing contains less than 20% (wt/wt) oil, and during this process, the bioactive material is not subjected to organic solvents and high temperatures, whereas mechanical energy is applied to the solid material either by batch hydraulic pressing or screw press (de Jesus & Filho, 2020), resulting in oils with less chemical alterations and preservation of bioactive compounds.

The conventional technologies to extract oils from plant seed sources involve the use of organic solvents, commonly hexane, which is a non-polar solvent with lower latent heat than ethanol. It is the most common organic solvent used for lipid extraction, since lipids dissolve easily and its recovery is simpler relative to the other organic solvents, making it economically attractive to the industry (Saini et al., 2021). However, hexane presents high toxicity and contributes to environmental pollution, generating the worldwide need to search for alternative solvents and technologies that are more sustainable and green according to the principles of green chemistry (Anastas & Warner, 1998). In general, volatile organic solvents used at industrial scale for pharmaceutical, chemical and food processing purposes represent a serious problem from the

sustainability perspective, due to their negative consequences at environmental and human health levels. For example, in humans, volatile organic solvents could produce dizziness, skin and eye problems, and at long term exposure, liver, kidney and central nervous system issues (Crinnion, 2010). As a result, the use of "green solvents", such as terpenes, supercritical carbon dioxide (SC-CO_2) and ionic liquids is becoming popular.

It is interesting to consider that to meet the criteria of a "green solvent", most of the 12 fundamental principles of green chemistry must be satisfied, which comprehend the rational and procedural use of renewable feedstock or innocuous chemicals, and the fact that the solvent used will not remain in the environment (Anastas & Kirchhoff, 2002). Some of the green organic solvents considered for lipid extraction are: a) organic-based solvents with low toxicity, high boiling point, biodegradable and easy to recycle; b) bio-based solvents derived from feedstock, usually from cellulose and starch, for example, alcohols, ethers, esters and terpenes; c) ionic liquids are organic salts which are liquid at low temperatures (below 100 °C), exhibit negligible vapour pressure below 400 °C, non-flammable and highly thermostable liquids; however, their classification as green solvents is controversial because fossil-based chemicals are used in their production, and d) SC-CO_2 is a non-polar solvent, which at ambient temperature is a gas allowing its easy recovery and it can be recycled to mitigate its greenhouse effect (de Jesus & Filho, 2020).

A modern technique investigated for seed oil extraction is an ultrasound-assisted process, which is based on the cavitation or oscillation phenomenon principle via ultrasound probe or bath. In this process, energy is transferred to solid material or particles through the generation of ultrasound vibration waves, while simultaneously, the collision of cavitation bubbles created on the solid surface occurs at higher amplitude, inducing a cell wall disruption, and resulting in more prominent transfer of the target lipid compounds in contact with the solvent (Senrayan &

Venkatachalam, 2019). This process offers a benefit compared with the conventional solvent extraction process, since it requires less amount of solvent and lower temperatures, reducing the risk of degradation of minor lipid compounds.

2.2.2. Vegetable oil refining process and alternative technologies

The conventional vegetable and seed crude oil refining process aims to obtain odorless, oxidatively stable and acceptable oil to customers. The overall process involves four main steps, which might vary based on the type of oil to be refined. The basic steps are degumming, neutralization, bleaching and deodorization. During the degumming process, the phospholipids and gums are removed from the crude oil. There are two types of degumming where conventionally water or acid have been used for this purpose, but other alternative processes have also emerged to improve the refined oil quality, for example, enzymatic degumming, membrane degumming, total degumming process and dry degumming (Ghazani & Marangoni, 2013). In the neutralization process (also called caustic refining or chemical refining method), sodium hydroxide or potassium hydroxide is added to the degummed oil to convert free fatty acids into insoluble soap, which are then removed by gravity or centrifugal separation. Other compounds removed in this step are metals, chlorophyll, and impurities (Fine et al., 2016). During this process, a strong base reactant is used, and heat might induce other chemical changes, for example, conversion of triacyglycerols into soap, and degradation of minor lipid compounds such as phytosterols, polyphenols and tocopherols (Ghazani & Marangoni, 2013). Later, in the bleaching process, impurities like color pigments, traces of soaps, phospholipids, metals and oxidation products from the neutralization process are removed by means of bleaching clays via adsorption and peroxides via catalytic decomposition. Those compounds must be removed because they negatively affect the final quality of the refined oil (Ghazani & Marangoni, 2013). The final step is the deodorization process, which

is a steam distillation process that aims to reduce the FFA% from ~1% to 0.05% in the bleached oil, where the oil is subjected to high temperature (230-260 °C) and steam pressure (3-5 mbar). (Ghazani & Marangoni, 2013). It is important to consider that the exposure of bioactive minor lipid compounds to high temperatures during the deodorization process might produce losses and oxidation of these compounds mainly due to thermal degradation.

As an alternative solution to reduce the amount of toxic chemicals used during the conventional refining process of vegetable and seed oils, membrane technology provides an interesting approach not only to reduce the chemical use but also to maintain the bioactivity of minor lipid compounds. For example, micelle-enhanced ultrafiltration membranes have been used for degumming to separate phospholipids and their ability to degum crude vegetable oils has been demonstrated (Rangaswamy et al., 2021). Another approach for the removal of wax content during the refining process involved the use of ultrafiltration or microfiltration membranes. Those membranes resulted in the reduction of low wax contents after the centrifugation and filtration steps (Rangaswamy et al., 2021).

2.2.3. Isolation of minor compounds from agri-food waste and vegetable oil-refining by-products

The biorefinery approach to enhance the value of agri-food waste considers the presence of high amounts of phytonutrients or bioactive compounds in the by-products or residues of food waste (Ben-Othman et al., 2020). Sustainability could be enhanced if the agri-food waste is used to produce value-added products, offering a great opportunity to the industry to generate additional income, as well as reducing the negative environmental impact (Ben-Othman et al., 2020). Some of the most common bioactive compounds isolated from agri-food waste and oil refining by-products are: a) polyphenols, tannins, sterols, flavonoids, flavanols, vitamins (A and E); fatty acids,

volatiles, anthocyanins and pigments from plant sources; and b) bioactive peptides from animal sources.

A major problem for the conventional oil refining process is that there are many factors negatively affecting the minor bioactive lipid compounds, inducing their loss, degradation and oxidation, making them unable to be extracted and reused as a value-added ingredient in human consumption products. For example, in their review article, Ghazani & Marangoni (2013) mentioned that a) during the degumming step of high-oleic acid safflower oil, the amounts of free and esterified sterols decreased mainly due to the effect of the phosphoric acid used and its catalytic effect on the hydrolysis of esterified sterols; b) during the neutralization step, total tocopherols in rapeseed oil was reduced from 685 to 552 ppm (24% loss), mainly due to the alkaline conditions of neutralization, while the phytosterol in rice bran oil was reduced by about 27%; c) bleaching step also affects the phytosterols amount, causing a reduction due to the hydrolysis of steryl esters by activated bleaching earth; and d) the deodorization step reduced the total tocopherols in canola oil by 36%, whereas in soybean oil, the total amount of esterified phytosterols increased from 59.5 to 97 mg/100 g and total free phytosterols decreased from 267 to 204 mg/100 g, which could be related to the esterification of free phytosterols occurring at high deodorization temperatures. Moreover, Fine et al. (2016) reported that phytosterols content was higher in crude rapeseed oil (821 mg/100 g), whereas it was 359 mg/100 g in soybean oil; however, during the refining process, there was 52% and 18% loss of phytosterols in rapeseed and soybean oils, respectively.

Due to the loss of bioactives during the oil refining process as highlighted above, several research studies intended to reduce the loss of those bioactive compounds through less severe processes to isolate those bioactive compounds with high efficiency while maintaining their bioactivity to increase their further use in human consumption products. For example, a) using

different alkaline reagents during the neutralization step demonstrated that $Ca(OH)_2$, MgO, and Na_2SiO_3 preserved tocopherols and phytosterols in rapeseed oil (Fine et al., 2016); b) enzymatic refining process resulted in better oil yield, reducing the losses of lecithin and oil while using less amount of water (Fine et al., 2016); c) membrane technology as detailed in the review of Rangaswamy et al. (2021), has been applied for the separation, recovery and concentration of bioactive compounds from agri-food wastes and vegetable oil industry by-products.

2.3. Supercritical fluid technology for the extraction of lipids and minor components

Supercritical carbon dioxide (SC-CO_2) has been widely used in food, pharmaceutical, nutraceutical, cosmetic and other industries due to its low cost, ease of accessibility at high purity, safe to manipulate and non-toxic at low levels; thus, it is approved for use as a solvent in the food processing industry without a declaration (Sahena et al., 2009). The properties of SC-CO_2 have been summarized by Aguilera & Del Valle (1999) and they are: a) due to its non-polar nature, it dissolves non-polar compounds and slightly polar compounds; b) exhibits affinity to oxygenated compounds of medium molecular weight; c) its density, which dictates its solvent power, can be manipulated by changing temperature and pressure; d) polysaccharides, sugars and mineral salts are insoluble in SC-CO_2; e) when SC-CO_2 pressure is enhanced, it can solubilize higher molecular weight compounds, which depends on its density and the properties of the solutes.

Lipid extraction using SC-CO_2 has been widely studied to extract lipids from plants and animal sources. CO_2 becomes a supercritical fluid at conditions above its critical point of 31.1 °C and 7.4 MPa, where its diffusivity is like a gas and its solvent power is like a liquid. It is suitable for lipid extraction and an excellent solvent to extract thermosensitive minor lipid compounds or lipid mixtures. There are critical aspects to be considered at the moment of lipid extraction using SC-CO_2: a) knowledge of the composition of the raw material; b) pretreatment of material to allow

better contact of CO_2 with the matrix containing the lipids, c) consideration of polarity of the target lipids to extract, since if those lipids are polar, it might be suitable to use a polar co-solvent to enhance their extraction efficiency. During this process, the sample is exposed to SC-CO_2 under controlled conditions of time, temperature, pressure and co-solvent flow or amount depending on the operation mode, to dissolve the oil or fat from the sample in CO_2 or CO_2 with a co-solvent. Then, the lipids dissolved in CO_2 are recovered by reducing the CO_2 pressure. If a co-solvent is used during the extraction process, an extra step is required to remove this solvent and get the solvent-free extract or lipid mixture.

An approach for the deacidification of vegetable and seed oils as well as the isolation minor lipid bioactive compounds has been considered in the supercritical fluid technology though the fractionation process using SC-CO_2. A more detailed explanation of this process and the experimental parameters affecting its efficiency will be explained in the following sections of this chapter.

2.3.1. Column fractionation of lipid classes and minor compounds using supercritical carbon dioxide

Supercritical fluid fractionation with CO_2 has been used to isolate minor components from complex mixtures such as crude and refined oils, oil refining by-products like DOD as well as mixtures of fatty acid methyl esters (FAME), fatty acid ethyl esters (FAEE) and other model mixtures since the early 1990s, as summarized in Table 2.1. This process has been considered to use the versatility of SC-CO_2 as a safe, innocuous and green solvent, with or without co-solvents to deodorize lipid mixtures or to recover bioactive compounds, which are prone to thermal degradation or conversion into undesired compounds during the conventional refining process, as discussed in the previous section for different bioactive compounds.

Table 2. 1. Research articles related to the fractionation of complex lipid mixtures and minor lipid compounds using supercritical carbon dioxide, and the operating conditions and packing materials used.

Reference	Feed	Operation mode	Temperature (°C)	Pressure (MPa)	S/F ratio	Packing arrangement	Material	Packing specifications
Brunner et al. (1991)	Soybean, rapeseed and colza DC	B	50, 70, 90	13 - 20		Random	SS and Teflon	Spirals (SS) and ring (Teflon)
Shen et al. (1996)	Rice bran oil	Continuous	39.85-49.85	8.6-11.2	300-330	Solid material	Solid rice bran	n.s.
Catchpole et al. (1997)	Shark liver oil	Continuous	39.85-49.86	12.5 - 20	n.s.	Random	Glass and SS	Raschig rings (glass), Fenske helices (glass), and wire wool (SS)
Sahle-Demessie (1997)	Glycerides mixtures	SB	65-95	20.7 - 34.5	n.s	Random	SS	Protruded SS packing Pro-Pak®
King et al. (1997)	Glycerides mixtures	SB	65-96	17.2 - 34.4	n.s.	Random	SS	Protruded Pro-Pak® (SS)
Fleck et al. (1998)	EPA-DHA ethyl esters, fish oil FAEE	Continuous CC	39.85, 69.85, 79.85	14.5, 17, 19.5	70–180	Structured	SS	Sulzer CY

Table 2. 1. (Continued)

Reference	Feed	Operation mode	Temperature (°C)	Pressure (MPa)	S/F ratio	Packing arrangement	Material	Packing specifications
Stockfleth and Brunner (1999)	Tocols, water, aqueous surfactant solution	CCC	39.85, 99.85	8, 30	n.s.	Structured	SS	Gauze Sulzer CY, EX
Catchpole, Grey, et al. (2000a)	Fish oil, fish oil/ethanol	CC	59.85	20-30	n.s.	Random	SS, glass	Fenske spirals (glass), Pall rings (SS)
Catchpole, Simões, et al. (2000)	Shark liver oil, olive oil DOD	Co-current or CC + ER	39.85-59.85	16-25	n.s.	Structured	SS	EX Sulzer
Riha and Brunner (2000)	Fish oil FAEE	CCC	39.85-79.85	9, 20	75-130	Structured	SS	CY Sulzer
Ruivo et al. (2001)	Squalene + methyl oleate	CCC	39.85	11.5	2-80	Structured	SS	EX Sulzer
Stockfleth and Brunner (2001)	Water, olive oil DOD	CC	39.85, 99.85	8, 30	n.s.	Structured and random	Glass, ceramic, SS	Raschig rings (glass) and Berl saddles (ceramic), Sulzer CY (SS) and Sulzer EX (SS)

Table 2. 1. (Continued)

Reference	Feed	Operation mode	Temperature (°C)	Pressure (MPa)	S/F ratio	Packing arrangement	Material	Packing specification
Ibáñez et al. (2002)	Olive oil	CC, SB	40	20	up to 41. 7	Random	SS, glass	Beads (glass) and Rashing rings (material n.s.), Fenske rings (glass), and Dixon rings (material n.s.)
Ruivo et al. (2002)	Squalene + methyl oleate	CC	39.85	11.5	2 to 80	Structured	SS	Corrugated Sulzer EX
King and Dunford (2002)	Rice bran and soybean oil DOD	SB	40-80	10.2-34	n.s.	Random	SS	Protruded Pro-Pak® (SS)
Dunford et al. (2003)	Crude rice bran oil	CCC	45-80	13.8–27.5	7	Random	SS	Protruded Pro-Pak® (SS)
Hurtado-Benavides et al. (2004)	Olive oil	CC	39.85	20	23-42	Random	Glass	Beads (glass) and Rashing rings (material n.s), Fenske rings (glass), and Dixon rings (material n.s)

Table 2. 1. (Continued)

Reference	Feed	Operation mode	Temperature (°C)	Pressure (MPa)	S/F ratio	Packing arrangement	Material	Packing specifications
Zacchi et al. (2006)	Cold pressed wheat germ oil	CC	65	35	n.s	Structured	SS	Sulzer BX
Pietsch and Jaeger (2007)	Shark liver oil	Semi-continuous CC	120	50	n.s.	Structured	SS	Sulzer BX
Güçlü-Üstündağ and Temelli (2007)	Canola DOD	Semi continuous, SB	70-100	20, 25	n.s.	Random	SS	Protruded Pro-Pak® (SS)
Fernández et al. (2007)	Squalene + methyl oleate	CC	39.85-59.85	11.5-18.5	20-30	Structured	SS	Corrugated Sulzer EX
Fang et al., (2007)	Soybean DOD	Semicontinous CC	39.85-79.85	14, 15, 16, 20	14-20	Random	SS	Dixon
Vázquez et al. (2007)	Olive oil DOD and complex lipid mixtures	CC	69.85	15 - 30	up to 20	Random	n.s.	Fenske rings
Perretti et al. (2007)	Fish oil FAEEs	B	40, 50, 60	10, 14, 15 and 30	9–65	Random	SS	Rashing rings

Table 2. 1. (Continued)

Reference	Feed	Operation mode	Temperature (°C)	Pressure (MPa)	S/F ratio	Packing arrangement	Material	Packing specifications
Chang et al. (2008)	Soft-shelled turtle fish oil	CC	79.85	20	250-1000	Random	Aluminium	Pieces of cylindraceous aluminum structured matrices
Zacchi et al. (2008)	Rapeseed oil	CC	60	20-26	20-50	Structured and random	Metal	Sulzer Mellapak 500.X, Shott Durapack and wire mesh
Chen et al. (2008)	Rice bran oil	n.s.	69.85-89.85	20-30	n.s.	n.s.	SS	n.s.
Vázquez et al. (2009)	Cold press olive oil	CCC	39.85	18, 23.4, 25	15	Random	n.s.	Fenske rings
Torres et al. (2009)	Soybean DOD and modified lipid mixture	CCC	45–55	20 - 28	n.s.	Random	n.s.	Fenske rings
Brunner and Machado, (2012)	Palm fatty acid distillates	CCC	99.85	26, 29	50-350	Structured	Metal	Sulzer EX
Hurtado et al. (2013)	Olive oil	Semicontinuous CC	24.8 -75.2	6.59 - 23.41	n.s.	Random	n.s.	Fenske rings
B: Batch; SB: semi-batch; CC: countercurrent; CCC: continuous countercurrent; ER: external reflux; FAEE: fatty acid ethyl esters; DC: deodorizer condensate; DOD: deodorizer distillate; SS: stainless steel								
n.s. Not specified								

For the fractionation of lipid mixtures, a packed column has been used in the different studies summarized in Table 2.1. Diverse operation modes have been evaluated, but the continuous countercurrent process has been identified as the most efficient operation mode. As shown in Figure 2.1, during such an operation CO_2 is pumped from the bottom of the packed column at supercritical conditions, while the feed mixture is pumped in from the top of the column at the desired temperature and pressure and the system is allowed to reach steady state condition. In this process, CO_2 is able to solubilize low molecular weight lipids in the feed mixture, removing them in the lighter phase or extract from the top of the column and separating them from the heavier molecular weight lipids collected in the raffinate fraction at the bottom of the column.

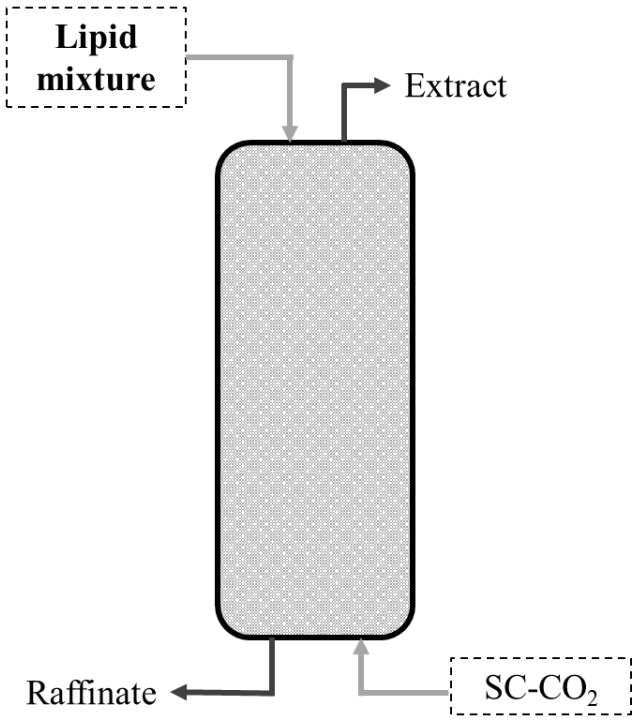

Figure 2.1. Fractionation of lipid mixtures in countercurrent continuous mode using SC-CO_2.

The optimization of this process relies on several experimental parameters and the interactions between the lipid components and SC-CO_2 as well as the packing material used to enhance the contact between the liquid and CO_2 phases. As detailed in Table 2.1, this process has been investigated to extract different bioactive compounds, optimizing experimental conditions of operation modes (batch, semi-continuous, continuous, co-current and countercurrent), temperature configurations (isothermal or thermal gradient), pressures (from below to above critical pressure of CO_2), using different packings (different materials and geometries as well as arrangements (random and structured)), solvent-to-feed ratios and chemical pre-treatments of feed lipid mixtures.

However, some challenges have emerged over the research and optimization of this process, as well as its scale-up, not only regarding the lack of physicochemical properties of the two phases in contact (i.e. CO_2 phase saturated with lipids and lipid phase saturated with CO_2), but also the absence of those parameters for individual compounds, which are fundamental knowledge needed to design, modify or improve processes that involve supercritical fluid technology using CO_2. As a result, the effects of temperature and pressure on the physicochemical parameters of FFA and TAG and lipid mixtures in CO_2 and vice versa will be discussed in the following sections.

2.3.2. Mass transfer and hydrodynamic behaviour

The mass transfer aspects of supercritical column operations has been evaluated following two different approaches: a) the conventional McCabe-Thiele method where mass balance, component balance and equilibrium data for lipid + CO_2 are needed to calculate the height of transfer unit (HTU) and the number of transfer units (NTU) to evaluate the packing efficiency, or in other words, if the packing is allowing enough contact between the phases and translating it to higher separation efficiency of target compound(s), and b) the modeling of mass transfer inside a

packed column, which is not only associated with the previous parameters mentioned, but also with the mass transfer model selected. Regarding mass transfer modeling of packed columns, de Haan and de Graauw (1991) developed the first study that addressed the mass transfer models for structured packed columns during the separation of hydrocarbons using SC-CO_2, specifically for the system hexadecane/2-methylnaphthalene/CO_2. However, focusing on the vegetable lipids, Simões et al. (1995) investigated the mass transfer inside a fractionation column packed with structured gauze packing and CO_2 as a solvent to fractionate a mixture of vegetable lipids such as terpenes. The authors pointed out that the mass transfer model selection depends on the physicochemical properties of the phases involved at the experimental conditions, as well as the hydrodynamic properties, highlighting the importance of surface tension. To the best knowledge of the author, this was one of the first studies to consider the possibility of partial wettability of packing area and its impact on mass transfer and hydrodynamic behaviour analysis, where the partial packing wettability was referred to as the liquid phase dispersed as a thin film that covered the packing area only partially. During their experimental work, Simões et al. (1995) faced challenges for the visual confirmation of the partial wettability of terpenes on gauze packing and their mass transfer coefficient predictions were limited by the lack of physicochemical properties data of CO_2 and liquid phases at experimental conditions, emphasizing the need for appropriate estimation of the wetted surface area of the packing by the lipid phase in contact with CO_2. Later, Ruivo et al. (2002) used olive oil DOD to test and develop a mass transfer model for supercritical fluid processes. Initially, they fractionated a model mixture of squalene/methyl oleate by SC-CO_2 using corrugated gauze packing material. Based on the data obtained, they presented a general correlation to predict the mass transfer efficiency of the high-pressure fractionation packed column, considering the film model approach due to the lack of film disruption on the packed bed

visualized during the experimental runs. It is important to consider that there is a correlation of the packing wettability of the liquid phase in the presence of CO_2 with the mass transfer behaviour, because lipid phase wettability on packing material not only dictates the interaction between the two phases, enhancing or reducing their contact, but it is also linked to the flow behaviour of the phases, and thus the hydrodynamic behaviour, referring to different flow patterns inside the column.

The hydrodynamic behaviour inside a continuous countercurrent packed column refers to the flow behaviour of the phases at the packing level that allows either an efficient or inadequate contact between the phases. In a continuous operation, it is expected that the phases flow continuously over the packing, avoiding the flooding of the packed column and undesired separation process outcomes. Flooding inside a packed column could occur by accumulation of liquid on top of the packing material, leading to inappropriate contact between phases, decreasing process efficiency. The role of packing is to improve the contact between the phases by enhancing mass transfer area to achieve the desired mass transfer between the phases involved. The flow of the phases at the packing level might be continuous or disrupted based on the experimental conditions and the type of packing, and therefore the type of packing is crucial to properly understand the hydrodynamic behaviour of this process. Furthermore, another important parameter to consider for the hydrodynamic behaviour inside a countercurrent column is the liquid hold-up. This parameter refers to the amount of liquid inside the column and it is classified as static (SH) and dynamic hold-up (DH). SH refers to the liquid attached to the packing material by adhesive forces; thus, it does not drain from the packing, and it must be removed by other means; whereas DH refers to the liquid that drains out of the column once the gas and liquid pumps are stopped (Stockfleth & Brunner, 2001).

In contrast to the film approach of Ruivo et al. (2002) to describe mass transfer, Stockfleth and Brunner (2001) considered the hydrodynamic behaviour under SC-CO_2 conditions to understand the flooding behaviour of packed columns, liquid hold-up and pressure drop using random and structured packings, investigating the systems water-CO_2 and olive oil-CO_2. The authors concluded that it was not possible to develop a universally applicable parameter to correlate packing and liquid phases in contact with CO_2 for the prediction of the flooding points because of the diverse physicochemical properties exhibited by lipid compounds in CO_2 as well as their interactions with the different packing materials. Furthermore, Zacchi et al. (2008) studied some parameters related to the hydrodynamic behaviour of packed columns using SC-CO_2, such as the static and dynamic hold-up as well as the residence time distribution among different packings, ranging from structured to random packing for rapeseed oil deacidification with SC-CO_2. Zacchi et al. (2008) mentioned that the static hold-up depended on packing density as well as gas phase density, but at high pressures the buoyancy effect caused by the dense gas on the liquid phase was considerable. As a result, the static hold-up could not be considered negligible based on the deviation of the flow model from plug flow (flow perfectly mixed in radial direction) to axial dispersion (diffusion and turbulent mixing occur, as in the case of countercurrent operation). Moreover, Pieck et al. (2017) proposed a new model to fractionate fish oil FAEEs using SC-CO_2, where they indicated that the flooding point during the fractionation of lipids with CO_2 inside packed columns must be determined considering the effect of interfacial tension and packing wettability. The authors mentioned that the increase or decrease of flooding capacity of the column might be caused by the degradation of packing elements, which is possible because of the energy variations that the packing is subjected to at different temperatures as well as chemical oxidation due to the different liquids it was in contact with and inappropriate cleaning procedure.

Furthermore, Pieck et al. (2021) developed a correlation to link hydrodynamic behaviour with flooding capacity inside a packed column using SC-CO_2. However, they indicated that there were challenges to investigate the influence of viscosity and interfacial phenomena though this correlation since only a few values of interfacial tensions and contact angles are available for systems involving a supercritical fluid.

Based on all the aspects mentioned above, there is a sensitive balance between mass transfer and hydrodynamic behaviour in countercurrent packed columns to fractionate lipids, which is related to the packing wettability by the lipid phase in SC-CO_2 medium and its inherent contribution to the variation of liquid flow pattern inside a packed column and packing surface energy, resulting in enhancement or reduction of mass transfer between phases, impacting the process efficiency. Therefore, to design an optimal fractionation process, the hydrodynamic behaviour inside a fractionation column must be considered, which relates the contact between the two streams at the packing material level.

Different studies have focused on understanding the hydrodynamic behaviour inside the packed column by using diverse packing materials and geometries, revealing a significant variation in the separation efficiencies of lipids (Stockfleth & Brunner, 1999, 2001; Ibáñez et al., 2002; Zacchi et al., 2006; Brunner & Machado, 2012). For example, Ibáñez et al. (2002) isolated phytosterols and tocopherols from olive oil using a semicontinuous countercurrent SC-CO_2 extraction process and evaluated the efficiency of different packing materials (Raschig rings, Dixon rings, Fenske rings, and glass beads) based on their selectivity towards a specific type of lipid (tocopherols and phytosterols). They concluded that the highest average concentration of tocopherols and phytosterols were obtained when glass beads and Fenske rings (made of glass) were used, highlighting that the chemical nature of the glass-based packing material allowed

uniform film formation, resulting in a high specific surface area, impacting positively the separation efficiency of those minor components. Based on visual observations of different systems (water-CO_2, aqueous surfactant solution-CO_2 and tocopherols-CO_2) inside a fractionation column with two different gauze packings, Stockfleth and Brunner (1999) reported that the Sulzer CY packing material did not show complete wettability, specifically for the tocopherols/CO_2 system. Previous studies revealed diverse separation efficiencies of lipids and minor components without explaining if the type of material and/or geometry of the packing had an impact on the selectivity of separation. Additionally, Bejarano et al. (2016) indicated that the understanding of the hydrodynamic behaviour inside a packed column might be linked to the contact angle (CA) and interfacial tension (IFT), since these parameters influence the limit of the interchange area and packing wettability; therefore, they are critical parameters.

The research to date has tended to focus on understanding the process performance based on different feed lipid mixtures and experimental conditions, including the type of packing, operation mode and solvent-to-feed ratio (Table 2.1). However, the experimental data and studies related to mass transfer and hydrodynamic behaviour are rather controversial, and there is no general agreement about the consideration of packing wettability and surface energy variation and their correlation to mass transfer models as well as the hydrodynamic behaviour inside the packed column. Based on the previous aspects mentioned, it is possible that some of the assumptions considered during the modeling, optimization, simulation and scale-up may not have been appropriate, and thus result in unrealistic economic feasibility outcomes, reducing the interest in industry to incorporate those processes as a sustainable solution in their operations.

2.4. Phase equilibria and physicochemical properties of lipid + supercritical carbon dioxide systems

It is essential to know the phase equilibria and physicochemical properties of lipid mixtures or their individual compounds in SC-CO_2 for the fractionation of lipid mixtures using SC-CO_2; however, there is a lack of such data in the literature due to the challenges associated with performing such measurements under high pressure. Pressure and temperature have a substantial effect on the physicochemical parameters of lipid + CO_2 systems, and it is essential to understand their impact at the molecular level for the individual compounds which constitute the lipid mixtures to understand properly the mass transfer phenomena as well as the fluid dynamics behaviour inside a packed column. There are various studies focusing on different lipid systems, including the behaviour of different lipid classes and model mixtures in SC-CO_2, but the diversity in the experimental conditions and the nature of the compounds considered has made it challenging to use the available data for modeling or simulation of the fractionation of a real complex lipid mixture inside a packed column with SC-CO_2. Considering the focus of this Ph.D. thesis, the discussion of solubility, phase behaviour, diffusion, density, and viscosity of lipid mixtures in the next sections will be limited to oleic acid (OA), canola oil (CanO) and triolein (OOO), with OA representing free fatty acids, and CanO and OOO representing triacyglycerols (TAG).

2.4.1. Phase equilibria, solubility behaviour and density

During the separation processes using SC-CO_2 to fractionate lipid mixtures or isolate lipid-based bioactive compounds, fundamental knowledge of the phase behaviour between the liquid lipid and the supercritical fluid phases is needed, to determine the number of transfer units (NTU) as well as the height of a transfer unit (HTU), which dictate the total height of the column needed to reach the target compound(s) separation. Several studies have focused on obtaining equilibrium

data for pure lipids and lipid mixtures in contact with CO_2 as shown in Table 2.2. Those studies could determine how much lipid can be solubilized in CO_2 as well as how much CO_2 can be solubilized in the specific lipid classes, which is critical for the understanding of fundamental aspects of mass transfer between phases. For example, Bharath et al. (1992) performed a phase equilibrium study of different binary and ternary lipid mixtures in SC-CO_2. For the system FFA/CO_2, specifically OA/CO_2, at isothermal conditions, the weight fraction of CO_2 in the liquid phase and that of OA in the vapour phase was enhanced as pressure increased. The authors also studied the phase equilibrium of OA/OOO/CO_2, finding that the solubility of OOO was much lower than that of OA and the dissolution of CO_2 in the liquid phase was less for the system OOO/CO_2. This ternary mixture phase behaviour approach allowed them to investigate the selectivity of SC-CO_2 towards the type of lipid class, concluding that the distribution coefficients of both lipids varied due to the effect of pressure and feed composition, and the CO_2 selectively dissolved lipids based on their carbon numbers.

Based on the equilibrium studies, solubility has been determined considering not only the solubility of lipids in SC-CO_2 but also how much CO_2 can be dissolved in different lipid classes and mixtures (Table 2.2), and some of those studies correlated this parameter and its impact on the physicochemical properties. For example, Güçlü-Üstündağ and Temelli (2000) correlated the solubility of different lipid classes in SC-CO_2. They highlighted that while OA was the most soluble compound in CO_2, OOO was not exhibiting the same trend. Also, the solubility of lipids in CO_2 increased with pressure, but FFA solubility in SC-CO_2 was strongly influenced by their molecular weight and vapour pressure. The crossover behaviour of solubility isotherms for lipid/CO_2 mixtures has been well established: at constant pressure, temperature enhancement increased the lipid vapour pressure, resulting in higher solubility, but a temperature increase

Table 2. 2. Phase behaviour and solubility data for lipid + CO_2 systems.

Property	Reference	System (lipid + CO_2)	Temperature (°C)	Pressure (MPa)
Phase behaviour	Bharath et al. (1992)	Oleic acid; triolein	OA:39.85 - 79.85 OOO: 39.85 - 59.85	OA: 10 – 30 OOO: 15 - 31
	Yu and Rizvi et al. (1992)	Oleic acid, methyl oleate and anhydrous milk fat	40 - 60	Up to 31
	Penedo et al. (2009)	Palmitic acid; stearic acid; oleic acid; linoleic acid; linolenic acid	40 - 80	6 - 12
	Gracia et al. (2009)	Oleic acid; triolein; oleic acid + triolein + CO_2	40 - 60	20 - 30
	Hong et al. (2010)	Oleic acid; palm oil; palm kernel oil	60.05 – 100.05	8.5 - 35
	Fernández-Ronco et al. (2010)	Oleic acid; triolein + sunflower oil	Up to 59.85	Up to 30.5
	Prado et al. (2011)	Sacha inchi oil	29.85 – 49.85	4.3 – 27.7
	Jenab and Temelli (2012)	CO_2 in canola oil and its blend with fully-hydrogenated canola oil	Canola oil: 40 and 70 Blend: 70	Up to 25
	Feihrmann et al. (2016)	Black sesame seed oil	29.85 - 59.85	Up to 20
	Garmus et al. (2019)	Oleic acid; oleic acid + sunflower oil; sunflower oil	39.85 - 75.85	10 - 40
	Yeo et al. (2021)	Palmitic acid; stearic acid; oleic acid; linoleic acid and linolenic acid	70 - 100	8 - 24
Solubility	Chrastil (1982)	Stearic acid; oleic acid; behenic acid; tributyrin; tripalmitin; triolein; trilinolein; palmityl behenate; behenyl behenate; tocopherol, cholesterol; water; cafestol	40 - 60	10.13 - 25.33
	Nilsson et al. (1991)	Oleic acid, methyl oleate; mono, di and triacylglycerol; triolein	50 – 60	Up to 20
	Maheshwari et al. (1992)	Lauric acid; linoleic acid; myristic acid; oleic acid; palmitic acid; stearic acid	39.85 – 59.85	13.8 – 27.6
	Ribeiro et al. (1995)	Triolein	34.85 – 54.85	Up to 20
	Soares et al. (2007)	Refined corn oil; sunflower seed oils; babassu oil; ucuuba oil; canola oil	40 – 80	20 – 35
	Regueira et al. (2013)	CO_2 in high oleic sunflower oil; castor oil; rapeseed oil	24.85 – 89.85	Up to 75
	Ilieva et al. (2016)	Rapeseed oil	40 – 80	Up to 31

also leads to a reduction in CO_2 density, causing the solubility to decrease; these two competing effects results in the phenomenon of crossover of solubility isotherms. Below the crossover pressure, the dominant mechanism of lipid solubility in CO_2 is governed by the decrease in CO_2 density, resulting in a solubility decrease with temperature whereas at higher pressures solubility increases with temperature with the vapour pressure effect being more dominant. Güçlü-Üstündağ and Temelli (2000) indicated that the molecular weight is a good indicator of vapour pressure/solubility since both vapour pressure and solubility decrease with increasing molecular weight. Following the aspects mentioned in this study, it is important to consider that when the lipid molecular weight increases, the solubility of the lipid in SC-CO_2 decreases since these parameters are intrinsically related to the solute physical state.

To define properly mass transfer and hydrodynamic behaviour in supercritical fluid separation processes, it is required to determine the density of the liquid lipid phase saturated by CO_2 and the density of the CO_2 phase saturated by the lipid(s), since the densities of these two phases in equilibrium are critical for the determination of packing wettability by lipids in SC-CO_2 medium as will be discussed in further sections. As Table 2.3 presents, different studies have determined the density of lipid saturated with CO_2 and vice versa. For example, Lockemann (1994a) determined the densities of both phases, CO_2 phase saturated with OA and liquid OA phase saturated with CO_2, concluding that: a) the density of the CO_2 saturated with OA was higher than that of pure CO_2; and b) density of OA saturated with CO_2 up to 13 MPa was also considerably higher than that of pure CO_2. The density of the lipid phase saturated with CO_2 increased with pressure as the CO_2 concentration in lipid phase increased. Later, Tegetmeier et al. (2000) conducted a study to determine the density of different vegetable oils (TAG mixtures) in contact with CO_2. The authors highlighted that the density of oils increased as more CO_2 was incorporated

into the lipid. Density of canola oil saturated with CO_2 was determined by Jenab and Temelli (2012) up to 70 °C and up to 30 MPa. The authors indicated that at isothermal conditions, the density of CO_2-saturated canola oil increased with pressure, while at isobaric conditions, the density decreased as temperature was enhanced. They mentioned that: a) the increase in density with pressure for lipid/CO_2 systems not only depended on the solubility of CO_2 in the lipid phase, but also on the compressibility of liquid lipid phase under high pressure, because at high pressure, more CO_2 was available to be localized among the TAG molecular spaces, acting as a lubricant and facilitating liquid phase compressibility; and b) at constant pressure and temperature, as the lipid degree of unsaturation increased, the density of lipid phase also increased.

Table 2. 3. Density of lipid + CO_2 systems

Reference	System	Method/principle/ Equipment	Temperature (°C)	Pressure (MPa)
Yu and Rizvi. (1992)	Oleic acid, methyl oleate, anhydrous milk fat	n.s.	40 – 60	Up to 31
Lockemann (1994a)	Oleic acid saturated with CO_2 and CO_2 saturated with lipid	Vibrating sensor tube	40 – 60	Up to 30
Tegetmeier et al. (2000)	Corn oil and palm oil saturated with CO_2	Magnetic suspension balance	Room – 80	0.1 – 30
Jenab and Temelli (2012)	Canola oil saturated with CO_2	Archimedes' principle	40 – 70	Up to 25
Ilieva et al. (2016)	Tristearin and rapeseed oil saturated with CO_2	U-tube principle	Tristearin: 70 – 100 Rapeseed oil: 60 and 80	Up to 20

n.s. Not specified

2.4.2. Diffusion coefficient and viscosity

Diffusion coefficient and viscosity are important transport properties needed for the design, modeling and simulation of separation processes that involve lipids and supercritical fluids. Diffusion is the process where atoms and molecules move from a phase of higher concentration to a phase of lower concentration. In supercritical fluid technology, there are studies related to the diffusion of FFA and TAG in CO_2. Different methods have been used to determine the diffusion coefficients of several lipid compounds and mixtures in CO_2 as indicated in Table 2.4. With respect to the diffusion coefficient of CO_2 in FFA, Lockemann and Schlünder (1996) determined the binary diffusion coefficient for different lipid/CO_2 systems, including CO_2-OA up to 13 MPa and up to 60 °C using the capillary technique. The authors mentioned that the solubility of CO_2 in the liquid phase was higher than that of the liquid phase in CO_2 and diffusivity was characterized by two parameters, the diffusion coefficient at infinite dilution (related to CO_2 molecules that interact with the surrounding fluid), and the diffusion coefficient in the saturated liquid phase present at the interface. Lockemann and Schlünder (1996) concluded that: a) CO_2 concentration in the liquid phase increased at a given pressure and temperature, enhancing its diffusivity in the lipid phase due to lipid phase viscosity reduction; b) higher values of diffusion coefficient at both infinite dilution and in the saturated systems were obtained when temperature was enhanced because high temperature resulted in low liquid viscosity; c) the mass transport at elevated temperatures in the liquid phase was strongly influenced by the CO_2 solubility decrease, generating lower mass transfer from the interface into the bulk of the liquid, balancing the diffusivity enhancement; d) the amount of CO_2 molecules which interacted with the surrounding fluid did not depend on pressure; e) liquid phase diffusivity is indirectly affected by temperature and pressure, due to the

Table 2. 4. Diffusion coefficients and viscosity studies of lipids in CO_2 and CO_2 in lipids.

Property	Reference	System	Method/ Equipment	Temperature (°C)	Pressure (MPa)
Diffusion Coefficients	Funazukuri et al. (1991)	C_{16}-C_{24} unsaturated fatty acids; oleic acid, fatty acid methyl esters/CO_2	Taylor-Aris tracer response technique	39.85	16
	Lockemann and Schlünder (1996)	CO_2 /(cis-9-octadecenoic acid), methyl myristate and methyl palmitate	Capillary technique	40 – 60	7 – 13
	Rezaei and Temelli (2000)	Fatty acids (oleic acid) and their esters, TAG/CO_2	Taylor-Aris peak broadening technique	40 – 60	25 – 35
	Cai et al. (2022)	Triolein in CO_2	Chromatographic impulse response method.	30 – 60	Up to 31.02
Viscosity	Kashulines et al. (1991)	Oleic acid/CO_2	High-pressure capillary viscometer	40 – 60	Up to 32
	Peter and Jakob (1991)	Oleic acid/CO_2	Capillary viscometer	40	Value specified in terms of CO_2 density
	Lockemann and Schlünder (1995)	Oleic acid/CO_2	n.s.	40 – 60	Up to 12.6
	Yener et al. (1998)	CO_2/oleic acid	Capillary viscometer	40 – 60	20.5 – 30
	Jenab and Temelli (2011)	Canola oil/CO_2	Rotational rheometer	40 – 75	Up to 12.45
	Ilieva et al. (2016)	Rapeseed oil/CO_2	U-tube principle	60 and 80	Up to 20

n.s. Not specified

fact that those parameters affect the viscosity, and f) changes in lipid phase diffusivity and viscosity relies on the CO_2 concentration increase.

Moreover, Rezaei and Temelli (2000) determined the binary diffusion coefficients of pure lipids, such as fatty acids and their esters, and triacyglycerols in SC-CO_2 at temperatures up to 60 °C and pressures up to 36 MPa using the Taylor–Aris peak broadening technique. For OA, the diffusion coefficient increased with temperature and decreased with pressure; however, the effect of pressure was negligible in the range of 25 to 30 MPa. The decrease of OA diffusion coefficient with increase in SC-CO_2 density (higher pressure) was mainly due to the change in medium density; once it became denser, the molecule collision frequency increased but the mean path of the molecules decreased. For the case of TAG, diffusivity was slower than that for FFA due to differences in molecular size and weight, degree of unsaturation, spatial configuration and molecule polarity. Overall, the diffusion coefficient decreased with an increase in the number of double bonds (degree of unsaturation of molecules) (Rezaei & Temelli, 2000).

Furthermore, Cai et al. (2022) studied diffusion of OOO in different solvents, including CO_2. Despite the challenges faced by the authors to determine the diffusivity of triolein in CO_2 due to the peak tailing observed using the chromatographic impulse response method, they reported the diffusivity of triolein in different fluids as CO_2 > hexane > methanol > ethanol. Despite such challenges, some data on diffusion coefficients of lipids in CO_2 are available, but more is required to properly characterize mass transport phenomena involved in the supercritical fluid technology and the processing of lipids with CO_2.

Considering the fractionation process using packed columns, viscosity plays a significant role in understanding and describing the hydrodynamic behaviour of the phases at the packing level, which also impacts mass transfer phenomena. Viscosity is an important property for lipid +

CO_2 systems, which measures the fluid resistance to flow. Several studies have investigated and determined the viscosity of CO_2 phase saturated with lipids as well as the liquid lipid phase saturated with CO_2 as shown in Table 2.4. For the case of FFA saturated with CO_2, viscosity of OA saturated with CO_2 was determined by Kashulines et al. (1991), finding that at isobaric conditions, the viscosity decreased with increasing temperature, exhibiting a Newtonian fluid behaviour. On the other hand, at isothermal conditions, the viscosity of FFA saturated with CO_2 decreased with pressure mainly because there was more CO_2 dissolved in FFA, reducing its viscosity value. As Kashulines et al. (1991) highlighted, important patterns in the viscosity behaviour of CO_2-saturated FFA systems must be considered when analyzing the effects of pressure and temperature because CO_2 solubility in the FFA decreases with temperature and increases with pressure. They expressed challenges regarding the study of temperature and pressure effects on the viscosity of lipid mixtures saturated with CO_2 because the mixture composition and the pure component viscosities must be known but such data may not be available. Similar to the previous study, Lockemann and Schlünder (1995) determined the OA + CO_2 lipid phase viscosity and explained the effect of pressure and temperature on this parameter. The CO_2 concentration in the liquid phase was related to the viscosity reduction. As pressure was elevated, the CO_2 concentration in the lipid phase increased, resulting in a viscosity decrease. At constant pressure if temperature was enhanced, the viscosity of lipid phase decreased. Based on the previous studies, the viscosity of FFA saturated with CO_2 is strongly affected by molecular structure, degree of unsaturation and temperature.

The viscosities of TAG mixtures, for example, canola oil, saturated with CO_2, has been determined by Jenab and Temelli (2011). The authors characterized CO_2-saturated canola oil as a non-Newtonian fluid (shear-thickening behaviour). Similar to the previous studies, Jenab and

Temelli (2011) confirmed that pressure and temperature exerted a significant effect on CO_2-saturated lipid phase viscosity. For example, as pressure increased, there was an exponential decrease in viscosity because of the CO_2 solubility enhancement in the lipid phase. However, at elevated pressures, the mass fraction of CO_2 in the lipid phase reached a plateau, resulting in viscosity values levelling off. At lower temperatures, the effect of pressure on viscosity was more pronounced due to the solubility of CO_2 in the lipid phase being enhanced with pressure and reduced with temperature increase. They explained that the shear-thickening behaviour of the canola oil in equilibrium with CO_2 could be related to the fact that the CO_2-expanded oil density varies with pressure. They linked this shear-thickening behaviour to the possible positioning of CO_2 among the void volumes of the triacylglycerol molecules at elevated pressure.

2.4.3. Wettability behaviour of lipids in dense gases

The hydrodynamic behaviour and mass transfer inside packed columns are intrinsically correlated with a property called wettability, describing the condition when a liquid is in contact with a solid surface in a given medium, and it is related to two parameters, interfacial tension (IFT) and contact angle (CA). Pieck et al. (2017), Simões et al. (1995) and Stockfleth & Brunner (2001) have highlighted the challenges of appropriate process modeling, simulation and scale up due to the lack of realistic approaches and assuming wettability patterns, which might be far from the real process behaviour. More information about the determination of each of these parameters for different systems will be detailed in the next sections.

2.4.3.1. Interfacial tension

IFT is the free energy per unit surface area needed to create an interface between two immiscible liquids. As Table 2.5 indicates, IFT has been determined for different lipid/CO_2 systems. The pendant drop method (Andreas et al., 1938) has been applied most commonly to

determine the IFT of lipids in the supercritical fluid environment using the Young-Laplace equation, which associates the contour of the pendant drop suspended in another fluid with the balances between gravitational, buoyant and interfacial forces acting at the interface level, as detailed in Eq. (2.1)

$$\frac{1}{\frac{R_1}{R_2}} + \frac{\sin\theta}{\frac{Z}{R_2}} = 2 + \frac{\Delta\rho * g * Z}{\sigma_{L/V}} * \frac{1}{R_2} \quad (2.1)$$

where $\sigma_{L/V}$ is the IFT between the liquid and vapour, $\Delta\rho$ is the density difference between the two phases, R is the radius of the curvature in the apex, g is the acceleration due to gravity, θ is the angle formed by the liquid at 90° with respect to Z, Z is the distance from the apex, R_1 and R_2 are the principal radii of the drop interface at distance Z from the apex, with R_1 being the radius of curvature in the vertical plane of the drop and R_2 the radius of curvature in a perpendicular plane as shown in Figure 2.2. The IFT of lipids in the surrounding CO_2 environment at different experimental conditions has been previously reported, including for corn oil (Jaeger, 1998; Jaeger et al., 1996; Simões et al., 2000; Sutjiadi-Sia et al., 2008a; Tegetmeier et al., 2000), oleic acid (Lockemann, 1994b), fish oil (Seifried & Temelli, 2010) and tristearin and rapeseed oil (Ilieva et al., 2016).

The impact of temperature and pressure on the IFT behaviour for lipid + CO_2 systems has been investigated over the years. For example, Lockemann (1994b) determined the IFT for several lipids (including oleic acid) in the presence of SC-CO_2, highlighting several aspects: a) at high pressure, the CO_2 was more absorbed at the interface level generating the disruption of a liquid film into droplet, b) the Marangoni effect is related to the gradient of the interfacial tension at the interface level; in a mixture, temperature differences generate variation in the component concentrations, increasing or reducing the effect of temperature on IFT. In this effect,

Table 2. 5. Interfacial tension studies on lipids in SC-CO_2

Reference	Drop phase	Technique	Temperature (°C)	Pressure (MPa)
Hiller et al. (1993)	Pelargonic acid; linoleic acid.	Capillary rise, Du Nouy Ring.	39.85 – 79.85	Up to 25
Lockemann (1994b)	Oleic acid; methyl myristate; methyl palmitate; methyl myristate-methyl palmitate system	Capillary rise	40 – 60	Up to 17.5
Jaeger et al. (1996)	Wheat oil; corn oil; walnut oil; citrus oil; coffee oil; olive oil	Pendant drop	40 – 120	0.1 to 50
Simões et al. (2000)	Olive oil; refined corn oil; coffee oil; citrus oil.	Pendant drop	39.85 – 79.85	Up to 40
Dittmar et al. (2002)	Corn germ oil; palm oil; wheat oil; olive oil	Pendant drop	40 – 120	Up to 40
Seifried and Temelli, (2010)	Triacyglycerols of fish oil; fatty acid ethyl esters	Pendant drop	40 – 70	Up to 25
Ilieva et al. (2016)	Tristearin; rapeseed oil	Pendant drop	80 – 100	Up to 20

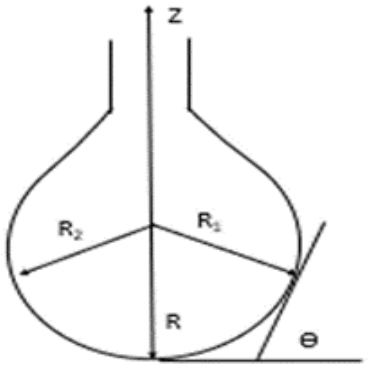

Figure 2. 2. Geometry of axisymmetric pendant drop, where θ is the angle formed by the liquid, R is the radius of the curvature in the apex, Z is the distance from the apex, R_1 and R_2 are the principal radii of the drop interface at distance Z from the apex.

the fluid with lower surface tension is going to flow towards the fluid with higher surface tension, reducing the IFT value. Moreover, Seifried and Temelli (2010) determined the IFT for TAG of fish oil and FAEEs in CO_2 and pointed several aspects: a) pressure significantly affected the volume of the pendant drop; b) composition of the phases as well as interactive forces between molecules close to the interface might vary based on CO_2 pressure and temperature and influence IFT values; c) at isothermal conditions, at low pressure the IFT is governed by lower intermolecular forces, whereas at high pressures, the CO_2 adsorption at the interface resulted in lower IFT values. Furthermore, Jaeger et al. (1996) considered TAG mixtures such as wheat, corn, walnut, citrus, coffee and olive oils for the IFT determination in the presence of CO_2. The authors addressed similar aspects of previous studies, but they centered their attention on the surface-active compounds at the interface level. When there was just one surface active compound, its concentration could vary over time until thermodynamic equilibrium was reached, so that IFT could be determined. However, when the mass transfer at the interface level was at non-steady condition due to the presence of several surface-active compounds, it influenced the decrease of the IFT values mainly due to the Marangoni effect. Another study on rapeseed oil and tristearin was performed by Ilieva et al. (2016), where the authors highlighted that a pressure increase at isothermal conditions resulted in a reduction of the IFT of the lipids in CO_2.

Research on the subject has been mostly restricted to vegetable oil and individual lipid compounds or classes in CO_2 and challenges have been raised for the determination of IFT for complex lipid mixtures, for example, deodorizer distillates. To determine IFT, the densities of the lipid drop and surrounding phases are needed, but this information is not available for real industrial lipid mixtures due to the variability of the composition of those real lipid mixtures. This situation generates the need to assume values that may be far from the actual values for the real

lipid mixture, when considering only the available data in the literature for the design, modeling and simulation of engineering process. These assumptions might result in unrealistic scale-up processing, and non-attractive approaches with deviations linked to economic feasibility studies, bringing challenges to investors, who are willing to consider supercritical fluid technology as a green and sustainable solution for the lipids or oil refining by-products processing.

2.4.3.2. Contact angle

The contact angle (CA) is the angle formed when a liquid is in contact with a surface and it is influenced by the molecular interactions between the solid, liquid and gas phases at the three-phase contact line (Law & Zhao, 2016b). When the kinetic energy of the droplet is dissipated on the solid surface, the static contact angle is obtained, which is characterized by its non-modified value over time. Once the liquid wets the surface, there is a reorganization of the liquid molecules and solid segments to their relaxed state. This process is referred to as the wetting phenomena and the relaxation state is influenced by the solid-liquid system and the solid substrate heterogeneity (chemical or geometrical) (Law & Zhao, 2016b) as shown in Figure 2.3.

As a result, different wetting dynamics emerge based on the type of surface (ideal or non-ideal), resulting in diverse contact angles (static CA_{stat} or equilibrium CA_{eq} and apparent CA_{app}) (Law & Zhao, 2016a).

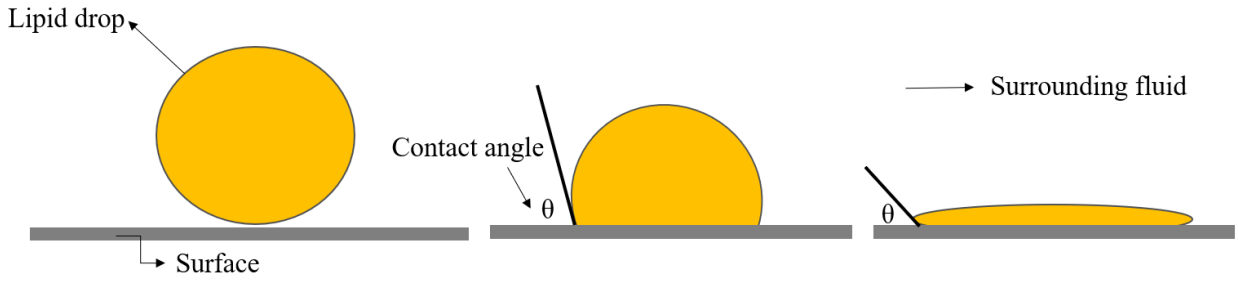

Figure 2. 3. Spreading phenomena of a liquid lipid drop on a solid surface in a specific medium.

CA can be determined using the sessile drop method and image analysis (Law & Zhao, 2016b), which depends on the CA value range, physical phenomena consideration and the symmetry between the right and left sides of the drop (Bateni et al., 2003; Mack & Lee, 1963). For small volume drops with CA values between 0º to 10º, the height/width method has been used (Aydar et al., 2016). The height/width method considers the sessile drop phase forming a circular arc on the surface since the small drops are only slightly affected by gravity as shown in Figure 2.4.

CA has been determined at atmospheric and high-pressure conditions for different systems. At atmospheric conditions, the CA of canola and olive oils on PTFE (polytetrafluoroethylene or Teflon) were determined in air and steam as the surrounding phases (Ashokkumar et al., 2012). At high-pressure conditions, Jaeger (1998) correlated the IFT and CA of TAG mixtures on smooth and rough surfaces in the presence of SC-CO_2 in an effort to link them with the mass transfer inside a column with glass and SS packing material to fractionate lipid mixtures using SC-CO_2. Another system that has been explored is water in CO_2 environment on glass surfaces modified with dichlorodimethylsilane and silanol, correlating the spreading coefficient of the liquid on the surface with the IFT of liquid/CO_2 and CA values (Dickson et al., 2006). The authors indicated that the spreading coefficient is the result of the differences between the surface energy of a dry surface and wet surface, which can be represented by $S= \sigma_{L/V} * (\cos \theta-1)$, where S is equal to the spreading coefficient, $\sigma_{L/V}$ is the interfacial tension between liquid and vapour, and θ is the contact

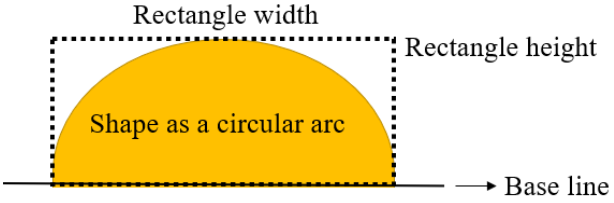

Figure 2. 4. Height/width method representation to determine CA.

angle between the liquid and solid surface in the vapour medium. This spreading coefficient value could be zero or negative if complete wetting (CA = 0) and partial wetting (CA > 0) are achieved. Dickson et al. (2006) concluded that the spreading coefficient values were less negative when CO_2 activity increased for their system CO_2/water/solid, mainly due to the decrease in the $\sigma_{L/V}$ values, resulting in wetting enhancement and a reduction in CA values. Sutjiadi-Sia et al. (2008) determined the CA of water, ethanol and their mixtures on PTFE, glass and SS in the presence of CO_2, and showed wettability variations on the surfaces as poor, intermediate and good for PTFE, SS and glass, respectively.

An important dimensionless parameter that relates the effect of gravity or surface tension over the interface of the pendant or sessile drop is the Bond number (Bo) expressed in Eq. (2.2),

$$Bo = \frac{\Delta\rho * g * R_O^2}{\sigma_{L/V}} \qquad (2.2)$$

where $\Delta\rho$ is the density difference between the liquid and gas phases, g acceleration due to gravity, R_o the drop radius based on the volume of the pendant or sessile drop and $\sigma_{L/V}$ is the interfacial tension between the liquid and gas interface. If Bo > 1, the gravity force dominates over the surface force of the drop shape, resulting in a flattening effect on the sessile drop and falling of the pendant drop (Kaveh et al., 2014). However, when the Bo < 1, the effect of gravity is neglected, and the sessile drop shape approaches a sphere while the pendant drop is hanging at the tip of the needle or capillary (Kaveh et al., 2014).

To correlate the IFT and CA with the wetting of different surfaces under CO_2 environment and evaluate the effects of pressure and temperature, several studies have been carried out in the oil and gas sector in relation to the enhanced oil recovery (EOR) systems, using different fluids (CO_2, brine at different sodium chloride (NaCl) %, deionized water) on different surfaces, (calcite, mica, quartz, uncoated and coated glass) under saturated and unsaturated CO_2 environments with

the purpose of evaluating the geo-storage of CO_2 in porous materials (Dickson et al., 2006; Kaveh et al., 2014). However, in these systems, the formation of carbonic acid in the presence of CO_2 and water modifies the energy of the solid surface and when NaCl is present (as in the case of brine), bicarbonate precipitates affecting the wettability and surface energy of the surface. Kaveh et al. (2014) considered the modification of the surrounding phase, saturated and not saturated, to evaluate the effects of the environmental conditions on wetting properties. They indicated that when the Bo<0.9, the variation of CA became insignificant with the maximum drop diameter of 2.3 mm, providing an accurate way to evaluate the effect of pressure on the contact angle (Kaveh et al., 2014).

2.5. Conclusion

There is considerable academic and industrial interest in separating lipids and isolating minor lipid compounds from complex lipid mixtures. Many conventional technologies involve the use of organic solvents based on their low cost and high availability, despite their toxicity and impact on the final quality of the lipid extracted in addition to their potential negative environmental effects. While the conventional techniques may lead to degradation and oxidation of minor lipid compounds such as tocopherols and sterols, due to the use of high operating temperatures and strong acids during their refining steps, different modern techniques have evolved to reduce the environmental impact and improve the quality of the final product, such as ultrasound-assisted processes, membrane and supercritical fluid technologies.

With a focus on the supercritical fluid technology, SC-CO_2 has been the most commonly used solvent for the extraction and isolation of lipids, due to its versatility by exhibiting density and solvent power as a liquid and diffusivity as a gas. Extraction and fractionation using packed columns have been studied extensively to separate lipids and minor lipid compounds from complex

lipid mixtures. To improve the fractionation process performance, different operating conditions, packing materials and lipid feed mixtures have been tested depending on the target lipid compound(s). However, there is still a lack of knowledge to understand properly the mass transfer and hydrodynamics of the phases at the packing level and their implications on the process performance.

Based on the literature review conducted, several challenges were highlighted from the engineering perspective to determine the implications of operating conditions and different packings on the design of the packed fractionation column with a focus on mass transfer and hydrodynamic behavior. Several studies have considered partial and complete wettability of the packing with lipids in SC-CO_2 environment; however, the reasons behind this wettability variation are not well understood. In addition, such wettability variations can lead to deviations in flow pattern, affecting the fluid dynamics inside the packed column, which might result in decreasing or enhancing process performance, depending on the characteristics of the system lipid-packing-CO_2 and experimental conditions.

To address the identified gaps in the mass transfer and hydrodynamic behaviour knowledge, there is a need for fundamental data, including phase equilibria and physicochemical properties (density, viscosity, interfacial tension, diffusion coefficient, contact angle). However, despite all the developments, there is a lack of such data for the lipid components targeted. Therefore, this Ph.D. thesis research was undertaken to determine interfacial tension and contact angle of selected lipids to better understand wettability behavior on different surfaces and to investigate the performance of a fractionation column packed with different materials and operating under different conditions.

Chapter 3. Interfacial tension and equilibrium contact angle of corn oil on polished stainless steel in supercritical carbon dioxide and nitrogen[a]

3.1. Introduction

Various processes have been developed using supercritical carbon dioxide (SC-CO_2) to separate different lipid components in high purity while avoiding the use of organic solvents. To design an optimal column fractionation process, there are many variables to consider, including, the mass transfer and hydrodynamic behaviour, which are related to the contact between the two streams and type of packing material. The contact between SC-CO_2 and of liquid streams involving edible oils and their by-products has been studied by different researchers. For example, Simões et al. (1995) reported two approaches to define the mass transfer models inside a packed column, considering partial and complete wettability of the packing by the liquid phase. Based on visual observations of the behaviour between diverse packings and different systems, Stockfleth and Brunner (1999a) concluded that the tocopherols-CO_2 mixture did not exhibit complete wettability of the Sulzer CY packing. Moreover, Bejarano et al. (2016) indicated the importance of contact angle (CA) and interfacial tension (IFT) to understand the hydrodynamic behaviour inside a packed column. These parameters have been investigated in spray columns but not in packed columns where the limit of the interchange area is regulated by wettability (Bejarano et al., 2016).

With the purpose to understand the hydrodynamic behaviour inside packed columns using SC-CO_2, a variety of packing materials have been used to enhance the mass transfer inside the columns. The predominant factor that influences the separation efficiency could be the packing

---

[a] A version of this chapter has been published as: Eileen Santos, Prashant Waghmare, Feral Temelli. Interfacial tension and equilibrium contact angle of corn oil on polished stainless steel in supercritical CO_2 and N_2. *Journal of Supercritical Fluids* (2020) 156, 104665 (https://doi.org/10.1016/j.supflu.2019.104665).

material and/or its geometry, but this aspect has not been studied yet. IFT has been reported for different types of lipids and surrounding phases, including corn oil (Dittmar et al., 2002; Jaeger et al., 1996; Simões et al., 2000). The pendant drop method has been applied most commonly to determine the IFT of lipids in the supercritical fluid environment using the Young Laplace equation as described in Chapter 2 (section 2.3.3.1).

On the other hand, when a liquid is in contact with a solid surface, molecular interactions of solid, liquid and gas phases at the three-phase contact line dictates the CA. For small volume drops with CA values between 0º to 10º, the height/width method (Mack & Lee, 1963) has been used, which involves the width of the sessile drop and the height at the apex. At atmospheric pressure and different temperatures, the CA of canola and olive oils on PTFE (polytetrafluoroethylene or Teflon) was determined under air and steam as surrounding phases (Aydar et al., 2016) and a similar approach was extended to other vegetable oils (Ashokkumar et al., 2012). At high pressure conditions, several studies reported the determination of CA under CO_2 environment for different types of liquids and solid surfaces (Dickson et al., 2006; Jaeger, 1998; Sutjiadi-Sia et al., 2008a).

The literature is limited in relation to the wettability of metal surfaces by lipids in SC-CO_2 environment, even though such information would be valuable for the design of various supercritical processes involving lipids. Therefore, the objective of this study was to determine the effect of pressure and temperature on IFT and equilibrium contact angle (CA_{eq}) of corn oil in air, SC-CO_2 and supercritical nitrogen (SC-N_2) on polished stainless steel metal sheet under unsaturated and saturated surrounding phases.

3.2. Materials and methods

3.2.1. Materials

Mirror-like highly corrosion-resistant 316 stainless steel (SS) sheet (304.8 x 304.8 mm and 0.914 mm thickness) was purchased from McMaster-Carr **(**code: 9759K72, Aurora, OH, USA) and cut by water jet into two different dimensions (25.40 x 25.40 mm and 25.91 x 15 mm, respectively) for roughness and contact angle analysis. Acetone (HPLC grade, Fisher Scientific, Ottawa, ON, Canada), isopropanol (>98% Food Grade, Sigma-Aldrich, Oakville, ON, Canada), deionized water and compressed air were used for the cleaning treatment of the polished SS substrates. The drop phase was corn oil ("Mazola", ACH Food Companies, Inc., Memphis, TN, USA) that was purchased from a local market.

3.2.2. Roughness determination

Three pieces of polished SS surfaces (25.40 x 25.40 mm) were used to determine the roughness factor using Zygo optical profilometer (model NewView 5000, Zygo Corporation, Middlefield, CT, USA) with lens of 10X. The roughness factor was measured 3 times at different sections of each SS surface and the mean ± standard deviation was reported.

3.2.3. Apparatus to determine the interfacial tension and contact angle

The system used for the determination of IFT and CA was DSA100 HP from Krüss GmbH (Hamburg, Germany), which was equipped with the High Pressure (HP) system model PD- E1700 MD (Eurotechnica GmbH, Barteheide, Germany) and the optic system DSA100 (Krüss GmbH, Hamburg, Germany) as shown in Figure 3.1. The dosing system is highlighted inside the dashed rectangle on the left, the pressurization section is on the right side and the view cell and the optical system (CCD camera and light source) are at the centre of the figure.

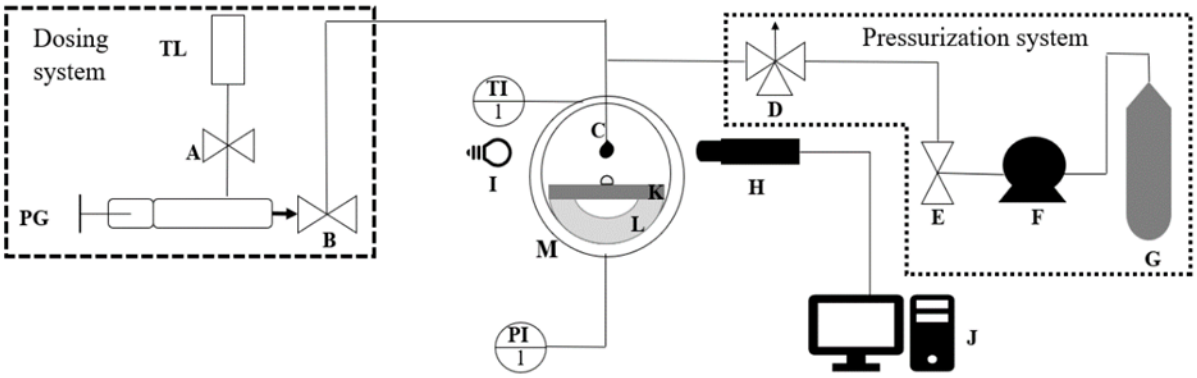

Figure 3. 1. Schematic of DSA 100 HP system. TL: drop phase liquids; A:inlet valve for liquid 1; PG: manual piston for liquid; B: discharge valve of liquid valve into capillary; C:capillary (1.65 or 1.1 mm OD); D: drain or vent valves; F: booster pump; G: CO_2 or N_2 cylinder; H: CCD camera, I: light source; J: computer; K: metal surface; L: glass solid substrate support; M: high pressure (HP) vessel; TI: thermocouple with temperature indicator; PI: pressure gauge.

3.2.4. Interfacial tension and contact angle measurements

The cleaning protocol of Becker et al. (2016) was followed, where each polished SS metal surface was cleaned using three different organic solvents: acetone, isopropanol and deionized water. First, each metal surface was submerged into 10 mL of acetone and placed in a sonicator (model 1510, Branson Ultrasonics Corp., Danbury, CT, USA) for 2 min. Then, the same procedure was applied using isopropanol and then with deionized water. Finally, the SS surface was removed and dried for 2 min using compressed air.

The IFT and CA measurements were performed at 40, 60, 80 °C and 0.1, 16, 20, 24 MPa in triplicate. To ensure that the drop phase did not contain any air bubbles, several drops were formed with the HP vessel being open until no more air bubbles were seen inside the drop at the tip of the capillary. Then, the vessel was cleaned using isopropanol. The HP vessel (42 mL) was pre-heated to reach the targeted temperature for 45 min. Different sets of measurements were performed, where the surrounding phase was either unsaturated or saturated. For the saturated conditions, 2 g corn oil was weighed inside the glass holder and then placed inside the HP vessel

for 4.5 h for the surrounding phase to reach saturation under the targeted temperature and pressure conditions, whereas for unsaturation conditions, this step was omitted. Reaching the saturation condition was verified since the IFT of the corn oil in saturated SC-CO_2 did not vary over time. The metal sheet was placed on top of the glass support, which was bigger than the metal sheet, allowing the contact between CO_2 and corn oil placed in the glass support. Then, the HP vessel was closed by tightening the two sapphire windows located at each side of the vessel. To pressurize the HP vessel, valves A, B and D were closed, and valve E was opened slowly until the desired pressure was reached using either N_2 or CO_2. Then, valve E was closed and 5, 7 and 9 min was allowed for stabilization of the target temperatures of 40, 60 and 80 ºC, respectively. A video was recorded at 35 frames per second for 6 min to capture all the phenomena (IFT and CA) under CO_2 and N_2 environments.

To create a drop, the reservoir (TL) was filled with corn oil. The valve A and manual piston (PG) were totally opened to allow the corn oil to fill the PG. Then, valve A was closed while simultaneously PG was closed, and valve B was slightly opened to push the corn oil into the capillary (outside diameter=1.65 and 1.1 mm for N_2 and CO_2, respectively). Once the drop was formed, valve B was closed to avoid the detachment of the drop and 3 min were allowed to stabilize the interface of the pendant drop inside the pressurized system. Then, by slowly closing PG and opening valve B, the pendant drop was allowed to fall on the metal surface and converted into a sessile drop. The recording was continued for another 3 min. Later, valve D was opened slowly to depressurize the system and the sapphire windows, metal sheet and support were removed. A different set of three metal sheets was used at each temperature tested.

The IFT and CA values were determined by the Young-Laplace equation and height/width method, respectively, using the pendant drop and sessile drop modules of the ADVANCE for Drop

Shape Analyzers (2014-2017) software (Krüss GmbH). To get the IFT value from the pendant drop, the video was converted into frames using the JPG video converter (free software). The densities of the drop phase in pressurized gases were taken from Tegetmeier et al. (2000), and densities of the surrounding phase (N_2 and CO_2) were taken from the National Institute of Standards and Technology (NIST, 2005). All measurements at each condition were performed in triplicate and two-way analysis of variance was performed using Microsoft Excel to assess the effects of pressure and temperature as well as their interaction effect on the IFT and CA_{eq}, at $p < 0.05$.

3.3. Results and discussion

3.3.1. Interfacial tension of corn oil in nitrogen and carbon dioxide under unsaturated and saturated conditions

To validate the experimental protocols and the results, the IFT of corn oil/N_2 and corn oil/CO_2 were determined and compared with the values reported in the literature for corn oil and other oils at 80 ºC and up to 40 MPa. As shown in Figure 3.2, the results were in agreement with previous studies (Dittmar et al., 2002; Jaeger et al., 1996; Seifried & Temelli, 2010; Simões et al., 2000). Then, IFT of corn oil in N_2 and CO_2 were determined at different pressures and temperatures (Figure 3.3). The Bond number (Bo) values (Eq. (2.2)) were from 0.62±0.01 to 0.74±0.06 for the corn oil/N_2 system and from 0.56±0.06 to 0.76±0.03 for corn oil/CO_2 system, which confirmed that the gravity did not affect the IFT values of both interfaces, and the pressure effect could be evaluated. As expected, there was a substantial difference in IFT depending on the surrounding medium (Figures 3.2 and 3.3). The corn oil/N_2 system displayed a moderate decrease in IFT with increasing pressure at constant temperature; however, the decrease was substantial for the corn oil/CO_2 system. This difference between the two systems was due to the lower solubility and

diffusion of N_2 in corn oil resulting in higher interfacial tension and lower mass transfer between the phases, whereas the higher solubility, diffusion and mass transfer of CO_2 in corn oil generated a remarkable decrease in IFT. Similar explanations were also provided previously (Dittmar et al., 2002; Jaeger et al., 1996; Simões et al., 2000).

During an isothermal process, as pressure increases, the density of CO_2 is enhanced, resulting in a reduction of the density differences between the two phases, decreasing the IFT. In terms of the effect of temperature, there was a cross-over of the isotherms at around 2.5 MPa, which was similar to that for fish oil reported by Seifried and Temelli (2010), who explained that at pressures up to 2.5 MPa, a temperature increase resulted in higher molecular mobility at the interface, with more distance between the molecules and thus lower cohesive forces between them, generating lower IFT values for the triacylglycerols (TAG) and fatty acid ethyl esters (FAEE) of fish oil.

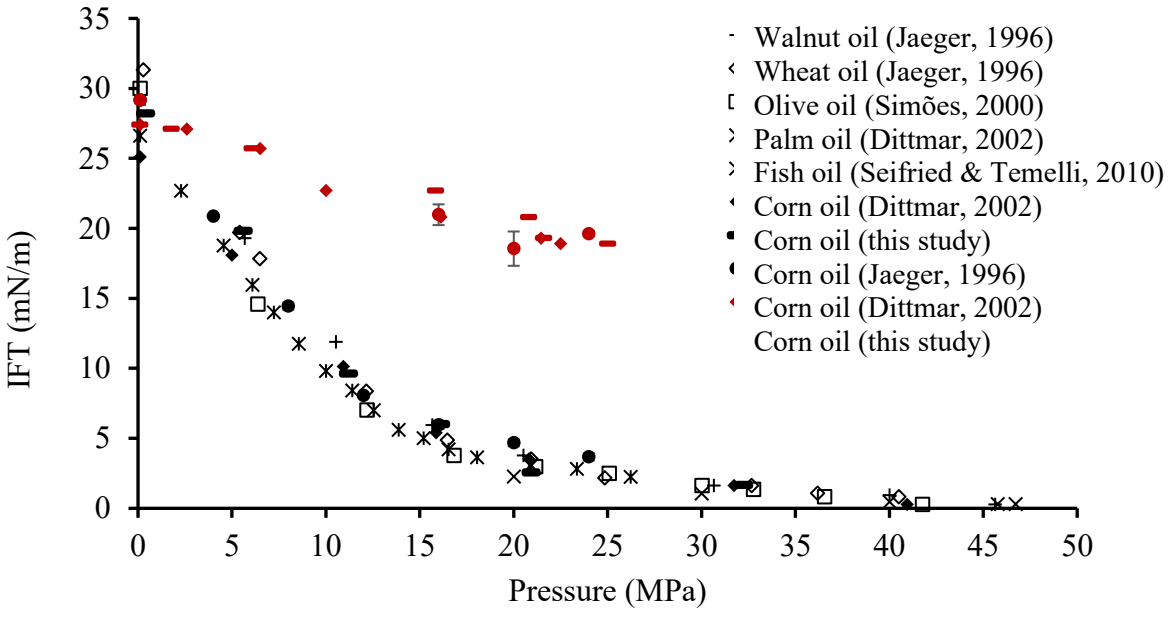

Figure 3. 2. IFT of different oils in CO_2 (black symbols) and N_2 (red symbols) at 80 ºC up to 47 MPa (fish oil was at 70ºC).

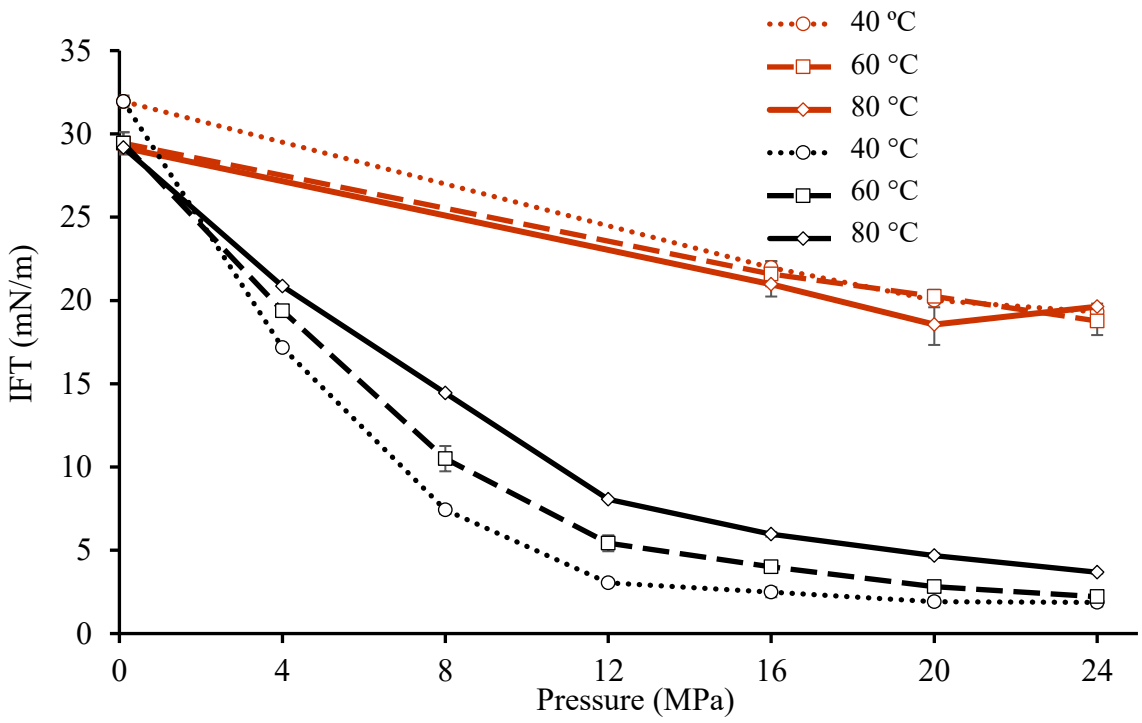

Figure 3. 3. IFT of corn oil in N_2 (red lines) and CO_2 (black lines) at different temperatures and pressures (Data presented in Appendix A, Tables A.1 and A.2).

Different justifications of the effect of CO_2 on the interfacial tension of the lipid/CO_2 systems have been provided in the literature. For example, Lockemann (1994) indicated that the IFT decreased when it was in contact with soluble gases, mainly due to the surfactant behaviour of the gas and that the reduction in the gas density with temperature caused a less remarkable surfactant effect of the gas. In contrast, Jaeger et al. (1996) explained that CO_2 was not acting as a surfactant at the interface, but it was adsorbed, and thus resulting in IFT decrease. Similarly, Seifried and Temelli (2010) explained that the CO_2 effect on the IFT was based on the diffusion of CO_2 into the drop, adsorption of CO_2 at the interface, nature of the components at the interface and diffusion of components from the drop to surrounding phase. They highlighted that the amount of CO_2 present close to the interface increased with pressure, resulting in less cohesive forces and

lower IFT (Seifried & Temelli, 2010). At higher pressures, the temperature influence on the IFT is related to CO_2 density, where the CO_2 density decreases with temperature, resulting in less CO_2 adsorption at the interface and higher IFT value (Simões et al., 1995).

For all the conditions tested, the pendant drop (3-5 µL) was allowed to hang for 3 min at the tip of the capillary in order to stabilize the interface. As shown in Figure 3.4, there was no impact of saturation of the surrounding phase on IFT under the tested conditions, considering that the solubility of the vegetable oil in SC-CO_2 is much lower than the solubility of the SC-CO_2 in the oil.

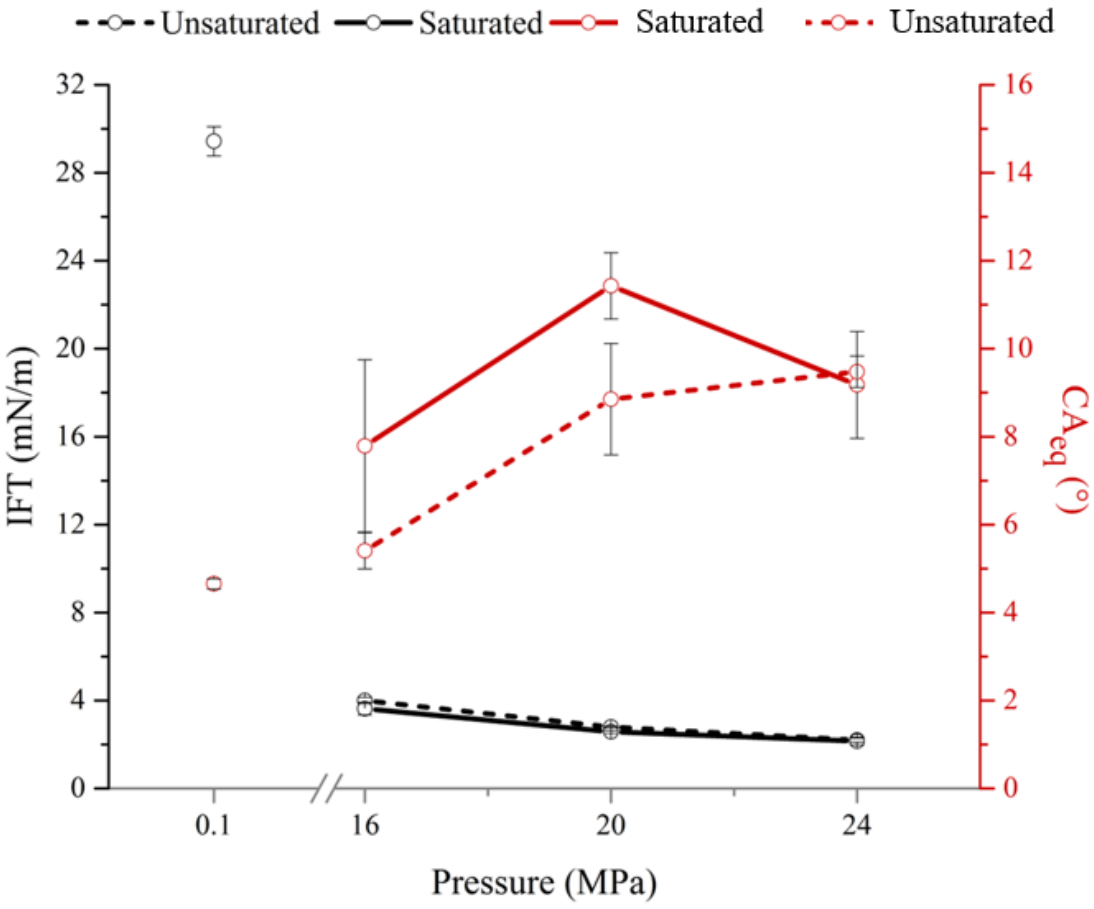

Figure 3. 4. IFT and CA_{eq} of corn oil on polished SS under unsaturated and saturated CO_2 at 60 ºC as a function of pressure (Data presented in Appendix A, Tables A.3 and A.4).

For example, the solubility of canola oil in CO_2 was 0.17 wt% (Stockfleth & Brunner, 2001) whereas the solubility of the CO_2 in the canola oil was 20.5 wt% at 40 ºC and 20 MPa (Fattori et al., 1988). Therefore, it seems that the 3 min allowed for the stabilization was sufficient for the saturation of the SC-CO_2 at the interface. Seifried and Temelli (2010) saturated the oil phase with CO_2 prior to the formation of the pendant drop and used the saturated liquid density and pure CO_2 density values in IFT calculations. However, most of the studies on IFT did not specify whether the phases were saturated or not, regardless, the oil/CO_2 interfaces exhibit similar behaviour with a substantial drop in IFT with pressure as shown in Figure 3.4.

3.3.2. Equilibrium contact angle of corn oil on polished stainless steel in unsaturated nitrogen and saturated and unsaturated carbon dioxide.

The roughness (R_a) values of polished SS sheets were measured in triplicate to determine if the solid surfaces could be characterized as an ideal surface. The R_a value was 46.1±1.5 nm, which allowed the identification of the polished SS surface as an ideal surface. To determine a reliable value of CA_{eq} of any liquid droplet on a surface, it is necessary to saturate the surrounding phase with the liquid phase; otherwise, volatilization and/or solubilization of the light components would impact the sessile drop volume, resulting in a variable value of CA_{eq} over time. The CA_{eq} of corn oil/N_2 and corn oil/CO_2 systems were determined over 12 s (Figure 3.5), where high interactions between the solid, liquid and gas phases were observed, resulting in a considerable decrease in CA over the first second as the drop energy was dissipated on the surface until reaching a value of zero where the CA_{eq} was obtained. The CA_{eq} of corn oil in N_2 and CO_2 media on polished SS surface indicated complete wetting with values ranging from 3.20±1.15° to 10.49±1.94º and 3.87±0.21° to 11.35±0.96° for N_2 and CO_2 environments, respectively (Figure 3.6). Based on the analysis of variance (ANOVA), the effects of pressure, temperature and their interaction were

significant ($p < 0.05$) on the CA_{eq} in both N_2 and CO_2 environments. Under CO_2 environment (Figure 3.6.(B)), there was an increase in CA_{eq} with pressure, which was not the case under N_2 environment (Figure 3.6(A)) due to the different interactions of the gases with the corn oil. With an increase in pressure, some deposition of oil was visible on the metal surface in CO_2 environment different from N_2, which can be attributed to the solubilization of some components of the drop phase to the surrounding phase, resulting in the formation of a thin vapour film. This film may reduce the surface energy, resulting in higher values of CA_{eq} in CO_2 than in N_2, especially at higher pressures. Thus, with a pressure increase under CO_2 environment, the interactions between the corn oil and SS surface might be reduced, resulting in strong interactions between the thin vapour film and surface, altering the affinity of the liquid to the surface (autophobic phenomenon) (Hare & Zisman, 1955; Jenab & Temelli, 2011).

The CA_{eq} of corn oil in SC-CO_2 was significantly ($p < 0.05$) affected by the saturation conditions of the CO_2 environment (Figure 3.4). At 60 °C, even though CA_{eq} under saturated conditions was higher than that at unsaturated conditions at 16 and 20 MPa (8.9±1.3° vs 11.4±0.8° at 20 MPa), there was no difference at 24 MPa.

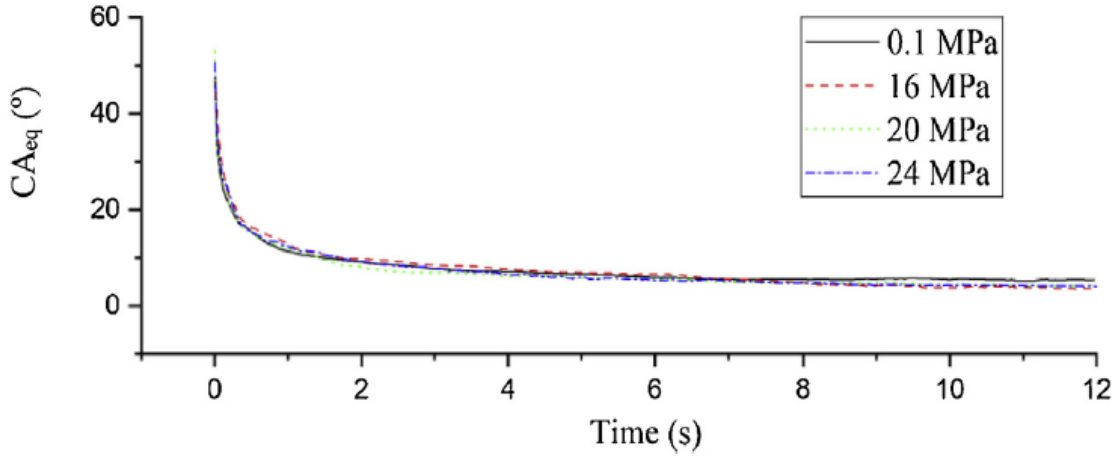

Figure 3. 5. CA_{eq} of corn oil on polished SS in N_2 environment at 60 ºC and different pressures as a function of time.

(A)

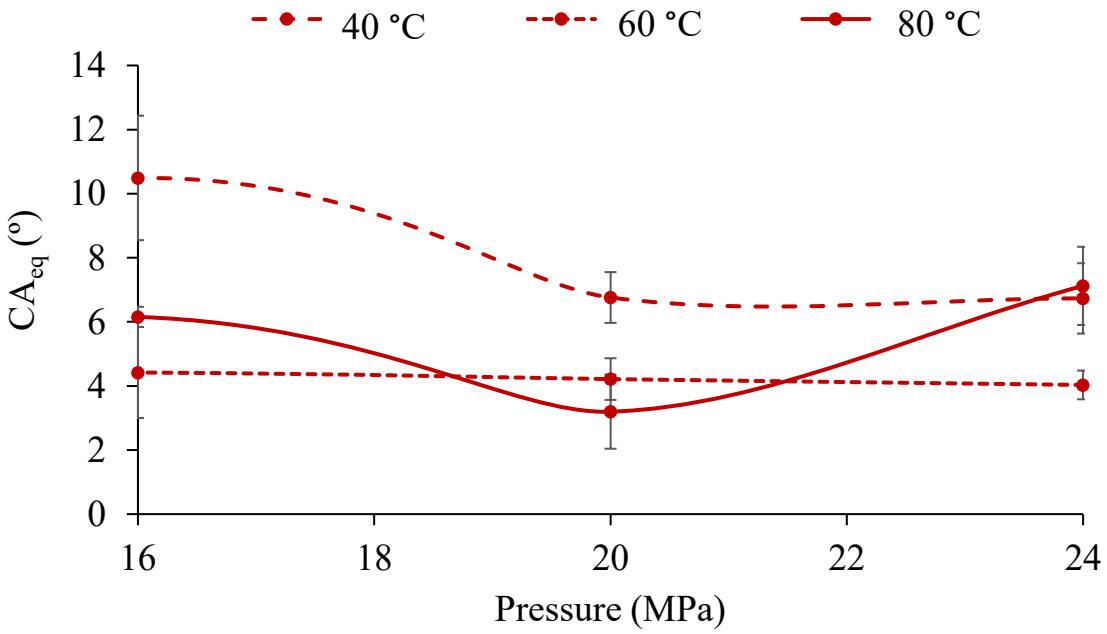

(B)

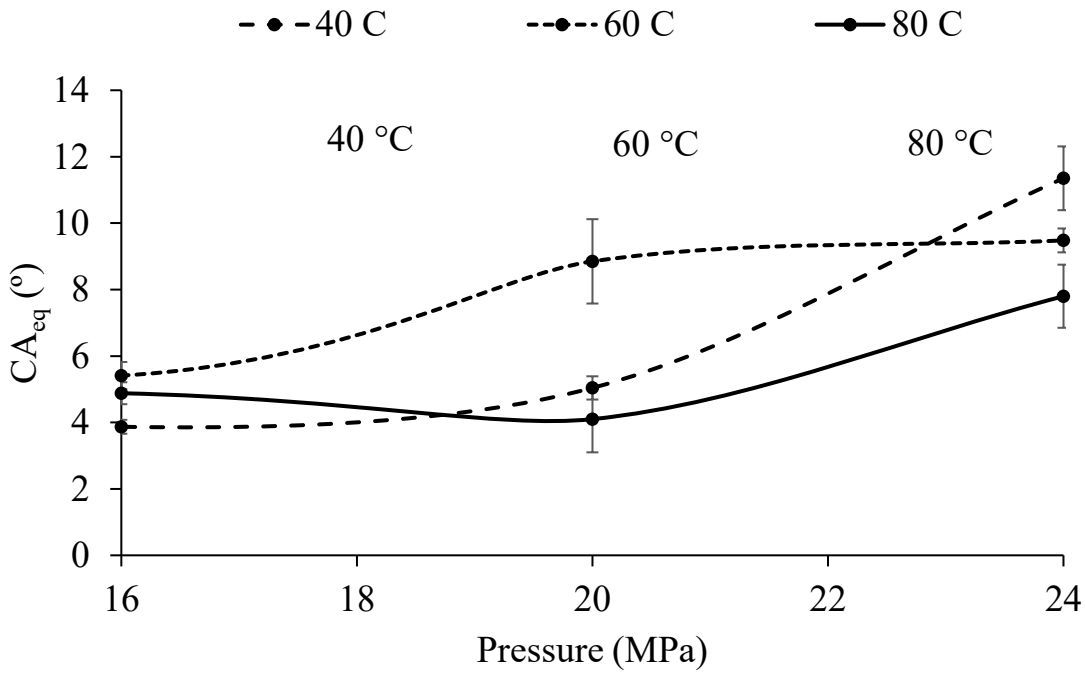

Figure 3. 6. CA_{eq} for (A) corn oil/N_2 (red lines) and (B) corn oil/CO_2 (black lines) under unsaturated medium at 40, 60 and 80 ºC and 16, 20 and 24 MPa. (Data presented in Appendix A, Table A.5)

This increase might be related to the preconditioning of the metal surface due to the surrounding phase saturation leading to deposition of tiny oil droplets on the surface, creating a thin vapour film with specific characteristics that may modify the surface energy. This effect might be minimal at higher pressures due to the higher solubility of oil in SC-CO_2 and the formation of a similar film on the solid surface regardless of whether the surrounding phase is previously saturated or not.

The limited information available about the wettability of lipids on metal surfaces has created some restrictions to compare the results of this study to the literature. However, different approaches have been reported to understand other complex wettable systems by experimental or simulation studies. For example, to improve the enhanced oil recovery (EOR) process in the oil and gas industry, an experimental approach was taken to understand the wettability of brine or CO_2 on different mineral surfaces, under saturated and unsaturated media. Kaveh et al. (2014) determined the wettability of CO_2 in Bentheimer sandstone under unsaturated and saturated water with CO_2 and flue gas (N_2 and CO_2), up to 15 MPa and 44.85 °C. The authors concluded that under unsaturated conditions, the CA values of the CO_2 bubble were influenced by the dissolution of CO_2 in the surrounding phase, resulting in a change in the bubble size, while the impact of the surface properties was not significant (Kaveh et al., 2014). When the medium was saturated with the flue gas, the CA was not affected by dissolution since the composition of the flue gas was 80% N_2 and 20% CO_2, showing higher values of the flue gas bubble IFT than just CO_2 bubble (Kaveh et al., 2014). They specified that the CA results would not be reliable and reproducible while the saturated medium was efficient since the effects of the dissolution and bubble size reduction were avoided (Kaveh et al., 2014). Another study by Arif et al. (2016) focused on the wettability of CO_2 on calcite surface in brine saturated with CO_2 at pressures of up to 20 MPa, and temperatures between 34.85-69.85 °C and 0-20% sodium chloride (NaCl) in brine. Their results showed that the

affinity of the calcite surface to water changed, once the CO_2 pressure was increased, resulting in a surface with less water wetting properties (Arif et al., 2016). The CA of CO_2 increased when the surrounding medium pressure was enhanced, showing poor wetting of CO_2 on calcite surface in the presence of brine (Arif et al., 2016). Moreover, the authors pointed out that the carbonic acid formed from the reaction between CO_2 and water in brine contacted the calcite surface and caused its dissolution (Arif et al., 2016). As a result of all these events, the CA value may be affected because of changes in mass transfer, and surface topography, chemistry and energy (Arif et al., 2016), which also apply for the case of lipids evaluated in this study.

On the simulation side, Arif et al. (2017) used the Neumann's equation of state to estimate the solid/CO_2 and solid/water surface energies based on the CA and IFT data from the literature obtained at different operating conditions using different types of surfaces. They indicated that the surface tension between solid/CO_2 decreased when pressure was increased at constant temperature. Based on the previous findings of Dickson et al. (2006), the cohesive energy density of CO_2 tends to be close to that of the solid with a pressure increase. As well, Arif et al. (2017) highlighted the reduction of the solid/CO_2 surface energy and more intermolecular interactions at the solid/CO_2 interface. They specified that for hydrophobic surfaces pre-wetted with oil, the water CA was higher, which could be explained with the decrease in the surface energy of the solid/gas interface. Nevertheless, hydrophilic surfaces pre-wetted with water showed lower water CA, due to the higher solid/gas surface energy (Arif et al., 2017). They found that when temperature was increased, the solid/CO_2 surface tension increased because of the reduction of the CO_2 cohesive energy density, which promoted less van der Waals interactions and less intermolecular interaction between solid and CO_2 (Arif et al., 2017).

The findings of the previous studies and the results of this study justify that the CA of a liquid or fluid under unsaturated environment generates relevant information related to the diffusion and mass transfer from the surrounding phase to drop phase and vice versa. However, under saturated medium, the mass transfer between phases is negligible resulting in an excellent approach to evaluate the wetting properties of the surface. In addition, the pressure, temperature and composition of the surrounding phase have a significant influence on the final value of the CA_{eq} since these parameters affect the molecular interactions between the surrounding phase-solid surface and surrounding phase-solid surface-drop phase, modifying the surface energy and thus resulting in different affinities of the liquid under investigation to the solid surface.

3.3.2.1. Spreading dynamics of corn oil droplet on polished stainless steel in supercritical nitrogen and supercritical carbon dioxide

Different studies have focused on understanding and characterizing the spreading dynamics of Newtonian and non-Newtonian fluids on different surfaces (Arif et al., 2016; Bertola, 2009; Carré & Eustache, 2000). However, diverse surrounding media, such as SC-N_2, and SC-CO_2 environments have not been reported. As presented in Figure 3.7, the drop radius over time at 60 °C and different pressures was higher under air and SC-N_2 compared to that under SC-CO_2, indicating higher spreading velocity. This difference could be explained considering the difference in the solubility of the gas in the oil droplet and the formation of a thin vapour film on top of the surface with different physicochemical properties, which might impact the spreading dynamics by allowing or avoiding faster contact between the corn oil droplet and the SS surface. The solubility of SC-N_2 in the corn oil droplet and the solubility of oil in SC-N_2 are negligible, so that a thin vapour film that may form on top of the solid surface does not affect the surface energy, resulting in faster contact of the liquid with the surface, enhancing the spreading velocity.

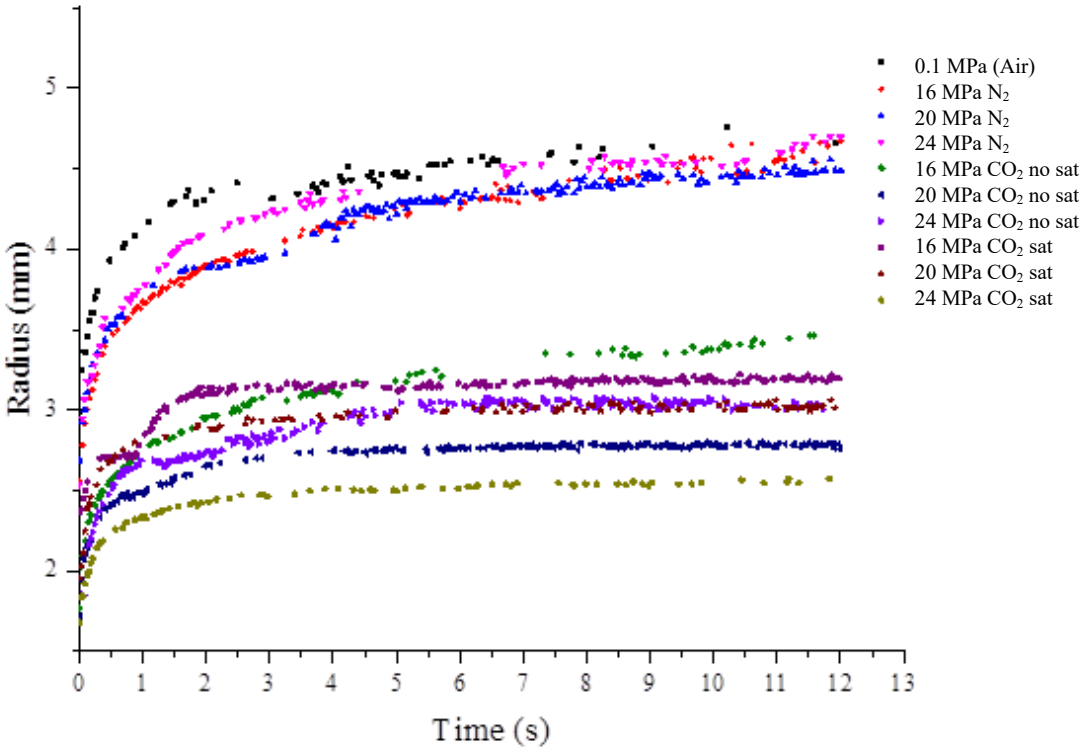

Figure 3. 7. Spreading radius versus time of corn oil droplet on SS surface at 60 °C at different pressures under SC-N_2 and SC-CO_2 (unsaturated and saturated) environments.

In contrast, under SC-CO_2 environment, the physicochemical properties of such a film would be different due to the solubility of the corn oil in SC-CO_2 and the solubility of the SC-CO_2 in the corn oil. Therefore, such a thin vapour film would momentarily affect the energy of the surface and thus the drop impact and spreading dynamics. There are multiple factors that affect the spreading dynamics of a droplet and its final shape: drop properties (initial drop volume, viscosity, density, surface tension) and interface properties (surface roughness, stiffness, inherent charges, elasticity (Chen & Bertola, 2016; Eddi et al., 2013). In most cases, the analysis of spreading dynamics of a droplet is represented with power law dynamics where the transient evolution of the base radius is observed under different scenarios. One of the power law models is Tanner's law,

representing the spreading of a viscous droplet that relies on hydrodynamic spreading radius (r), which depends on the initial droplet radius (R_0), interfacial tension (γ), viscosity (μ) and spreading time (Kavehpour et al., 2002). The initial stages of spreading dynamics of viscous droplets do not follow a simple power law in the form of $r \sim f(t)^{\propto}$ (Tanner's Law equation) and are independent of the surface spreading.

To determine the experimental stages during spreading of a liquid droplet on a surface, the exponent α is determined based on the Tanner's law equation. When $0.5 < \alpha < 0.1$, it represents fast dynamics at shorter times, while $0.1 < \alpha < 0.2$, describes the drop reaching a plateau (consistent with Tanner's law) (Chen & Bertola, 2016). In addition, the late stage spreading of viscous drops can also be predicted by Tanner's law (Chen & Bertola, 2016). In order to characterize the stages of the spreading dynamics of the corn oil droplet on SS surface under SC-N_2 and SC-CO_2 environments, the power law exponent of Tanner's law was determined. This was possible through the log-log plot of drop radius versus time and the determination of the slope of each curve (Figure 3.8). The values of the power law exponent were between the range of $0.05 < \alpha < 0.09$, which according to Eddi et al. (2013) characterized that the drop reached a plateau. Two different approaches, hydrodynamic model (James et al., 2018) and molecular kinetics model (Rahman et al., 2018) are commonly used to describe spreading dynamics of a droplet on a solid surface. The hydrodynamic model relies on the resultant energy dissipation due to the viscous drag inside the droplet whereas in the molecular kinetics model, the friction at the three-phase contact line is the origin of the dissipation (Blake & Haynes, 1969). In the molecular kinetics, the adsorption along the solid-air interface is considered by ignoring the influence of bulk viscosity (James et al., 2018).

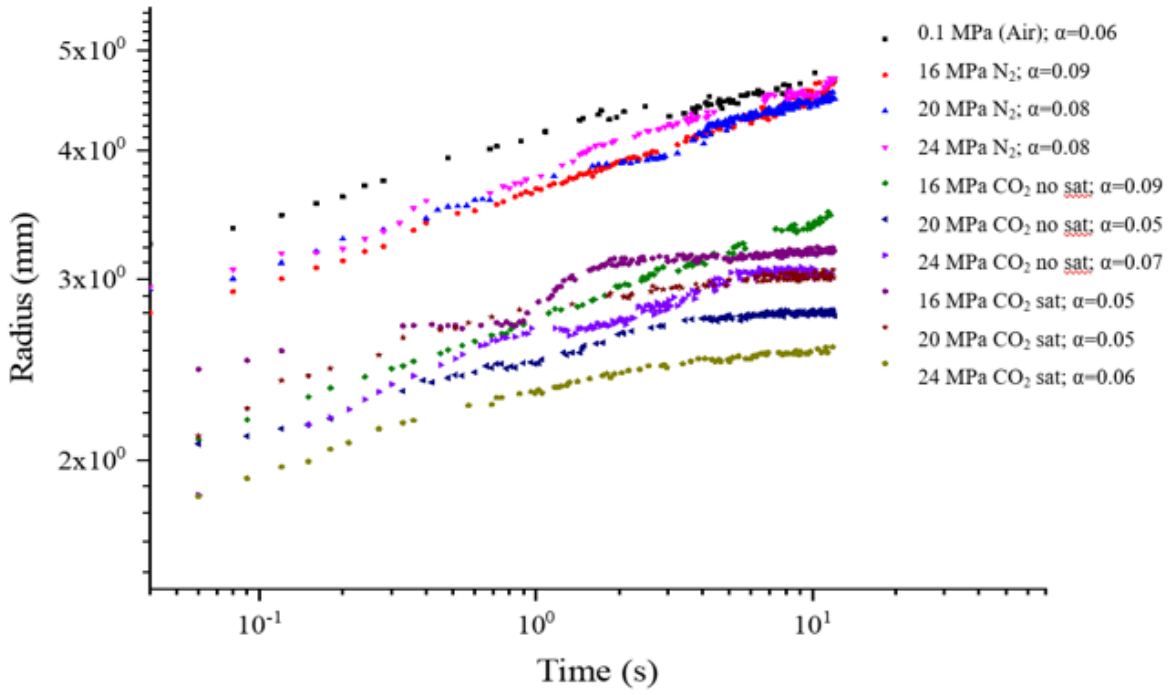

Figure 3. 8. Log-log representation of the spreading radius versus time of corn oil droplet on SS surface at 60 °C at different pressures under SC-N_2 and SC-CO_2 (unsaturated and saturated) environments, with their respective power-law exponents (α).

Based on the time resolution at which the spreading dynamics is observed, three stages can be visualized, starting from early stage to late stage spreading and in between an intermediate stage (Von Bahr et al., 2001). In these stages, the competition between three interfacial energies, solid-medium, drop-medium and drop-solid dictate the dynamics of the drop spreading (Carlson et al., 2011; James et al., 2018). interfacial energies, solid-medium, drop-medium and drop-solid dictate the dynamics of the drop spreading (Carlson et al., 2011; James et al., 2018). The viscosity of the liquid and resistance offered at the three- phase contact line as well as across the drop medium interface dampens the oscillations and eventually the drop attains the equilibrium configuration with Young's contact angle (Carlson et al., 2011). The findings of this study are novel in the area of supercritical fluids in terms of the differences in the spreading velocity of the corn oil droplet

on SS surface in SC-N_2 and SC-CO_2 environments. It would be interesting to determine the early and intermediate stages of oil droplet spreading under dense gases to be able to formulate and to evaluate the fundamental understanding of the phenomena observed in this study, for example, the bouncing of the corn oil droplet before the spreading phenomena occurs under SC-CO_2 conditions as discussed next.

3.3.2.2. Bouncing of corn oil droplets on stainless steel surface in supercritical carbon dioxide environment

The bouncing of the corn oil droplet on SS surface was observed under unsaturated and saturated SC-CO_2 environments (Figure 3.9), but not under SC-N_2 (Figure 3.10). Such phenomenon has not been reported previously for lipid/SC-CO_2 systems. The ability of a drop to bounce on a surface depends on the presence of a thin vapour film of the gas or liquid between the droplet and the solid (Chen & Li, 2010), which can momentarily modify the surface energy by covering a significant section of the wetted area and changing the liquid's affinity to the surface (Seifried & Temelli, 2011). Also, this phenomenon could be affected by the viscosity differences between the drop phase, its interface and surrounding phase, where the effect of the solubilization of the liquid into the surrounding phase and density differences in the system, promote the bouncing of the liquid droplet on the solid surface, specifically for the system corn oil/SC-CO_2/polished SS surface. Moreover, the time scale is a relevant aspect to consider because part of the gas may be trapped between the falling drop and the substrate, and the time required to dissipate that gas may not be enough to avoid this phenomenon.

It is interesting to note that at high pressure CO_2 conditions, the mass transfer phenomena could promote the formation of a thin film (nanometric), with specific rheological behaviour, on the surface causing the drops to bounce (Figure 3.9) because of the dissolution of the drop phase

in SC-CO_2. Moreover, the formation of this thin vapour film and its characteristics might be different depending on the type of supercritical fluid that forms the surrounding phase and its conditions (saturated or unsaturated). Chen and Bertola (2016), who studied the spreading dynamics of viscoplastic drops, pointed out that at high pressure, the formation of a thin vapour film might be possible, causing the droplets to bounce. This layer may work as an elastic cushion opposing the droplet impact velocity. Similar phenomena might be related to the corn oil droplet in SC-CO_2 environment observed in this study, and its rheological behaviour could be similar to those of canola oil (Fattori et al., 1988) and fish oil (Seifried & Temelli, 2011) saturated with CO_2 under high pressure, which were characterized as a dilatant or shear-thickening fluid when pressure was increased at constant temperature. In contrast, the corn oil droplet in SC-N_2 is not expected to have similar rheological behaviour since the solubility of N_2 in the oil is negligible. Therefore, the viscosity of the thin vapour film formed by the system corn oil/SC-N_2 did not promote strong and proper film formation that would allow the bouncing of the corn oil droplet (Figure 3.10). During the initial stage of drop spreading of a viscoelastic fluid, it may accumulate some of the impact energy like elastic energy and deliver it at the retraction step, decreasing the overall mechanical energy dissipation and increasing the bouncing effect (Chen & Li, 2010).

Furthermore, when a thin vapour film (nanometers in thickness) acts as an impact absorber of the droplet, the physical effect is called the dynamic Leidenfrost phenomenon (Carré & Eustache, 2000; Quéré, 2013). After this initial spreading followed by drop impact, the drop takes back its initial spherical shape, minimizing its surface energy (Carré & Eustache, 2000). Because of the presence of the vapour film, the liquid drop does not spread on the surface, resulting in the reduction of the energy dissipation and allowing the bouncing phenomena to occur because more of the initial kinetic energy is available for its bounce until all of the drop's kinetic energy is

dissipated (Carré & Eustache, 2000). To better understand the stability of the thin vapour film and its role in the spreading dynamics and bouncing, different aspects need to be considered, for

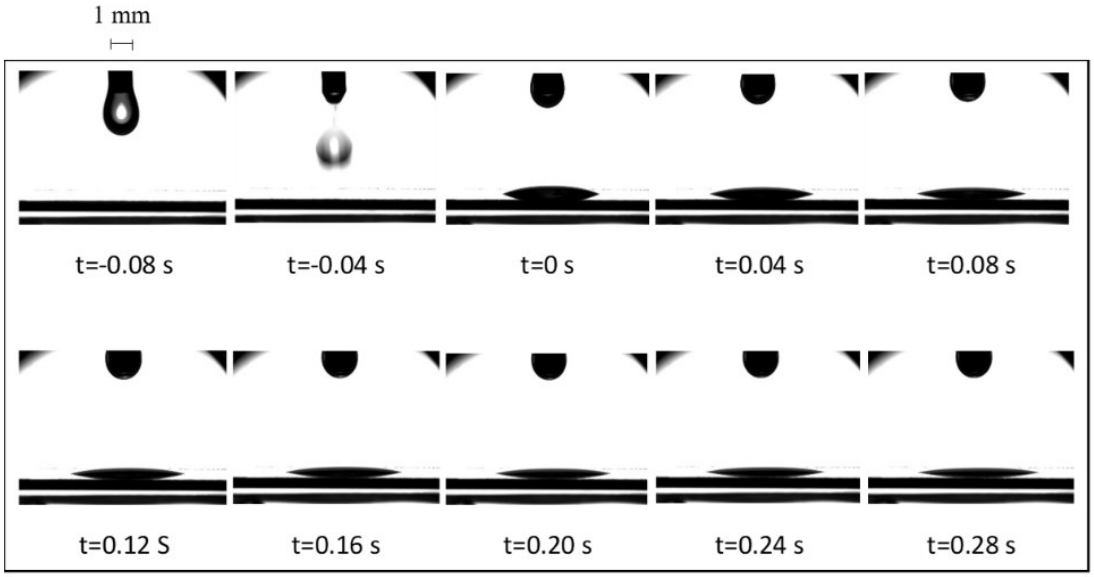

Figure 3. 9. Bouncing of corn oil droplet on SS surface in unsaturated SC-CO_2 at 60 ºC and 20 MPa.

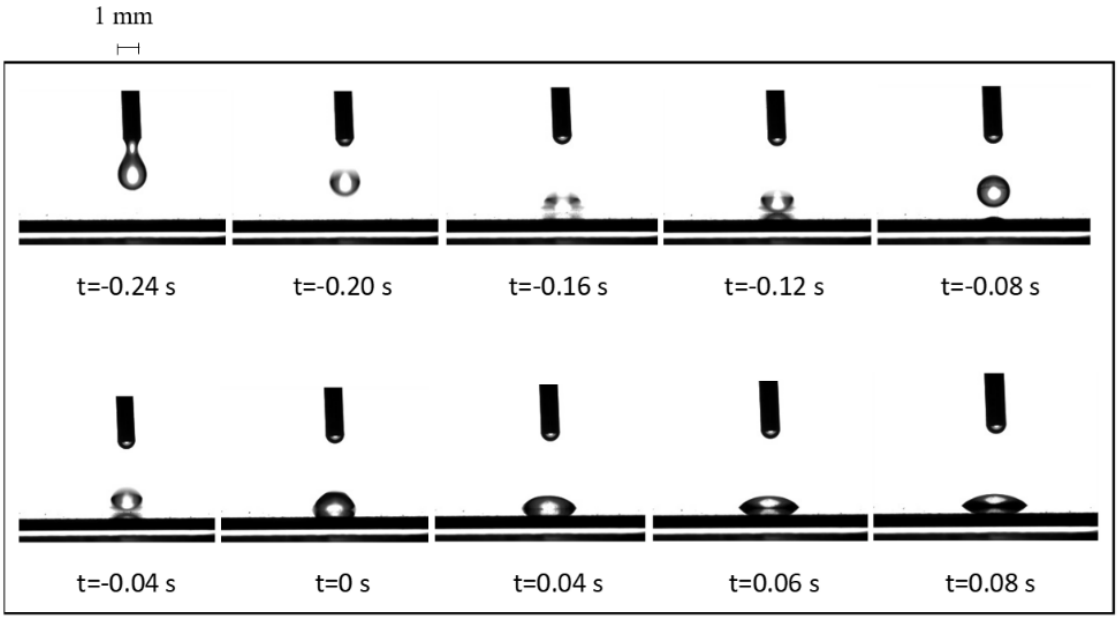

Figure 3. 10. Wetting phenomenon of the corn oil droplet on SS surface in SC-N_2 at 60 ºC and 20 MPa.

instance, formation of the vapour film, impact height, impact velocity, viscosity and/or elasticity of the film and instabilities in the film.

Different studies have been performed to understand the bouncing behaviour of fluids on surfaces. For example, at atmospheric conditions, different studies have focused on the spreading dynamics of different fluid droplets on diverse types of surfaces (Carré & Eustache, 2000); for non-Newtonian fluids such as shear-thinning (Arif et al., 2016), viscoplastic (Bertola, 2009) and viscoelastic (water with small amounts of polyethylene oxide that changes viscosity but does not affect surface tension and shear viscosity) fluids (Carré & Eustache, 2000). Kolinski et al. (2014) indicated that drops can bounce perfectly at ambient conditions on hydrophilic surfaces. Therefore, more information is needed on the influence of the type of fluid and its composition on the bouncing effect of drops on different surfaces.

As a result, there is a growing interest in the spreading dynamics of non-Newtonian fluids because of their practical application in different fields of the industry, for instance, cosmetics, drug delivery systems, formulation of new food products, agro-chemicals and bioactive encapsulation. To the best of the author's knowledge, this interesting phenomenon has not been reported in the literature previously under supercritical conditions and further research is required to understand it better and promote its potential process implications.

3.4. Conclusions

The interfacial tension of corn oil/N_2 and corn oil/CO_2 showed a remarkable difference depending on pressure and temperature conditions of the N_2 or CO_2, which impacts their density values. This difference between the two systems was due to the lower density, solubility and diffusion of N_2 in corn oil resulting in higher interfacial tension, once equilibrium is reached; whereas the higher solubility, diffusion and mass transfer of CO_2 in corn oil generated a substantial

decrease in IFT with pressure at constant temperature, as the density of CO_2 approached that of the liquid. In contrast, during an isobaric operation, when temperature was increased above the cross-over pressure, the IFT was enhanced due to the decrease in CO_2 density.

The wetting behaviour of corn oil on polished stainless steel surface under dense N_2 and CO_2 was characterized as complete wetting, showing values of CA_{eq} below 10°. Based on the ANOVA results, there were significant effects of pressure and temperature on the equilibrium contact angle. The unsaturated and SC-CO_2 saturated with corn oil exhibited variations in the CA_{eq} at 12 s, where at 60 °C and 16 and 20 MPa, the CA_{eq} showed a noticeable increase under saturation conditions. It was interesting that the bouncing of corn oil droplet was visualized on a completely wettable substrate (polished SS) under SC-CO_2 environment, but not in SC-N_2 environment, which can be linked with the higher values of CA_{eq} of corn oil droplet under saturated CO_2 as well as physicochemical characteristics of the phases at the experimental conditions. Further research is required to better understand the bouncing effect of lipid droplets on SS surface in SC-CO_2 environment and its potential processing implications.

Chapter 4. Interfacial tension and equilibrium contact angle of lipids on polished glass in supercritical carbon dioxide[b]

4.1. Introduction

Supercritical fluid fractionation employing CO_2 has been used to isolate minor lipid components with health benefits from complex mixtures such as deodorizer distillates (Ibáñez et al., 2002; Stockfleth & Brunner, 1999). To design an optimal fractionation process, different aspects must be considered, including the hydrodynamic behaviour in a fractionation column, which relates the contact between the two streams and the packing material. Different studies have focused on understanding the hydrodynamic behaviour inside the packed column by using diverse packing materials, and geometries, revealing a significant variation in the separation efficiencies of lipids as summarized in Chapter 2 (Table 2.1) (Brunner et al., 1991; Stockfleth & Brunner, 1999; Simões, et al., 2000; Ibáñez et al., 2002; Hurtado-Benavides et al., 2004; Güçlü-Üstündağ & Temelli, 2007; Fornari et al., 2008). Those studies revealed diverse separation efficiencies of lipids and minor components without explaining if the type of material and/or geometry of the packing had an impact on the selectivity of separation. Additionally, Bejarano et al. (2016) indicated that the understanding of the hydrodynamic behaviour inside a packed column might be linked to the contact angle (CA) and interfacial tension (IFT), since these parameters influence the limit of the interchange area and packing wettability; therefore, they are critical parameters to analyze the interfacial phenomena inside a packed column. The IFT of lipids in the surrounding CO_2 environment at different experimental conditions has been previously reported, including

---

[b] A version of this chapter has been published as: Eileen Santos, Prashant Waghmare, Feral Temelli. Interfacial tension and equilibrium contact angle of lipids on polished glass in supercritical CO_2. *Journal of Supercritical Fluids* (2022) 181, 105486 (https://doi.org/10.1016/j.supflu.2021.105486).

corn oil (Jaeger et al., 1996; Jaeger, 1998; Simões et al., 2000; Tegetmeier et al., 2000; Sutjiadi-Sia et al., 2008a), oleic acid (Lockemann, 1994b), fish oil (Seifried & Temelli, 2010) and tristearin and rapeseed oil (Ilieva et al., 2016).

The pendant drop method (Andreas et al., 1938) has been applied most commonly to determine the IFT of lipids in the supercritical fluid environment using the Young-Laplace equation. On the other hand, CA is the result of the contact of a liquid with a solid surface, where molecular interactions among the phases (solid/liquid/gas) occur at the three-phase contact line until they achieve their relaxed state, which is affected by multiple factors, including the solid substrate heterogeneity (chemical or geometrical) and the solid-liquid system properties (Law & Zhao, 2016a; Chapter 3). CA has been determined at atmospheric and high-pressure conditions for different systems. At atmospheric conditions, the CA of canola and olive oils on PTFE (polytetrafluoroethylene or Teflon) were determined in air and steam as the surrounding phases (Ashokkumar et al., 2012). At high-pressure conditions, the CA of different fluids on diverse surfaces as been determined for different applications (Dickson et al., 2006; Jaeger, 1998; Sutjiadi-Sia, 2008). In Chapter 3, it was determined that corn oil completely wetted the polished stainless steel (SS) surfaces under unsaturated SC-N_2 and SC-CO_2, and saturated SC-CO_2 at 40 to 80 °C and 0.1 to 24 MPa, exhibiting CA values of less than 10º. In an effort to enhance our knowledge on the wettability behaviour of lipids and their mixtures on diverse surfaces in the presence of SC-CO_2, which is fundamental information needed for supercritical process design, this study is focused on polished glass surface building on the previous study on polished SS surface (Chapter 3). As well, two different lipid classes (oleic acid (OA) representing free fatty acids (FFA) and canola oil (CanO) representing triacyglycerols (TAG)) were targeted in this study as opposed to the use of corn oil only in the previous study (Chapter 3) to expand the database on different types

of lipids. The objective of this study was to determine the effect of pressure and temperature on IFT and equilibrium contact angle (CA_{eq}) of oleic acid and canola oil on polished glass in SC-N_2 and SC-CO_2 environments.

4.2. Materials and methods

4.2.1. Materials

Two different ideal surfaces were used in this study polished glass and SS (same as that used in Chapter 3). The glass surface was plain glass microscope slides (25 x 75 mm and 1 mm thickness) that were purchased from Fisher Scientific (code: 12550A3, Fisher Scientific, Ottawa, ON, Canada) and manually cut in a specific dimension (25 x 25 mm). The surface roughness of the glass was determined as described in Chapter 3 (section 3.2.2.).

Acetone (HPLC grade, Fisher Scientific, Ottawa, ON, Canada), isopropanol (>98% Food Grade, Sigma-Aldrich, Oakville, ON, Canada), deionized water and compressed air were used for the cleaning treatment of glass and SS surfaces. The drop phases were oleic acid (100% pure) and canola oil purchased from VWR International (Mississauga, ON, Canada) and a local market ("Mazola", ACH Food Companies, Inc., Memphis, TN, USA), respectively.

4.2.2. Apparatus to determine the interfacial tension and contact angle

The determination of IFT and CA was performed using the equipment described in detail in Chapter 3 (section 3.2.3). The unit is DSA100 HP from Krüss GmbH (Hamburg, Germany), which is equipped with a High Pressure (HP) system model PD- E1700 MD, (Eurotechnica GmbH, Barteheide, Germany) and an optic system DSA100, (Krüss GmbH, Hamburg, Germany). Briefly, a custom-made glass holder was placed inside the HP vessel (42 mL) and a sufficient amount of the lipid sample was put into the glass holder to saturate the surrounding SC-CO_2 phase. The polished glass surface was placed on the glass holder with sufficient opening to allow contact

between the lipid and SC-CO_2. Then, the system was pressurized to the desired level and allowed to equilibrate at the target temperature. The test lipid was filled into the liquid reservoir and a drop was formed at the tip of the capillary needle (OD = 1.65 and 1.1 mm for N_2 and CO_2, respectively) by adjusting the valves in the dosing system. First, IFT was determined from the pendant drop, then the drop was allowed to fall on the glass surface and the CA was determined from the sessile drop using the images captured over time.

4.2.3. Interfacial tension and contact angle measurements

The IFT measurements of OA and CanO were performed at 60 ºC, and 0.1, 16, 20 and 24 MPa. These experiments were performed under extreme care, considering cleaning and avoidance of the presence of air bubbles at the tip of the needle. To guarantee the thermodynamic equilibrium and saturation of the surrounding media inside the HP vessel with each lipid type, approximately 1.2 g of lipid was weighed in a glass holder (amount determined based on vessel size and solubility of OA and CanO in SC-CO_2 (Nilsson et al., 1991; Soares et al., 2007) and placed inside the HP vessel. The vessel was heated up to the desired temperature and held for 1 and 2 h, for OA and CanO experiments, respectively. The saturation of the surrounding media was verified when IFT values did not change over time. Based on the negligible solubility of lipids in SC-N_2 and vice versa, the experiments under this gas environment were performed without consideration of saturation conditions. The experimental procedure was similar to that reported in Chapter 3 (section 3.2.4). For calculations, the densities of the oleic acid and canola oil saturated with SC-CO_2 (drop phases) were taken from Lockemann (1994a), and Jenab and Temelli (2011), respectively, while the density of CO_2 (surrounding phase) was taken from NIST (2005).

The cleaning protocol of glass and SS surfaces was adopted from Becker et al. (2016), where each surface was cleaned using deionized water and two different organic solvents, acetone

and isopropanol, in the order of acetone, isopropanol and deionized water. The CA measurements of OA and CanO were performed on polished glass at 40, 60 and 80 ºC, and 0.1, 16, 20 and 24 MPa in SC-CO_2, following the procedure described in Chapter 3 (section 3.2.3.) to allow comparison of the behaviour of different lipids on diverse surfaces. To compare the effect of the type of surrounding media on the wettability of OA and CanO on glass, experiments in SC-N_2 were performed at 60 ºC and up to 24 MPa of pressure. Moreover, to determine the difference in wettability of CanO on different surfaces, the same surface used in Chapter 3, polished SS, was employed for CA determination of CanO at 60 ºC and 20 MPa in SC-CO_2.

The IFT and CA values were determined using the pendant drop and sessile drop modules, respectively, of the ADVANCE for Drop Shape Analyzers (2014-2017) software (Krüss GmbH). To obtain the IFT value from the pendant drop images, the video was converted into frames using the JPG video converter (free software). All measurements at each condition were performed in triplicate and two-way analysis of variance was performed using Microsoft Excel to assess the effects of pressure and temperature as well as their interaction effect on the IFT and CA_{eq} at a significance level of $p < 0.05$.

4.3. Results and discussion

4.3.1. Interfacial tension of oleic acid and canola oil in supercritical carbon dioxide

The IFT of OA and CanO in SC-CO_2 were determined at 60 ºC and pressures of up to 24 MPa (Figure 4.1). As expected, a remarkable decrease in IFT values for both systems were observed due to the increase in CO_2 density as pressure was enhanced under isothermal conditions, resulting in a smaller density difference between the drop and surrounding phases and higher miscibility between the phases. The observed trend of the decrease in IFT of lipids with pressure (Figure 4.1) was similar to that reported in previous studies for IFT of other oils, such as corn oil

(Chapter 3; Dittmar et al., 2002; Jaeger et al., 1996), oleic acid (Yu et al., 1992; Lockemann, 1994b), olive oil (Simões et al., 2000), fish oil (Seifried & Temelli, 2010) and palm oil (Dittmar et al., 2002). However, there was a noticeable difference in IFT values, especially at lower pressures, between the results of this study and literature values for the system OA-CO_2, which might be due to the differences in the methods used (capillary rise method vs pendant drop method) and the purity of OA. Lockemann (1994a, 1994b), subjected the OA to a freezing process to enhance its purity from 70 % to 90%, and identified the impurities as stearic acid; whereas the OA used in this study was 100% pure.

At atmospheric pressure and 60 ºC, the IFT values of lipids were determined, considering the density difference between the two phases, using the density values of 860 kg/m^3 (Lockemann, 1994a), 890.76 kg/m^3 (Jenab & Temelli, 2012) and 1.5943 kg/m^3 (NIST, 2005) for OA, CanO and CO_2, respectively.

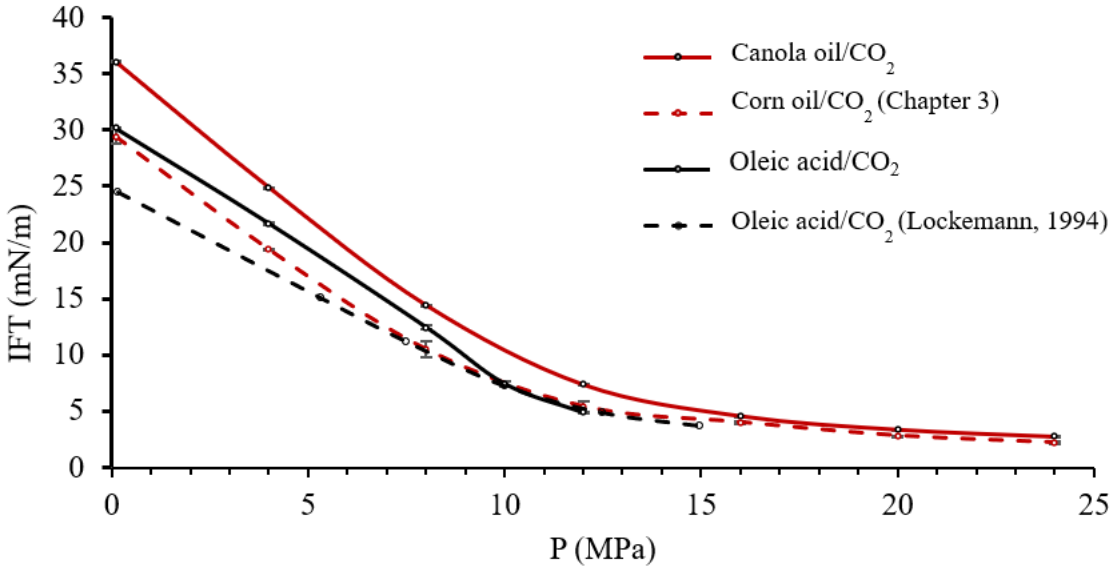

Figure 4. 1. IFT of lipids in saturated SC-CO_2 at 60 °C as a function of pressure (Data presented in Appendix B, Table B.1).

The resulting IFT values were 30.17 and 36.06 mN/m for OA and CanO, respectively, compared to 29.44 mN/m for corn oil determined previously in Chapter 3. The oil densities, in part, depend on the fatty acid composition and the degree of unsaturation, where saturated fat content is 6.4 mol% and 13.1 mol% for CanO and corn oil, respectively (Moreau, 2005; Przybylski et al., 2005) In the case of corn oil, different density values were reported at 60 ºC and 0.1 MPa (Sahasrabudhe et al., 2017; Tegetmeier et al., 2000), which might be related to the composition of the corn oils used in those studies, impacting the results for physicochemical properties (especially density), making comparison of the results for the IFT values of CanO vs corn oil more challenging. Similar to the other reports in the literature, the vegetable oils used in this study and in Chapter 3 were purchased from commercial sources, and the exact composition and quantities of minor lipid compounds are not known. The presence of some minor lipid components may intrinsically impact the IFT since they may act as surface active agents, leading to low IFT values. Even though progress has been made over the years to characterize the physicochemical parameters of lipids and their complex mixtures under SC-CO_2 environment under a wide range of experimental conditions (Chapter 2), many physicochemical parameters are still unknown for complex lipid mixtures. Considering the lipid composition of canola oil (94.4-99.1 wt% triacyglycerols (TAG); 0.4-1.2 wt% free fatty acids (FFA)) and its TAG profile (22.4% triolein (OOO); 22.5% LOO; 10.4% LnOO) (Przybylski et al., 2005) as well as the availability of physicochemical properties, triolein was selected as the representative TAG to explain differences in the behaviour of the complex lipid mixture of canola oil in comparison to OA in this study to overcome the challenge of unavailable physicochemical parameters for canola oil.

The type of lipid used (OA-CO_2, CanO-CO_2) had an effect on the IFT values, especially at pressures up to around 15 MPa, which was intrinsically related to the intermolecular interactions

affected by pressure and temperature, impacting the solubility and diffusion of the lipid into SC-CO_2 and vice versa. Regarding the solubility of SC-CO_2 in the lipid phases, some studies have reported the solubility of CO_2 in TAG and fatty acid ethyl esters (FAEE), for example, Jenab and Temelli (2011) determined the solubility of CO_2 in canola oil and its blend with canola stearin (30 wt%) at 40 and 65 ºC, and up to 20 MPa, where they concluded that the solubility of CO_2 increased with pressure and decreased with temperature. Similarly, Seifried and Temelli (2011) obtained the solubility of CO_2 in fish oil at 40 and 55ºC up to 20 MPa. At pressures above the crossover region, an increase in temperature resulted in a decrease in CO_2 solubility in the oil. Also, they highlighted that CO_2 would be located in between the large TAG molecules upon dissolution in the fish oil, increasing spatial distance between TAG molecules, leading to a decrease in the molecular interactions, and thus, to the volumetric expansion of the CO_2-saturated liquid phase. The solubility of CO_2 in FAEE was significantly higher than that in TAG, exhibiting higher volumetric expansion (Seifried & Temelli, 2011).

These previous studies demonstrate that the solubility of CO_2 in lipids is affected by temperature and pressure as well as the structural complexity of the lipid molecule. For simpler and smaller molecules, like FAEE and possibly OA, CO_2 could solubilize in the lipid phase to a greater extent, whereas for TAG, the CO_2 solubility is less. The extent of CO_2 solubilization into the lipid droplet may impact the IFT values presented in Figure 4.1. In terms of diffusion, for simpler and smaller lipid molecule like OA, which is more symmetrical and with a lower degree of unsaturation, the solubility and diffusion of CO_2 into the lipid are higher than those for more complex molecules like triacyglycerols (OOO), resulting in lower IFT values.

4.3.2. Contact angle of oleic acid and canola oil on glass in supercritical nitrogen and supercritical carbon dioxide

The roughness (R_a) values of polished glass sheets were measured in triplicate to determine if the solid surfaces could be characterized as an ideal surface. The R_a of glass surface was 7.13 ± 0.82 nm, compared to R_a value of 46.1 ± 1.5 nm for the SS surface used in the previous study reported in Chapter 3. This measurement allowed the identification of the polished glass and SS sheets as ideal surfaces. For the CA determination of lipids on surfaces in supercritical fluids, it is important to understand the interactions between the phases in an effort to better analyze the results. The phases present during the CA measurement experiments are depicted in Figure 4.2: liquid lipid phase saturated with SC-CO_2 (L), which is present as the sessile drop; vapour phase making up the surrounding medium (V), which is SC-CO_2 saturated with lipid and a thin vapour film on the solid surface; and the solid phase (S), which is the surface under investigation. The sensitive balance between the compositions of the vapour and liquid phases under equilibrium is highly dependent on the experimental temperature and pressure, which also impact the physicochemical properties of the phases involved (density, interfacial tension, contact angle, diffusion and viscosity). As a result, wettability of lipids on different surfaces in a SC fluid environment not only depends on the experimental conditions, but also on the composition of both phases, which remarkably influences the net effect on wettability and surface phenomenon.

For determination of the CA_{eq} of lipids in supercritical fluids at 60 ºC and 16, 20 and 24 MPa, the saturation condition was implemented for the lipid/SC-CO_2 systems, considering the extent of solubility of CO_2 into lipid phase and vice versa, to reduce the negative impact of mass transfer effects that can affect the CA values. Conversely, for the lipid/SC-N_2 systems, the saturation condition was not implemented since the mutual solubility between the two phases is

almost negligible. CA_{eq} results for OA and CanO on glass surface in SC-N_2 and SC-CO_2 media are presented in Figure 4.3, where CA_{eq} values in SC-N_2 were higher than those in SC-CO_2 medium, over the range of pressures tested for both lipids. The CA_{eq} values for CanO were higher than those for OA, which might be related to the lower solubility of CO_2 in CanO compared to that in OA, leading to a lower reduction of viscosity of the CO_2-saturated lipid phase as well as differences in the diffusion of CO_2 into lipids. Limited data are available in relation to the wettability of liquids on surfaces in dense gases and the determination of solid surface energy at SC-CO_2 conditions. Jaeger (1998), Dickson et al. (2006), Sutjiadi-Sia et al. (2008a, 2008b) and Sutjiadi-Sia (2008) reported the interfacial phenomena of liquids on surfaces in dense gases, trying to relate the surface energy and interfacial tension with CA to analyze the wettability of liquids on solid surfaces, under high pressure. However, comparison of available data is challenging because of the different liquids and modified, and non-modified surfaces used with different roughness and chemical composition.

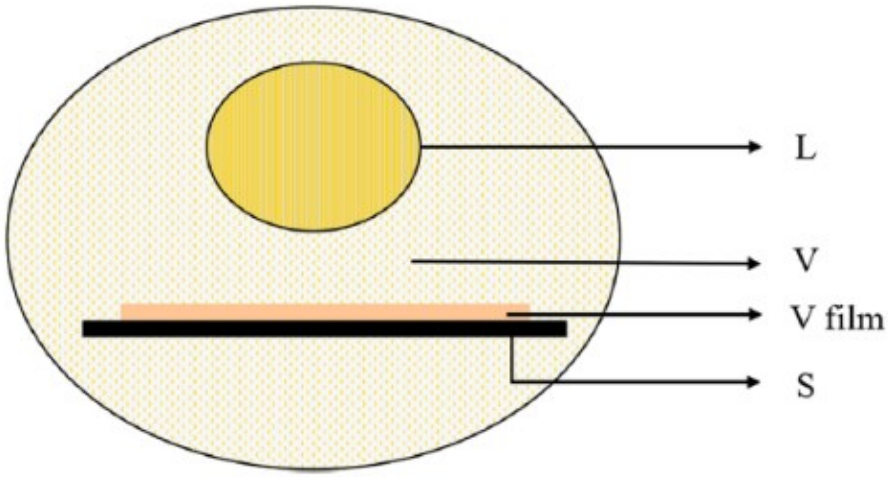

Figure 4. 2. Phases present in wetting of lipids on surfaces in saturated SC-CO_2 environment (L: liquid; V: vapour; V film: vapour film; S: solid phase (surface)).

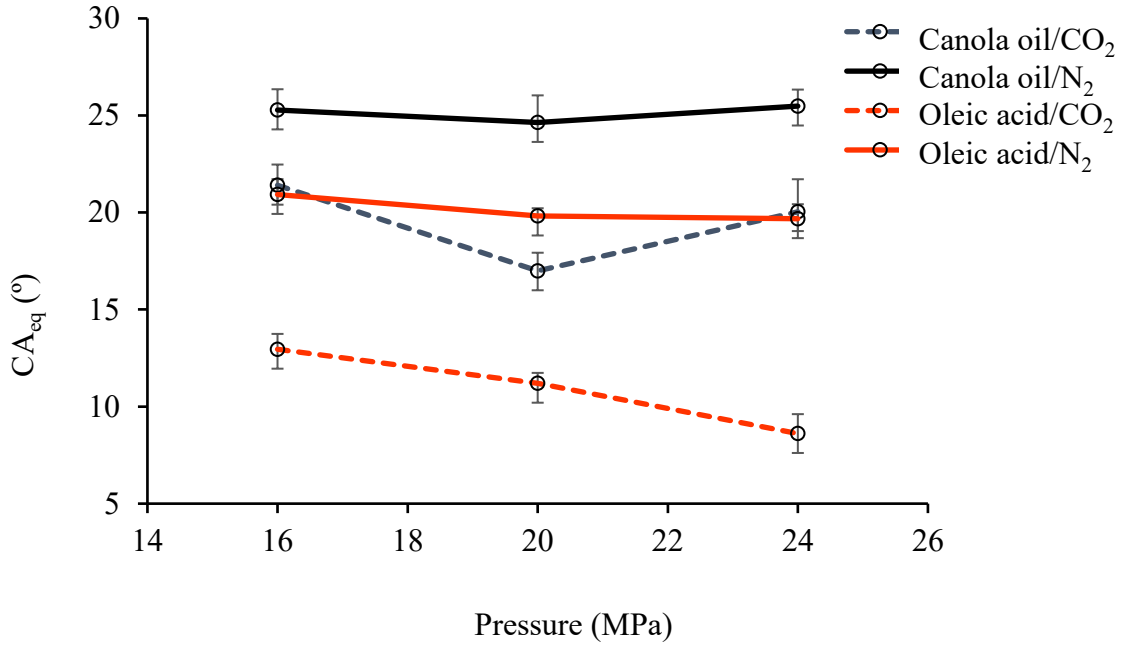

Figure 4. 3. CA_{eq} for oleic acid and canola oil on glass in SC-N_2 (solid line) SC-CO_2 (dashed line) at 60 ºC as a function of pressure. (The curves are included to guide the eye Data presented in Appendix B, Table B.2).

Dickson et al. (2006) determined the CA of water on modified glass surfaces with different hydrophilicities at 23 ºC and up to 20.4 MPa, where they concluded that interactions of CO_2 with the solid surface were improved at elevated pressure because the CO_2 cohesive energy density became closer to that of the solid surface, causing the solid-vapour interfacial tension ($\sigma_{S/V}$) to decrease. Moreover, Sutjiadi-Sia et al. (2008b) determined the $\sigma_{S/V}$ of PTFE (Teflon), glass and SS with water and ethanol in CO_2 at 39.85 ºC and up to 27 MPa and compared to that of PTFE/N_2 system. They highlighted that the $\sigma_{S/V}$ was remarkably influenced by the type of fluid used as the surrounding environment, whereas the $\sigma_{S/V}$ in N_2 environment was not significantly affected in contrast to that in CO_2. Also, they mentioned that the liquid-vapour interfacial tension ($\sigma_{L/V}$) variations generated different wettability of liquids on surfaces, and the adsorption of the gas on

the surface strongly influenced the final value of $\sigma_{S/V}$ (Sutjiadi-Sia et al., 2008b). In addition, Sutjiadi-Sia et al. (2008a) determined the CA of water on a glass surface at 39.85 ºC and up to 27 MPa to be in the range of 31º and 78º, which exhibited an increase as pressure was increased up to the critical conditions; above which, the CA values were approximately constant. The $\sigma_{S/V}$ of Teflon, glass and steel in CO_2 were determined up to 99.85 ºC and up to 27 MPa, considering the theory of Good and Girifalco (1960), which associates the miscibility between phases at atmospheric conditions, the interaction parameter, $\sigma_{L/V}$ and CA values. The results showed that ethanol wetted better than water on all studied surfaces, but glass was the best wetted surface, highlighting that the $\sigma_{S/V}$ relied on the nature of the solid surface and the surrounding fluid.

There are several aspects mentioned by Sutjiadi-Sia (2008) that might not apply for all surfaces analyzed in liquid/SC fluid systems. For example, for the determination of the $\sigma_{S/V}$ of glass surface, the system was defined as highly polar, considering only water and ethanol interactions with the surface, but not CO_2. Also, the presence of CO_2 solubilized in the drop phase was excluded during the evaluation of the intermolecular interactions between the drop phase and solid material. In addition, the $\sigma_{S/V}$ value of any solid surface surrounded by any type of vapour or fluid was considered absolute and of the same order of magnitude, regardless of the type of liquid deposited on the surface. Moreover, pre-saturation of the system to determine wetting angle (equal to CA) did not impact the final CA value (Good & Girifalco, 1960).

In contrast to those statements, the present study demonstrates important aspects to consider during the analysis of the interaction of a liquid deposited on a solid surface in dense gases. The solubility of the liquid into the surrounding phase and vice versa at experimental conditions influences the physicochemical parameters (density, viscosity and IFT) of both phases, which impact the wetting phenomena of the liquid deposited on a surface in a saturated medium.

In addition, the surface energy can be modified by the formation of a saturated vapour film on the surface, known as the Leidenfrost phenomenon (Bertola, 2009), resulting in noticeable differences in CA. For example, at 60 ºC and 16 MPa, the CA_{eq} of OA in SC-N_2 and SC-CO_2 were 20.93±0.40º and 12.95±0.53º, respectively. This difference was mainly due to two aspects: a) difference in the solubility of the two SC fluids in the lipid phase, where the more soluble SC-CO_2 promotes film formation on the surface, altering the liquid/surface interactions; b) the lower impact of N_2 in comparison to CO_2 on $\sigma_{S/V}$ values, which might be related to the adsorption of CO_2 only by the glass surface, as was previously explained for the PTFE surface in both fluids (Sutjiadi-Sia et al., 2008b). It is important to recognize that each system (liquid/solid/SC-fluid) is unique, and diverse interactions between phases at different experimental conditions might lead to variations in CA values, which have a major impact on the design and optimization of processes involving those systems and must not be analyzed considering general approaches.

4.3.3. Contact angle of oil on different surfaces in supercritical carbon dioxide

In an effort to understand the wettability of different oils on different surfaces in SC-CO_2 medium, the CA of canola oil on SS and glass was determined at 60 ºC and 20 MPa and compared with the previous CA data for corn oil on SS at the same experimental conditions in Chapter 3, which presented remarkable differences based on the type of vegetable oil and surface. The CA of CanO and corn oil on SS in saturated environment were 2.3±0.30º and 11.4±0.8º, respectively; whereas the CA of CanO on glass was 17.0±1.67º. To explain the differences in CA values, different aspects of the liquid/solid/SC fluid system must be considered: a) phases identified during CA determination of lipids on surfaces in saturated lipid/SC-CO_2 system (Figure 4.2); (b) diffusion and solubility of lipids in SC-CO_2 and vice versa as well as the viscosity of L and V phases at

experimental conditions; c) possible adsorption of CO_2 on the surfaces, which exhibit weak intermolecular forces, for example, PTFE and glass.

As also discussed in Chapter 3, under lipid-saturated SC-CO_2 environment, the solid/liquid/SC-CO_2 system exhibited the formation of a thin vapour film on the surface, constituted by CO_2-saturated with lipid, which might impact the direct contact of the lipid droplet with the solid surface. This film has specific physicochemical characteristics that influence the wettability phenomena based on the type of liquid/solid/SC fluid and interactions among the three phases. The difference observed in the CA values of CanO and corn oil on SS in SC-CO_2 was not relevant since both triacyglycerols wet the SS surface completely, exhibiting values lower than 10º. In contrast, the CA of CanO on SS and glass showed a remarkable difference, 2.3 ± 0.30º and 17.0±1.67º, respectively, which was related to the difference in the chemical compositions of those surfaces, impacting their surfaces energies. When the surface energy is high and IFT of the liquid is low, the liquid will wet the surface completely, whereas at low surface energies, the liquid will not wet the surface completely, as reflected in the CA values of canola oil on SS and glass surfaces, respectively.

To understand this difference in surface wettability, it is relevant to mention that the surface energy is a result of atomic and molecular level interactions, which might contribute to the difference in surface energy depending on the type of material that is in contact with the lipid and SC fluid. This parameter has been determined using different methods, and one of the pioneers, Fowkes (1964) considered the additivity of intermolecular forces at interfaces as an approach to determine IFT and CA. The author further separated those contributions into dispersion force and "the rest part" to determine the solid surface energy, where the first type was linked with dispersion forces (Van der Waals) and the latter type was related to hydrogen bond, metallic bond and dipole

interactions. Thus, considering the predominance of metallic bonding in SS, based on its chemical composition, it would exhibit higher energy than glass, which is mainly composed of silicon dioxide and barium oxide with the weakest intermolecular forces (Van der Waals), contributing to its low surface energy.

The cleaning of both surfaces was performed following the same procedure described in Chapter 3, to avoid any effect of different solvents and their potential residues, which might have affected the reproducibility and comparison of the results between the two studies. In addition, considering the challenges associated with the estimation of surface energy, determination of the surface energies of SS and glass surfaces used were outside the scope of this study.

4.3.4. Contact angle of oleic acid and canola oil on glass in supercritical carbon dioxide at different temperatures and pressures

To determine the effect of pressure, temperature and type of lipid on CA, the CA_{eq} of OA and CanO on polished glass surface were determined in saturated SC-CO_2 at 40, 60 and 80 ºC and 16, 20 and 24 MPa (Figure 4.4). Based on the analysis of variance (ANOVA), there was a significant effect of pressure, temperature and their interaction ($p < 0.05$) on the CA_{eq} for both OA and CanO. For the OA/SC-CO_2 system (Figure 4.4(A)), the CA exhibited partial to complete wettability trend at 40 ºC and 60 ºC from 16 to 24 MPa with values in range of 11.78±0.55º–3.74±1.03º and 12.9±0.54º–8.61±0.51º, respectively, which is related to the pressure effect at isothermal conditions. With an increase in pressure, the density of the SC-CO_2 was enhanced, resulting in higher solubility of the lipid in SC-CO_2, which could be related to the formation of a thin vapour film on the surface, modifying the interaction between the lipid droplet and the glass surface, and influencing the wetting of OA on glass in SC-CO_2.The formation of such a film was also previously reported for the corn oil/SC-CO_2/SS surface system in Chapter 3.

(A)

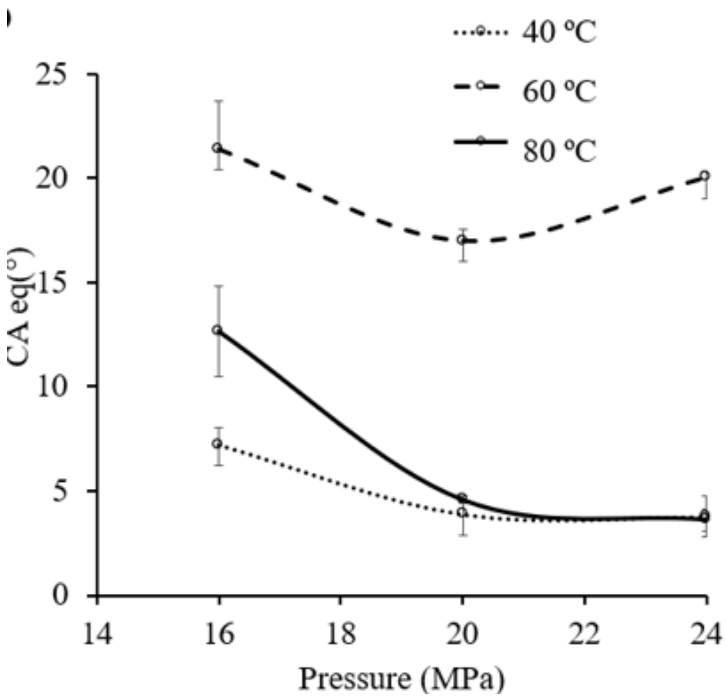

(B)

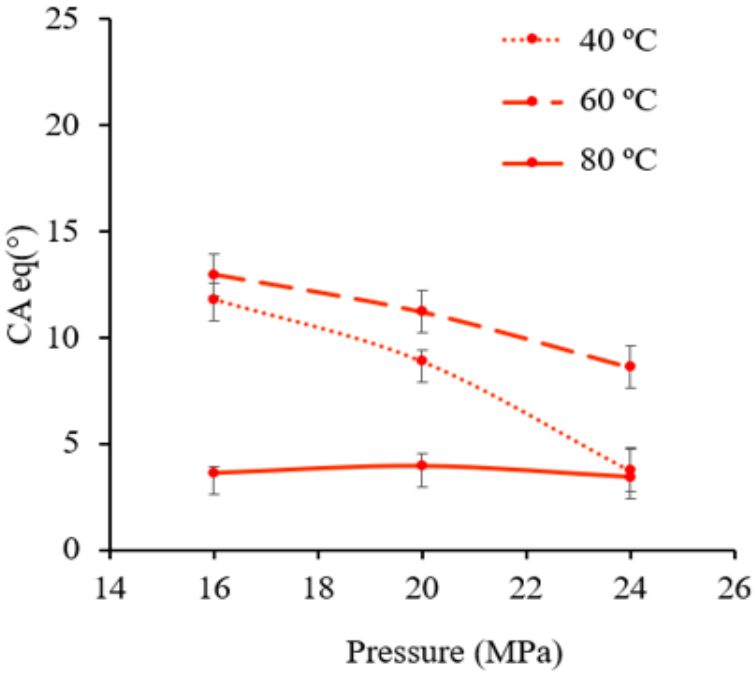

Figure 4. 4. CA_{eq} for (A) oleic acid and (B) canola oil in SC-CO_2 surrounding medium under saturated conditions at 40 ºC (------), 60 ºC (– – –) and 80 ºC (———) as a function of pressure. (The curves are included to guide the eye and data presented in Appendix B, Table B.3).

In contrast to the wetting trend of OA on glass in SC-CO_2 at 40 ºC and 60 ºC, complete wettability was obtained at 80 ºC from 16 to 24 MPa (3.62±0.57º–3.43±0.63º), which is related to several effects, including the increase in the vapour pressure of the lipid, decrease of OA and CO_2 densities, and decrease of CO_2 solubility in OA at 80 ºC, but the final impact of those density differences on the complete wettability of OA on glass in SC-CO_2 is still unknown. In addition to the solubility effect, previous studies have also reported the effect of pressure and temperature of CO_2 on solids wetted by liquids. For example, Arif et al. (2016) used the Neumann's equation of state to determine the solid/CO_2 and solid/water surface energies based on the CA and IFT data from the literature using different types of surfaces, where they mentioned a similar fact indicated previously by Dickson et al. (2006) that the $\sigma_{S/V}$ values decreased when CO_2 pressure was increased at isothermal conditions. In contrast, $\sigma_{S/V}$ values increased with temperature because CO_2 cohesive energy density decreased, reducing the intermolecular interactions between solid/CO_2 (Arif et al., 2016). The findings of this study are in agreement with these previous studies, demonstrating that pressure and temperature significantly impact the wettability of lipids on glass surface in SC-CO_2 environment, not only due to the changes in the solubility of SC-CO_2 in lipids, but also the surface energy of those systems.

For the system of CanO/SC-CO_2 (Figure 4.4(B)), there were three different wetting patterns over the isotherms as pressure was enhanced from 16 to 24 MPa, such as complete wettability at 40ºC (7.24 ± 0.76º–3.77±0.35º), partial wettability at 60º C (21.40 ± 0.93º–20.04 ± 3.15º) and partial to complete wettability at 80º C (12.67 ± 2.17º– 3.64 ± 0.53º). At 40 ºC and 80 ºC, the CA decreased with pressure, as expected, based on the increased solubility of lipids in SC-CO_2 as well as the increased solubility of SC-CO_2 in the lipid phase. A similar trend could be visualized for the OA/SC-CO_2 system (Figure 4.4(A)). Both systems showed a similar behaviour in terms of the

overlapping of 40 ºC and 80 ºC isotherms above a certain pressure and higher CA values at 60 ºC. While for the OA/SC-CO_2 system the isotherms overlapped at 24 MPa (Figure 4.4(A)), it happened at >21 MPa to 24 MPa for CanO/SC-CO_2 (Figure 4.4(B)). These pressures were similar to the cross-over pressures of the solubility isotherms of lipids in SC-CO_2 (Güçlü-Üstündag & Temelli, 2004), due to the variations of density and vapour pressure as described above. Higher solubility of both lipids in SC-CO_2 at the higher pressures dominated the wettability behaviour on glass, resulting in lower CA_{eq} values. There was a remarkable enhancement of CA values at 60 ºC for both systems. The overall variation in CA values with temperature and pressure in the systems studied emphasizes the delicate balance between the two phases in equilibrium: drop phase of lipid saturated with CO_2 and the surrounding phase of SC-CO_2 saturated with lipid, which also results in the formation of a thin film on the solid surface. In addition to the effect of temperature on lipid solubility in SC-CO_2 described above, an increase in temperature also negatively affects CO_2 solubility in the lipid phase. As well, the formation of the thin vapour film located on the solid surface and its physicochemical properties would be also affected by temperature and pressure, shifting the CA values to a higher level at 60 °C. However, the unknown physicochemical properties of the CO_2-saturated vapour film of OA and CanO on the glass surface generates challenges to explain its role in the wetting phenomena. The conditions of higher solubility of SC-CO_2 in the lipid (i.e. high pressure and low temperature) led to low CA values, and the glass surface was completely wetted. In addition, higher interaction and affinity of the more polar OA with the OH groups of the silicon dioxide or barium oxide present in the glass contributed to more enhanced wetting than CanO.

4.3.4.1. Spreading dynamics of lipid droplets on glass in supercritical carbon dioxide

Previous studies have investigated the spreading dynamics of Newtonian and non-Newtonian fluids on different surfaces (Bertola, 2009; Carré & Eustache, 2000; Chen & Bertola, 2016); however, lipid/SC-CO_2 systems on different surfaces were not considered. For the first time, the spreading dynamics of corn oil on SS surface in SC-N_2 and SC-CO_2, was reported in Chapter 3, where the drop radius over time exhibited lower spreading velocity in SC-CO_2 than in SC-N_2 environment, which was associated to the higher solubility of CO_2 in the lipid phase and the formation of a thin film on the surface, but that was not the case for N_2. As presented in Figure 4.5, the evolution of the drop radius over time on glass surface was higher for the OA than for CanO under SC-CO_2 at 60 °C and 20 to 24 MPa. While for corn oil/N_2 and corn oil/CO_2 on the SS surface, the drop radius was up to 4.5 mm and 3 mm (Chapter 3), in the present study for the glass surface the drop radius for OA/CO_2 and CanO/CO_2 were up to 15 mm and 11 mm, respectively (Figure 4.5), and up to 5.5 mm for OA and CanO on glass in SC-N_2 (Figure B.1 in Appendix B). It is interesting to mention that even though the drop sizes were similar for lipids on surfaces in CO_2 environment, the drop diameter increased from 3 mm on SS up to 15 mm. This difference for lipid/CO_2 system could be related with several effects: a) solubility and rheological behaviour of different lipids saturated with SC-CO_2, b) type of surrounding fluid and c) the solid surface material.

As more SC-CO_2 was soluble in the lipid (as in OA) reducing its viscosity, the spreading velocity of the drop on the glass surface was higher, leading to a larger drop radius. As well, as pressure was increased at isothermal conditions, the wettability of both OA and CanO on glass in SC-CO_2 was enhanced. In contrast, when the CO_2 was less soluble in the lipid (as in CanO), the spreading velocity was lower. Therefore, solubility might play a significant role on the

(A)

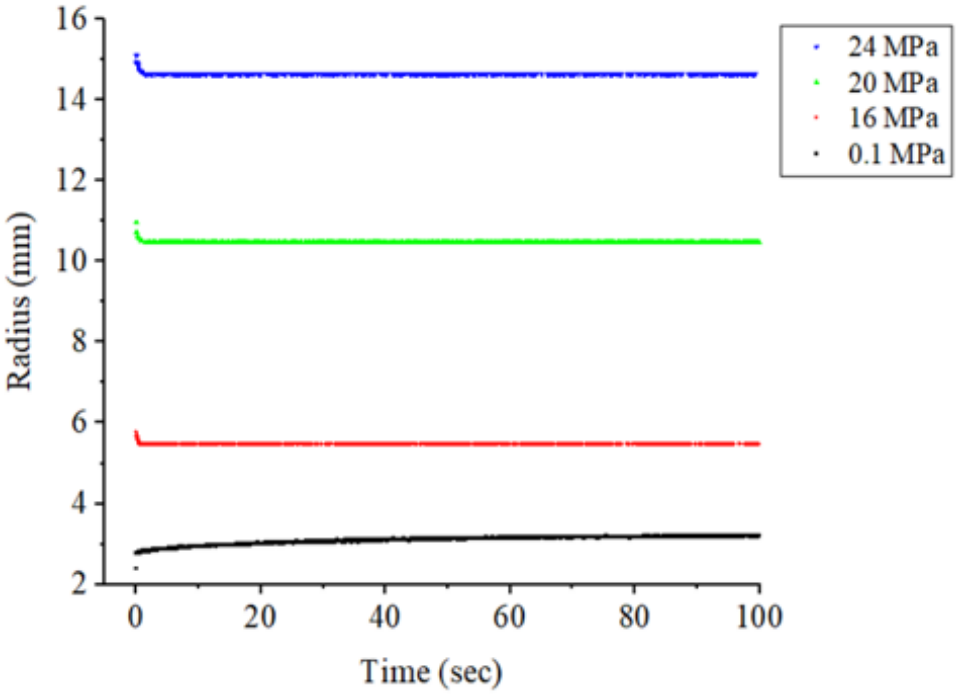

(B)

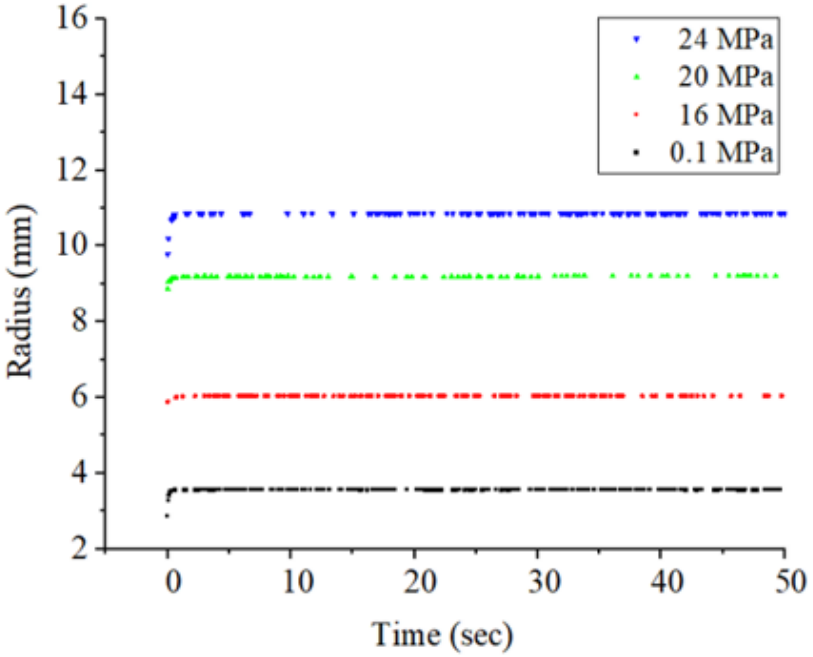

Figure 4. 5. Spreading radius versus time for (A) oleic acid and (B) canola oil in SC-CO_2 surrounding medium at 60 °C as a function of pressure.

characteristics of the thin vapour film on top of the glass surface, speeding or retarding the spreading velocity of lipids on glass in SC-CO_2, which could be associated with the unknown film physicochemical characteristics (density, viscosity, IFT). In addition, there are noticeable differences between the viscosities and rheological behaviour of the phases identified in the system (Figure 4.2). For the vapour phase of CO_2 saturated with lipids, the viscosity increased with pressure, exhibiting the common behaviour of a Newtonian fluid (Peter & Jakob, 1991; Yener et al., 1998); whereas forthe liquid phase of lipids saturated with CO_2, the viscosity decreased substantially with pressure, showing typical characteristic of a non-Newtonian, dilatant fluid (Ilieva et al., 2016; Jenab & Temelli, 2011; Seifried & Temelli, 2011, 2014). Therefore, considering the previous differences, it is important to deeply investigate and understand the effect of viscosity variations of both phases under different pressure and temperature conditions in relation to the formation of a droplet from dosing to its contact on the solid surface and spreading dynamics on different surfaces in SC-CO_2 environment. Also, those differences might induce the thin vapour film formed on the surface to have different viscosities, and thus different thicknesses as affected by the purity and composition of the lipid used; consequently, leading to different droplet phenomenon during dosing and contact with the surface.

Similar to Chapter 3, spreading dynamics was studied considering the power law dynamics, specifically Tanner's law, which represents the spreading of a viscous droplet that relies on the hydrodynamic spreading radius (r). It depends on diverse parameters such as the initial droplet radius (R_0), interfacial tension (γ), viscosity (μ) and spreading time (James et al., 2018), and its form ($r \sim f(t)^{\propto}$) varies independently of the surface wettability, where α is the apparent exponent, which describes the type of dynamics during spreading. The range of this apparent exponent allows the identification of the stage during the spreading dynamics, where $0.5 < \alpha < 1$ represents fast

dynamics at shorter times, while $0.1 < \alpha < 0.2$, describes the drop reaching a plateau (consistent with Tanner's law) (Eddi et al., 2013). In addition, the late stage spreading of viscous drops can also be predicted by Tanner's law (Eddi et al., 2013). Therefore, to identify the stages of the spreading dynamics of the OA and CanO droplets on glass surface in SC-CO_2 environment, the power law exponent of Tanner's law was determined at the different experimental conditions tested detailed in Table 4.1. This was possible through the log-log plot of drop radius versus time and the determination of the slope of each curve (Figure 4.6 for SC-CO_2 and Figure B.2 in Appendix B for SC-N_2). The values of the power law exponent were in the range of $0.00004 < \alpha < 0.05$ (Table 4.1), indicating that the drop had reached a plateau (Eddi et al., 2013).

Table 4. 1. Tanner's law exponent for oleic acid and canola oil on glass in SC-CO_2 environment as a function of pressure and temperature

Oleic acid			**Canola oil**		
Temperature (°C)	**Pressure (MPa)**	**α**	**Temperature (°C)**	**Pressure (MPa)**	**α**
40	0.1	0.029	40	0.1	0.001
	16	0.017		16	0.004
	20	0.019		20	0.049
	24	0.003		24	0.048
60	0.1	0.03	60	0.1	0.005
	16	0.00004		16	0.003
	20	0.003		20	0.005
	24	0.004		24	0.002
80	0.1	0.025	80	0.1	0.001
	16	0.005		16	0.003
	20	0.003		20	0.038
	24	0.055		24	0.021

α: Tanner's law exponent

(A)

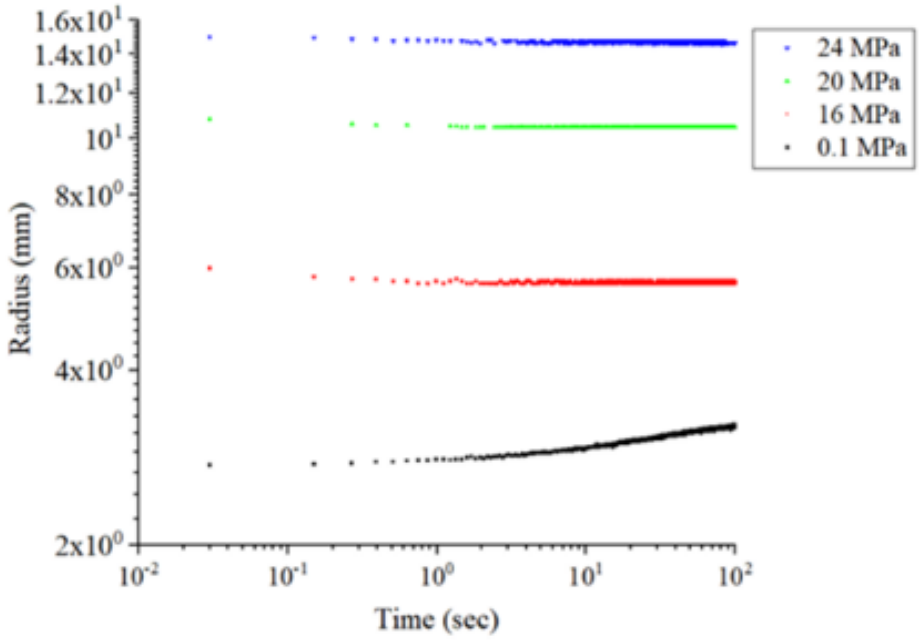

(B)

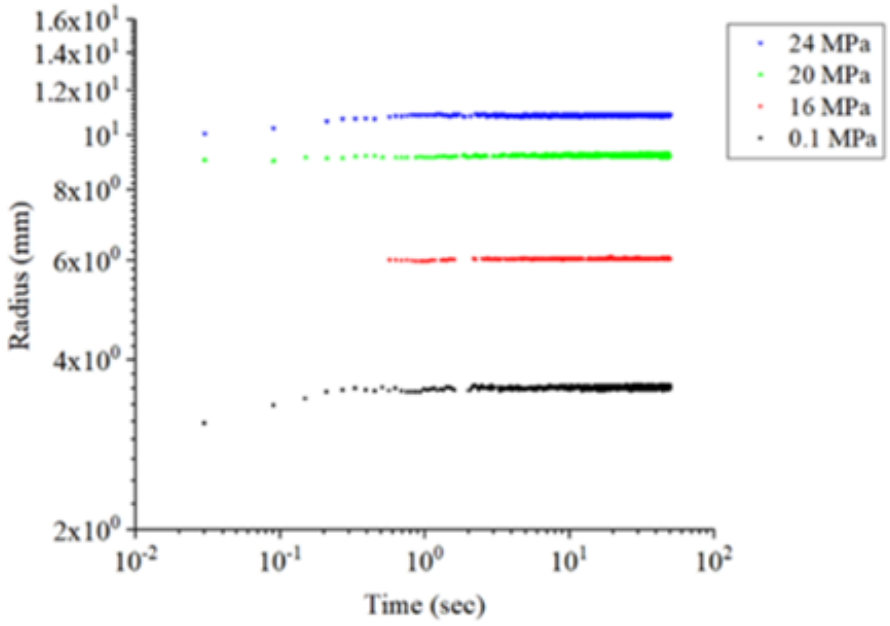

Figure 4. 6. Log-log representation of the spreading radius versus time for (A) oleic acid and (B) canola oil in SC-CO_2 surrounding medium at 60 ºC as a function of pressure.

However, it might be relevant to research the early and intermediate spreading dynamics under dense gases to better understand the phenomena observed in this study, for example, the formation of satellite droplets and SC fluid cavity observed in SC-CO_2, as described in the next section, which were not visualized in the previous study or under SC-N_2. The findings of this study together with those presented in Chapter 3 are novel in the field of the supercritical fluids in terms of the differences in the spreading velocity of the different lipid classes (OA, CanO and corn oil) on surfaces of different materials (SS and glass) in SC-CO_2.

4.3.5. Droplet phenomena of lipids on surfaces in supercritical carbon dioxide

4.3.5.1. Formation of satellite droplet of canola oil in supercritical carbon dioxide

Several studies have reported the formation of satellite and daughter droplets for different fluid systems (Ahmed et al., 2018; Banitabaei & Amirfazli, 2016; Lakdawala et al., 2015; Tjahjadi et al., 1992). For example, Ahmed et al. (2018) focused on the droplet deposition and detachment of a drop from the needle and the formation of satellite and daughter droplets in ferrofluid droplets on surfaces in the presence of a magnetic field. They generated the droplet similar to this study, considering that the droplet was detached from the needle because of its weight. Ahmed et al. (2018) explained that during the detachment process, there is a neck formation related to the opposition of body force and interfacial stress, which could be identified as a bridge between the needle and drop. Initially, the detachment process forms a large curvature that induces the neck to break. The lower side of the neck represents a new free surface that retracts towards the needle due to interfacial forces. Then, the other end of the fluid is detached from the needle by the action of breakup pressure and viscous nature of the fluid. Later, the two free sides of the neck minimize surface energy forming a satellite droplet, completely different from the first big droplet generated (Ahmed et al., 2018).

As shown in Figure 4.7, there was a satellite droplet (indicated with black arrow at -0.12 s) of canola oil saturated with CO_2 formed after the first liquid droplet was dosed, which was not observed for canola oil/SC-N_2 in this study or for the corn oil/SC-N_2 in the previous study (Chapter 3). This novel phenomenon in SC-CO_2 has not been reported previously, even though, it has been related to multiple other industrial processes, where the drop size is significant during the mass transfer between phases and interfacial chemical interactions, modelling transport processes and mechanical properties of blends (Tjahjadi et al., 1992). The understanding of this phenomenon in supercritical fluid technology will require further research to generate enhanced knowledge of fluid dynamics that might contribute to better design of various supercritical processes, including particle formation.

4.3.5.2. Cavity formation during spreading of lipid droplet on glass surface in supercritical carbon dioxide environment

The dynamics of droplet impact is a common phenomenon linked to several technical applications, for example, drug delivery, paints and coatings, delivery of pesticides and fertilizers in agriculture, and also related to atmospheric science (Caswell, 2014). There are possibilities of bubble entrapment of SC phase under the lipid droplet as shown in Figure 4.7 (indicated with red arrow at -0.09 s), where the formation of a SC fluid cavity was visualized during the spreading of lipid droplets on glass in SC-CO_2, but not in SC-N_2. As Chen et al. (2017) explained, two versions of bubble entrapment had been identified at different time scales during the impact of liquid droplets on surfaces. During early spreading dynamics (< 1 ms), at the moment of the droplet contact with the surface, there is the formation of a small bubble ranging from a few tens to hundreds of micrometers trapped beneath. As a consequence of the bubble formed between the droplet and thin film, there is a pressure build-up that deformed the lower cap of the droplet. Later,

at times between 1 to 10 ms and low impact velocities, a cylindrical CO_2 cavity is generated in the centre of the droplet by a series of capillary wave oscillations propagated along the droplet impact on the surface. This cavity is closed during the bouncing of the droplet, forming a submillimetre-sized surrounding fluid bubble. Moreover, there are aspects which might influence the occurrence of this SC fluid cavity formation in lipid/solid/SC-CO_2 systems, for example, surface wettability (Chen et al., 2017) , viscosity of phases, roughness and material of the surface.

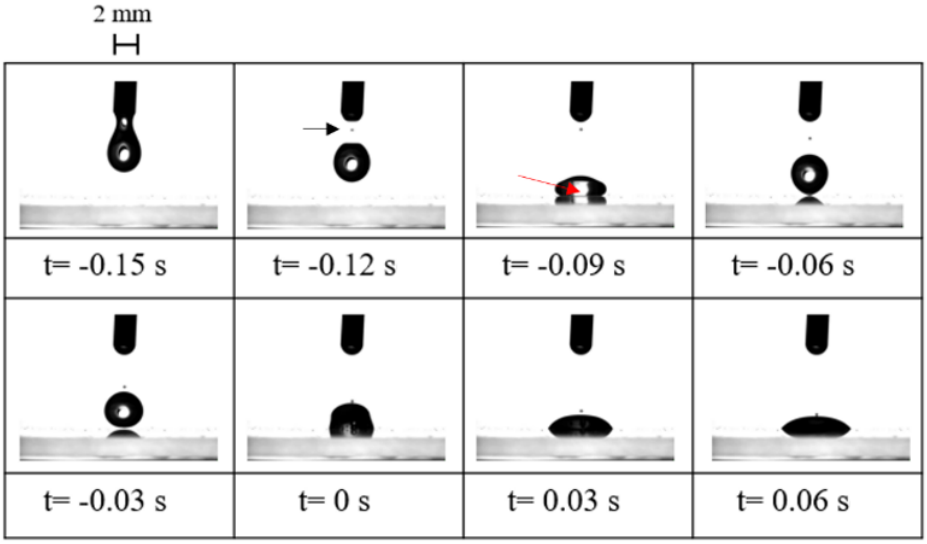

Figure 4. 7. Bouncing of the canola oil droplet on glass surface in saturated SC-CO_2 at 60 ºC and 16 MPa with identification of satellite droplet and cavity formation (black and red arrows, respectively).

In this study, it is challenging to clarify the occurrence of this event based on the late spreading dynamics (section 4.3.4.1) characterization of these experiments. It is possible to infer that based on the differences in the viscosity and density of SC-N_2 and SC-CO_2, their solubility differences in lipids, and the formation of thin vapour film on top of the surface before drop impact and spreading (Leidenfrost phenomena) contributed to the formation of the SC fluid cavity underneath the lipid droplet and bouncing phenomena. However, future studies on spreading of

droplet dynamics of lipids on surfaces in a SC fluid environment might be developed to better understand all the novel findings, considering more sophisticated dosing systems and having a complete dataset for all the physicochemical properties of phases at the high-pressure conditions for binary, ternary and multicomponent lipid mixtures.

4.3.5.3. Bouncing and sliding of lipid droplets on polished glass surface in supercritical carbon dioxide environment

Bouncing of corn oil droplets on SS surfaces in SC-CO_2 but not in SC-N_2, was a novel phenomenon visualized in Chapter 3. A similar bouncing phenomenon was observed in this study for the systems OA and CanO on glass surface in SC-CO_2 but not under SC-N_2 (Figure 4.7 at -0.03 s). Previously, in Chapter 3, the bouncing of corn oil on SS surface in SC-CO_2 was linked with the dynamic-Leidenfrost phenomenon, which also applies in the present case, where the thin vapour film formed on the solid surface absorbs the initial energy of the lipid droplet and results in the bouncing of droplet, with the drop taking back its initial spherical shape to minimize its surface energy (Carré & Eustache, 2000). Initially, the liquid drop does not spread on the surface, due to the presence of the vapour film on the surface, and thus the energy dissipation is reduced with more of the initial kinetic energy being available for its bounce until all of the drop's kinetic energy is dissipated (Carré & Eustache, 2000). There may be several reasons behind the occurrence of bouncing phenomena of lipids on surfaces in SC-CO_2, including the viscosity and solubility differences between the two phases as described above. In addition, the presence of the thin vapour film might modify the surface energy variation and the liquid's affinity to the surface by covering a significant portion of the wetted area. Van der Waals forces between the solid and thin vapour film might be responsible for film collapse when the vapour film becomes unstable on the smallest length scales (Chen et al., 2017). However, the bouncing phenomenon observed here is not

serendipity since it can be observed with any liquid-solid combination when the minimal impact conditions (impact velocity, density of phases, surface tension, wettability, and roughness of the surface) are present.

The bouncing was not observed in SC-N_2 due to its negligible solubility in the lipids and vice versa, reducing the possibility of thin vapour film formation and bouncing in this environment. Therefore, more information is needed on the influence of the type of fluid and its physicochemical parameters at supercritical conditions on the bouncing of drops on different surfaces. Another interesting phenomenon visualized in this study, which to the best of the author's knowledge has not been reported previously, was the sliding of canola oil droplet on glass surface in SC-CO_2 at 40 ºC and 16 MPa (Figure 4.8). It is a novel phenomenon, which requires further research and understanding to evaluate the implications for potential process design.

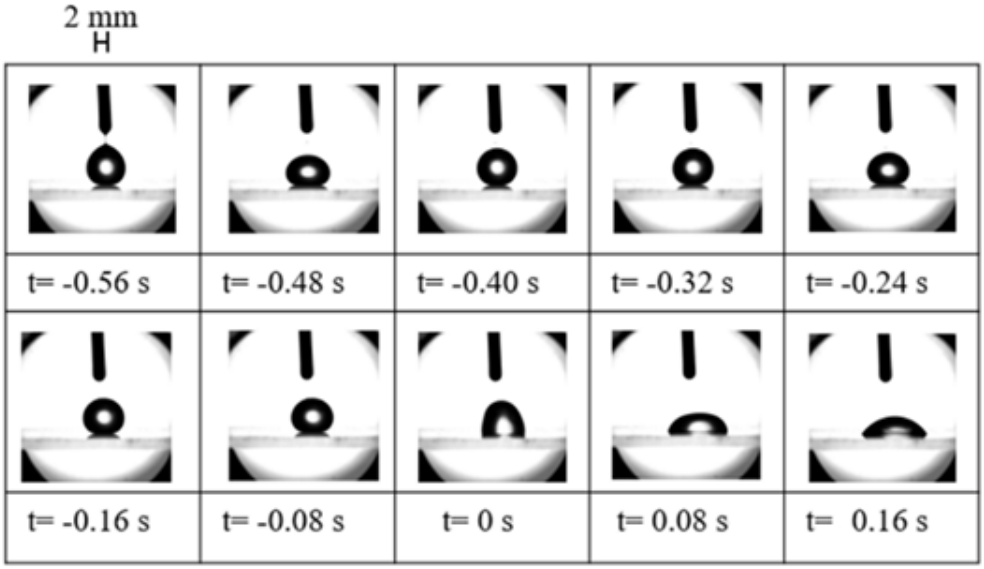

Figure 4. 8. Sliding of the canola oil droplet on glass surface in saturated SC-CO_2 at 40 ºC and 16 MPa.

4.4. Conclusions

The interfacial tension of OA and CanO in SC-CO_2 determined at 60 ºC and pressures of up to 24 MPa showed a remarkable decrease with pressure due to the increase in CO_2 density, resulting in a smaller density difference between the drop and surrounding phases and higher miscibility between the phases. The wettability behaviour of different types of lipids on diverse surfaces in SC fluids was determined by the CA_{eq} of OA on glass, and CanO on glass and SS surfaces in SC-CO_2 and SC-N_2 environments at different temperatures and pressures. The CA_{eq} of OA and CanO on glass surface showed a similar trend, with higher values in SC-N_2 than in SC-CO_2 environment at 60 ºC and pressures of up to 24 MPa. Higher solubility of SC-CO_2 in the lipid phase, film formation on the surface, altering the liquid/surface interactions, CO_2 adsorption on the glass surface contribute to the lower CA_{eq} values obtained in SC-CO_2 medium.

Diverse wetting patterns were observed for the lipids (OA vs CanO) tested on glass. While the OA/SC-CO_2 system on glass exhibited partial to complete wettability at 40 ºC and 60 ºC, complete wettability was obtained at 80 ºC from 16 to 24 MPa. In contrast, the system of CanO/SC-CO_2 on glass surface exhibited three different wetting patterns with complete wettability at 40 ºC, partial wettability at 60 ºC and partial to complete wettability at 80 ºC with an increase in pressure. With respect to the type of surface, while the CA values of CanO on SS surface was <10º (similar to that of corn oil reported previously in Chapter 3) it was >15º on glass at 60 ºC and 20 MPa due to the differences in surface composition and energy. In relation to the spreading dynamics, the radius of the OA and CanO droplets on glass surface in SC-CO_2 (up to15 and 11 mm, respectively) were higher than those reported previously in Chapter 3 for corn oil/N_2 and corn oil/CO_2 on SS surface (up to 4.5 and 3 mm, respectively). Also, the values of the power law exponent indicated that the drop had reached a plateau.

The wettability experiments of the lipids on different surfaces in SC-CO_2 (but not in SC-N_2) showed diverse and novel phenomena in the field of SC fluids, for example, a) the formation of a satellite droplet of canola oil saturated with CO_2, which was observed after the first liquid droplet was dosed, and b) formation of SC fluid cavity during the spreading of lipid droplets on glass in SC-CO_2. In addition, the bouncing of OA and CanO droplets on glass surface in SC-CO_2 was observed, similar to the corn oil/CO_2 system on SS surface reported in Chapter 3. Another interesting phenomenon visualized, which to the best of the author's knowledge has not been reported previously, was the sliding of canola oil droplet on glass surface in SC-CO_2 at 40 ºC and 16 MPa and further research is needed to evaluate the implications for potential process design.

Chapter 5. Effect of packing material on free fatty acid separation efficiency and liquid hold-up during countercurrent fractionation of a lipid mixture using supercritical carbon dioxide[c]

5.1. Introduction

Lipids and bioactive components have been isolated from complex lipid mixtures using conventional solvent extraction and supercritical fluid extraction, including column fractionation with supercritical carbon dioxide (SC-CO_2) to either separate heavier from lighter molecular weight lipids (glycerides, fatty acids, fatty acid esters) or recover minor lipid compounds (phytosterols, tocopherols, carotenoids, eicosapentaenoic acid, docosahexaenoic acid) from fish oil or oil refining by-products such as deodorizer distillates (DOD). Previous studies detailed in Chapter 2 (Table 2.1) (Stockfleth & Brunner, 1999, 2001; Ibáñez et al., 2002; Zacchi et al., 2006; Brunner & Machado, 2012) on the fractionation of complex lipid mixtures using random and structured packings of different materials (stainless steel (SS), Teflon, glass) and geometries have revealed diverse separation efficiencies of lipids without explaining if the type of packing material and/or geometry has an impact on the liquid hold-up within the column and separation efficiency of target compounds. The amount of liquid inside the column is called liquid hold-up and it is classified as static (SH) and dynamic hold-up (DH). DH is the liquid that drains out of the column once the gas and liquid pumps are stopped; in contrast, the SH does not drain from the column because it is adhered on the packing elements by adhesive forces, and must be removed by other means, for example, by pumping CO_2 inside the system at higher pressure and temperature

---

[c] A version of this chapter is in preparation to be submitted to the *Journal of Supercritical Fluids* for consideration for publication.

(Stockfleth & Brunner, 2001). Lack of information about the role of the type of packing on the liquid hold-up (SH and DH) for different lipid mixtures while they interact with SC-CO_2 medium under different processing conditions has been the motivation of this study. The objective of this study was to determine the effect of the type of packing on the separation efficiency of lipid classes and liquid hold-up during the fractionation of a complex lipid mixture using a countercurrent column with SC-CO_2 as the solvent at different experimental conditions (solvent-to-feed (S/F) ratios of 15 and 25, pressures of 16 and 24 MPa and temperatures of 40°C, 60°C and thermal gradient of 60-100°C).

5.2. Materials and methods

5.2.1. Materials

A model mixture of 85 wt% free fatty acids (FFA) and 15 wt% triacyglycerols (TAG) was used as the feed for the fractionation process. Even though the original goal was to isolate free and esterified phytosterols from canola DOD and evaluate the effect of the type of packing on their separation efficiencies, this had to be modified and the feed mixture had to be simplified due to the different challenges encountered. It was challenging to pump the canola DOD as well as model mixtures containing phytosterols into the fractionation column due to equipment limitations, resulting in the need to reformulate the lipid mixture composition of this study. The initial canola DOD and the model mixture of phytosterols exhibited crystalized solid lipid particles at room temperature (22 °C) and even after heating up to 40 °C, which was the upper limit of the operating temperature range for the feed pump. The presence of these solid lipid particles resulted in the blockage and damage of the feed pump, forcing the reformulation of the feed mixture. Considering the previously reported composition of canola DOD by Güçlü-Üstündağ and Temelli (2007) (GC area (%): volatiles: 7.10%; FFA: 61.52%; monoacylglycerols: 4.78%; squalene: 0.43%;

tocopherols: 6.66%; phytosterols: 11.53%, diacylglycerols: 2.42% and triacyglycerols: 1.86%), the model mixture formulated for this study was composed of 85% FFA and 15% TAG, intended to mimic the ratio of FFA to acylglycerols in canola DOD while avoiding further equipment problems and operational issues. This ratio was selected based on experiments performed by combining different ratios of FFA and TAG, where lipid solid particles were suspended in the lipid mixture when FFA% was 20%, and therefore 85% FFA and 15% TAG was the most favorable ratio in combination with equipment specifications.

The FFA mixture (based on supplier information, composed of 79.2% oleic acid (OA), 7.5% stearic acid and 12.4% linoleic acid based on GC area %) was purchased from Bulk Natural Oils (Braintree, MA, USA), and canola oil ("Mazola", ACH Food Companies, Inc., Memphis, TN, USA) was purchased from a local market for use as TAG in the model mixture. The following chemicals were used for the FFA percentage determination: 99% stearic acid (Nu-Chek Prep Inc, Elysian, MN, USA) to test the modified analytical method; sodium hydroxide (1 N) and all solvents, including toluene, ethanol, isopropanol, and methanol were ACS grade (≤95% purity), and they were obtained from Fisher Scientific Canada (Ottawa, ON, Canada). Phenolphthalein, used as the indicator during the titrations, was obtained from Tero Chem Laboratories Ltd. (Edmonton, AB, Canada).

5.2.2. Fractionation column

The supercritical fluid fractionation packed column used during this study was previously built and described in detail by Güçlü-Üstündağ and Temelli (2007), which operated in semi-batch mode to isolate minor lipid compounds from canola deodorizer distillate. However, to achieve the objectives of this study, the fractionation column was modified substantially and rebuilt to operate in continuous countercurrent mode, as shown in Figure 5.1. The packed column (height: 218 cm,

2.54 cm o.d., 1.75 cm i.d.) consisted of four sections (42 cm each) and a calming section (36 cm), which were connected by cross or tee fittings (five along the column, 10 cm each). The column was packed three times with different packing materials, which consisted of perforated stainless-steel Pro-Pak® (PS) (Cannon Instrument Company, State College, PA, USA), stainless steel beads (SB) (Abbott Ball Company, Inc., West Hartford, CT, USA) and glass (borosilicate) beads (GS) (DWK Life Sciences, LLC, Rockwood, TN, USA), with the specifications detailed in Table 5.1.

For the introduction of CO_2, a pneumatic booster pump (Haskel booster pump; model AG-152; Serial No. 607-226; Burbank, CA, USA) was used. A loop with a back pressure regulator (BPR) (TESCOM 26-1721, Mississauga, ON, Canada) was installed around the pump to control column pressure while maintaining CO_2 flow. The pump transported the CO_2 from the gas cylinder to the column at the bottom of section 4 (Figure 5.1). On the other hand, the feed was introduced at the bottom of section 1 (Figure 5.1) using a reciprocating pump (ReaXus Model 6010R Reciprocating pump, Teledyne ISCO, Lincoln, NE, USA) at the specified volumetric flow rate.

The column can be operated isothermally or with a thermal gradient through heating jackets and thermocouples (Type J), placed on the outer wall in the middle of each section and connected to temperature controllers (Omega Environmental, St-Eustache, QC, Canada), allowing individual control of this parameter for each section. The inlet (feed and CO_2) and exit lines (extract and raffinate) of the column, as well as the micrometering valve at the end of the extract line, were also equipped with heating ropes and thermocouples attached to separate controllers and were thus temperature controlled. Throughout the process, the pressure was monitored in the column, and inlet and exit lines by pressure gauges.

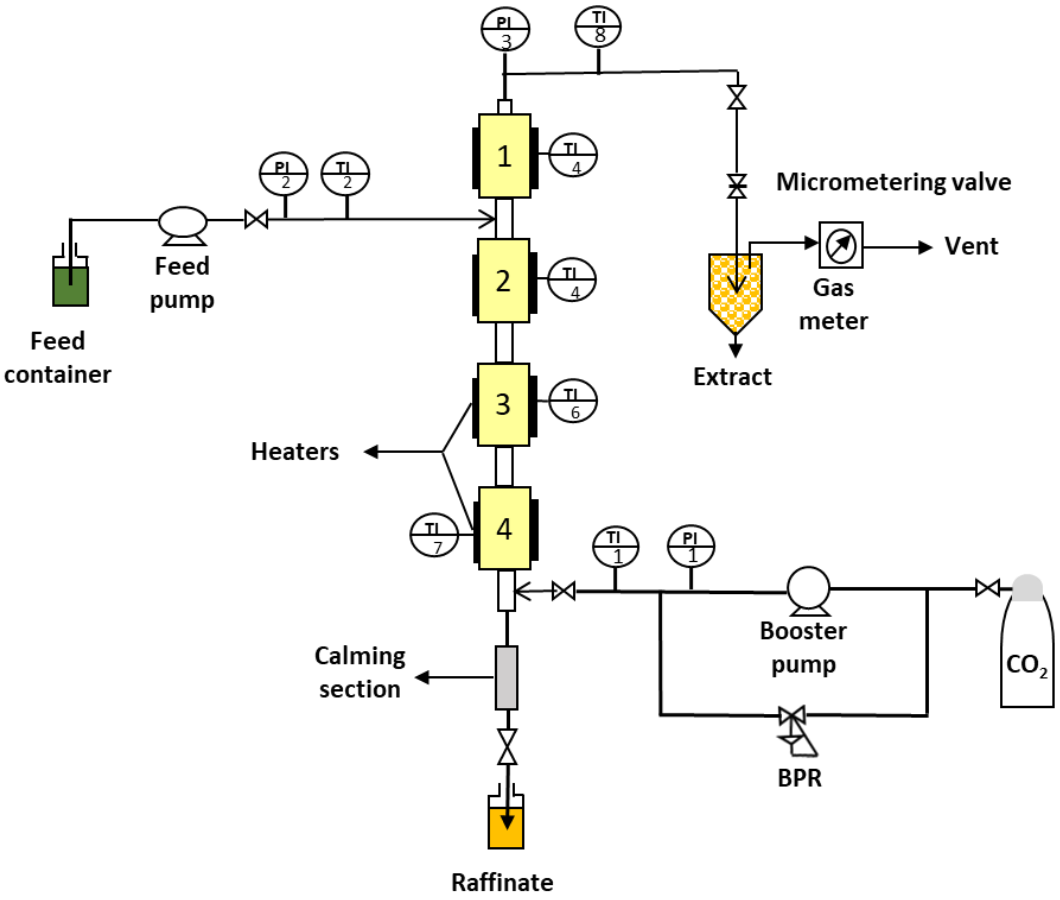

Figure 5. 1. Schematic of the supercritical fractionation column equipment with respective column sections (1, 2, 3 and 4), pressure indicators (PI) and temperature indicator (TI).

To achieve the desired solvent-to-feed ratio (S/F, wt/wt), feed and CO_2 pumps were calibrated at process conditions simultaneously, controlling the extract flow rate using the micrometering valve. The raffinate fraction accumulated in the calming section and was removed every 30 min from the bottom of the column, using an on/off valve, at the end of this section. In contrast, the extract fraction flowed out from the top of the column continuously through the extract line before passing through the micrometering valve and depressurized. The depressurized liquid extract was collected in a vial placed inside a heating jacket maintained at 25 °C to avoid the freezing of collection tubing, and CO_2 was passed through a gas meter to determine the volume

of gas prior to venting to the exhaust. All column components (rated at 68.8 MPa) were manufactured by Autoclave Engineers Inc. (Erie, PA, USA) and purchased from Zimco Valves and Tubings (Calgary, AB, Canada). All electrical/heating components were supplied by Tru-temp Electric Heat Ltd. (Edmonton, AB, Canada).

Table 5. 1. Packing characteristics

Packing Material		Packing size (cm)	Void volume (%)	Packing density (kg/m^3)	Surface area (cm^2/cm^3)
Pro-Pak® (PS)		0.4 x 0.4	94	437.30	18.89
SS beads (SB)		0.6	44	4622.84	6.97
Glass beads (GB)		0.6	40	1293.86	7.43

5.2.3. Fractionation column operation

Continuous countercurrent fractionation of a model mixture (85% FFA and 15% TAG) was carried out to determine the influence of the type of packing (PS, SB, GB), pressure (16 and 24 MPa), temperature configuration (isothermal at 40, 60 °C and thermal gradient (60-100 °C)), and S/F ratio (15 and 25 wt/wt, where feed flow rate was 0.67 g/min at 15 S/F and 0.4 g/min at 25 S/F and CO_2 flow rate was constant at 10 g/min) on the extract yield (%), separation efficiency (SE)

of free fatty acids (FFA) and liquid hold-up. The thermal gradient was established by independent control of the temperature of each of the 4 sections of the column at 60, 70, 90 and 100 °C, increasing from the bottom to the top of the column. Each section was equipped with an independent heating jacket, thermocouple and temperature controller, which allowed to operate the column in thermal gradient mode.

First, the column, and inlet and exit lines were heated to achieve the desired experimental thermal condition. Then, the system was pressurized at the CO_2 cylinder pressure and allowed to stabilize. After that, the targeted column operating pressure was reached utilizing the pneumatic booster pump. Once the temperature and pressure reached the desired levels and stabilized, the operation was started by pumping both feed and CO_2 into the column, ensuring the pressure in the liquid feed line was at least 0.7 MPa higher than that in the CO_2 line, to achieve countercurrent mode of operation. The gas flow rate and S/F ratio were regulated by manually adjusting the micrometering valve, placed at the end of the extract line.

The extract stream leaving the column was depressurized to atmospheric conditions and hence the liquid extract was separated from the CO_2 stream and collected in a vial, whereas the CO_2 was vented. Extract fractions were collected every 30 min and each experiment was continued for 180 min. The extract vials were placed inside a desiccator overnight to release the remaining CO_2 prior to FFA% quantification as described in section 5.2.4 The total extract amount was determined gravimetrically as the sum of the weights of extract fractions collected from 60 to 180 min. It is important to mention that no sample was collected in the first half hour at some experimental conditions, and therefore data for the total of five fractions were reported. Based on Güçlü-Üstündağ and Temelli (2007), the first 30 min corresponded to the residence time depending on the column dimensions, CO_2 flow rate and column volume.

After each 3 h run, the DH was collected by shutting down gas and feed pumps, closing the on/off valves on CO_2, feed and extract lines, and opening the on/off valve located at the bottom of the calming section. After the collection of DH, the column was pressurized again with CO_2 at the same experimental conditions, and the lipids remaining on the packing material were allowed to solubilize into the CO_2 phase over 60 min in a batch mode operation.

The column was cleaned with CO_2 at 25 MPa and the same temperature at which the experiment was performed for 90 min after each run or until no more liquid was removed from the column.

5.2.4. FFA content and FFA separation efficiency

FFA content was determined following the ASTM official method (ASTM-D5555-95) (ASTM International, 2017) to evaluate the acid value applicable to all neutral and synthetic drying oils, epoxidized, fatty alcohols and fatty esters. However, this method was modified to be able to handle the small sample sizes of 0.4 g or less, representing the extract fractions collected in this study.

Initially, 0.4 g of sample was added into 125 mL Erlenmeyer flask, together with 20 mL of 50/50 v/v/ of solvent mixture (isopropanol and toluene) and 40 µL of phenolphthalein (indicator solution) (1% in 95% ethanol) (solution #1). Another solution was prepared as a blank with 20 mL of distilled water and 40 µL of indicator solution (solution #2). Then, the NaOH solution was standardized from 1 N to 0.05 N. First, 50 mL of 1 N NaOH were added into 2 L calibrated volumetric flask and completed with methanol (solution #3). Secondly, 0.2 g of potassium phthalate monobasic was added into a 100 mL volumetric flask, where 40 µL of indicator solution was added and completed with distilled water (solution #4). Third, the solution #4 was used to

titrate solution #3 to determine the final normality of the NaOH (N_{std}) to be standardized, based on Eq. (5.1)

$$N_{std}=\frac{1000 \text{ x g phthalate}}{\text{MW phthalate x NaOH vol consumed}} \quad (5.1)$$

where, "g phthalate" is 0.2 g, molecular weight (MW) phthalate is 204.22 g/mol and "NaOH vol consumed" is the volume of NaOH required to neutralize solution #3. After knowing the normality of the NaOH, it was used to titrate the sample solution or solution #1 and solution #2 to get the acid value (AV), which is commonly defined as the amount of alkali needed to neutralize 1 g of sample. The AV was determined using Eq. (5.2).

$$AV=\frac{\text{volume of NaOH consumed x Nstd x 56.1}}{\text{mass of test sample (g)}} \quad (5.2)$$

where, the "volume of NaOH consumed" is the difference between the volume of alkali consumed to neutralize a blank solution (solution #2) and the volume of alkali used to neutralize sample solution (solution #1); N_{std} is the normality of NaOH determined by standardization; and 56.1 g/mol is the molecular weight of alkali (KOH), which is used for the conversion factor given in the ASTM method. The level of FFA is commonly expressed as acid value instead of FFA%. However, to convert AV into FFA%, the AV is multiplied by 1.99 based on the ASTM standard method.

5.2.4.1. Confirmation of the modified analytical method for FFA content determination

The modified method was confirmed by establishing a calibration curve of FFA content for FFA + TAG mixtures, with FFA content ranging from 0 to 100% and the result is shown in Figure 5.2 with R^2 value of 0.999. Then, a pure stearic acid sample (99% purity) was analyzed three times and its acid value was determined as 201.14±2.16 and the FFA% was 101.07±1.08%,

confirming that the modified ASTM-D5555-95 method was accurate enough to determine the FFA% in the lipid samples obtained in this study.

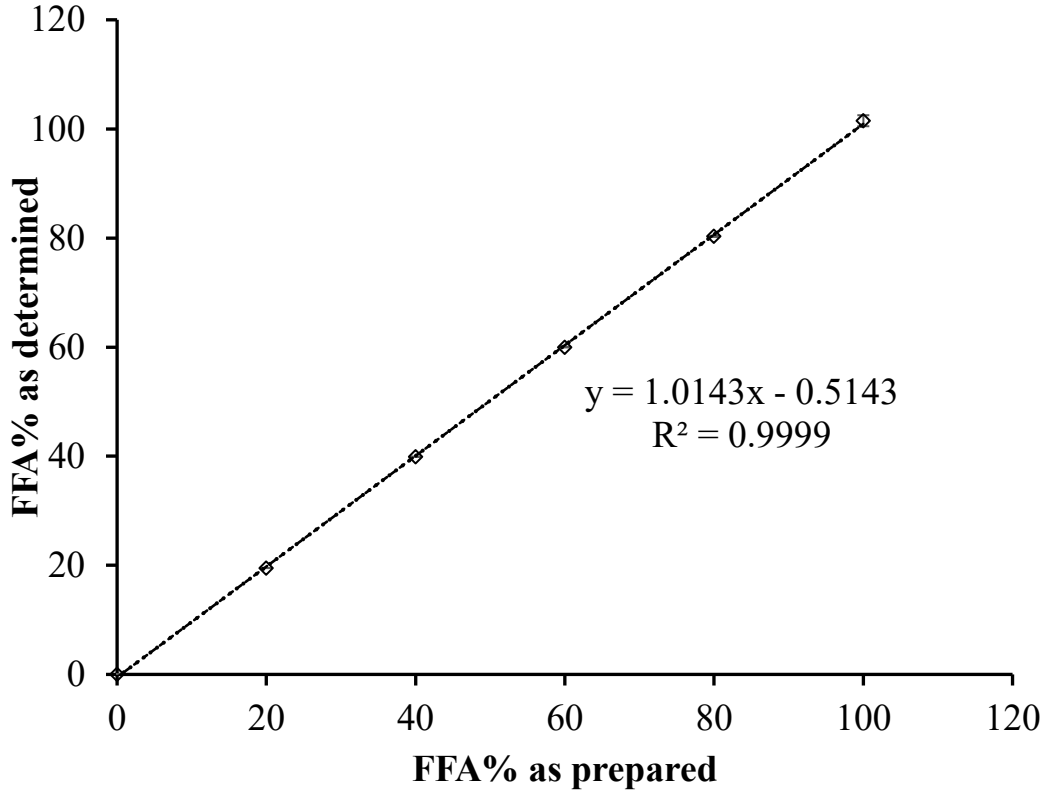

Figure 5. 2. Calibration curve for the modified method for FFA content

5.2.4.2. Extract yield (%) and FFA separation efficiency (FFA-SE)

The extract yield was determined based on the ratio between the overall amounts of extract collected and feed pumped in over 180 min of operation for each experiment, multiplied by 100, according to Eq. (5.3):

$$\text{Extract yield (\%)} = \frac{\text{extract amount over 180 min (g)}}{\text{feed amount over 180 min (g)}} * 100 \quad (5.3)$$

The FFA-SE was determined for each run based on the ratio of the FFA amount in the extract collected to that in the feed according to Eq. (5.4):

$$\text{FFA} - \text{SE} = \frac{\text{FFA (g) extract}}{\text{FFA (g) feed}} \text{ x } 100 \quad (5.4)$$

where, the 'FFA(g) extract' is the amount of FFA in the extract collected over a specific period of time, and the 'FFA (g) feed' is the amount of FFA in the feed, which was determined by multiplying the amount of feed sample pumped into the column over the same specific period of time and the FFA% in the feed mixture (85%).

5.2.5. Statistical analysis

Two sets of experiments were performed: Set 1 was designed to evaluate the effects of temperature (40 °C and 60-100 °C) and types of packing at constant pressure of 16 MPa at 15 S/F ratio, while Set 2 focused on the effects of S/F ratio (15, 25), pressure (16, 24 MPa) and types of packing at the constant temperature of 60 °C. Experiments in Set 1 were performed in duplicate whereas those in Set 2 were carried out in triplicate. Results were presented as mean ± standard deviation (SD). Analysis of variance (ANOVA) and Tukey's test at a significance level of $\alpha = 0.05$ were performed using the Minitab® Statistical Software (version 21.3.1.0, Minitab Inc., State College, PA, USA), to determine the effects of the pressure, temperature, S/F ratio and type of packing on the extract yield, FFA-SE, and DH amount Moreover, Pearson correlation analysis was performed between FFA-SE and DH amounts using Microsoft Excel.

5.3. Results and discussion

5.3.1. Steady state condition

To confirm that steady-state condition, based on constant weight and composition of the extract (Dunford et al., 2003), was reached during the column operation, extract fractions were collected every 30 min over 3 h, weighed and FFA concentration was determined. Some of the

results are presented in Figure 5.3 for the case of the column packed with GB and SB, operating at 60 °C, 16 MPa and 25 S/F ratio, which were typical for the other conditions tested. According to the previous studies on the fractionation of lipid mixtures at different experimental conditions (Dunford et al., 2003; Riha & Brunner, 2000; Ruivo et al., 2001), it was expected to reach steady state after 1 h. The average amount of each extract fraction collected over time from 60 to 180 min was approximately 1 g (Figure 5.3(A)) despite some variation and the FFA content of each fraction was consistently around 100%, compared to the feed model mixture containing 85% FFA. Therefore, it was concluded that steady state was reached after 60 min of operation.

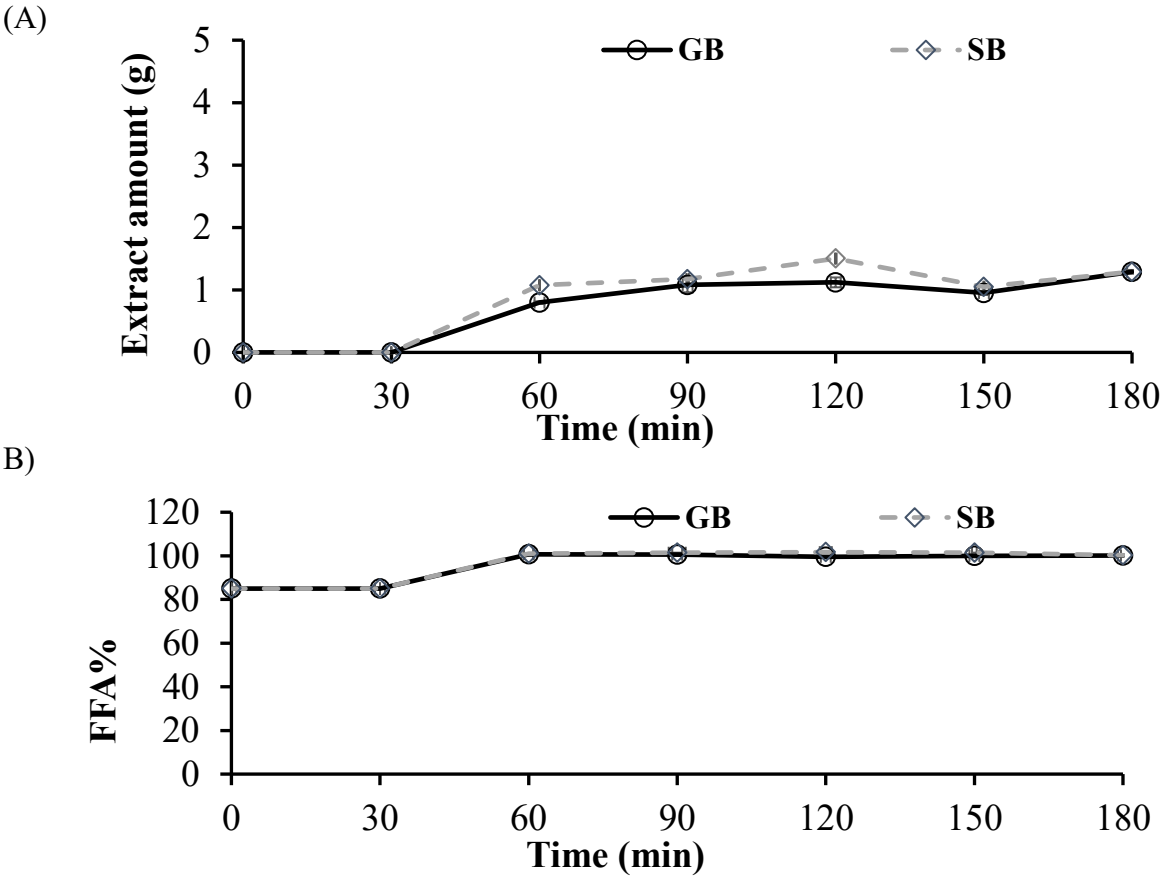

Figure 5. 3. (A) Extract amount and (B) FFA% of extract fractions when glass beads (GB-continuous black line) and stainless-steel beads (SB-dashed grey line) were used as packing at 60 ºC, 16 MPa, 25 S/F ratio collected every 30 min over 3 h of operation.

5.3.2. Effect of process conditions on extract yield

5.3.2.1. Effect of temperature configuration and type of packing

To understand the effect of temperature on the extract yield, isothermal (40 °C) and thermal gradient (60-100 °C) conditions were considered for the three types of packings at 16 MPa and 15 S/F ratio as shown in Figure 5.4. There was a significant effect of temperature ($p < 0.05$), whereas the effects of packing and interaction between the variables were not significant ($p > 0.05$). This was expected based on the effect of temperature on CO_2 density, which dictates the lipid solubility behaviour. The CO_2 density was 794.90 kg/m^3 at the isothermal condition of 40 °C and 16 MPa, whereas it decreased from 637.50 kg/m^3 at 60 °C to 363.69 kg/m^3 at 100 °C for the thermal gradient (NIST, 2005) showing that CO_2 has higher solvent power at lower temperature. Additionally, on the solubility aspect, at 16 MPa and 40 °C, the OA solubility was reported as 4.98 g of OA/100 g CO_2, while at 60 °C it was 4.13 g of OA/100 g CO_2 (Zou et al., 1990), demonstrating higher solubility at lower temperature and higher CO_2 density. Therefore, it was expected that at 40 °C, lipid solubility in the CO_2 phase would be higher, enhancing the extract yield at this condition relative to those at 60-100°C (Figure 5.4). Moreover, there was no effect of packing on extract yield because it is possible that at constant pressure and S/F ratio, the temperature effect on CO_2 density dominates any variability of extract yield due to packing geometry and material.

5.3.2.2. Effect of pressure, S/F ratio and type of packing

To determine the effects pressure, S/F ratio and type of packing on the extract yield, the experiments were performed at constant temperature of 60 °C and different pressures (16 and 24 MPa), S/F ratio (15 and 25) and types of packings (PS, SB, GB) and the results were presented in Figure 5.5. At each S/F ratio, the effects of the type of packing, pressure and the interaction between these two variables were significant ($p < 0.05$).

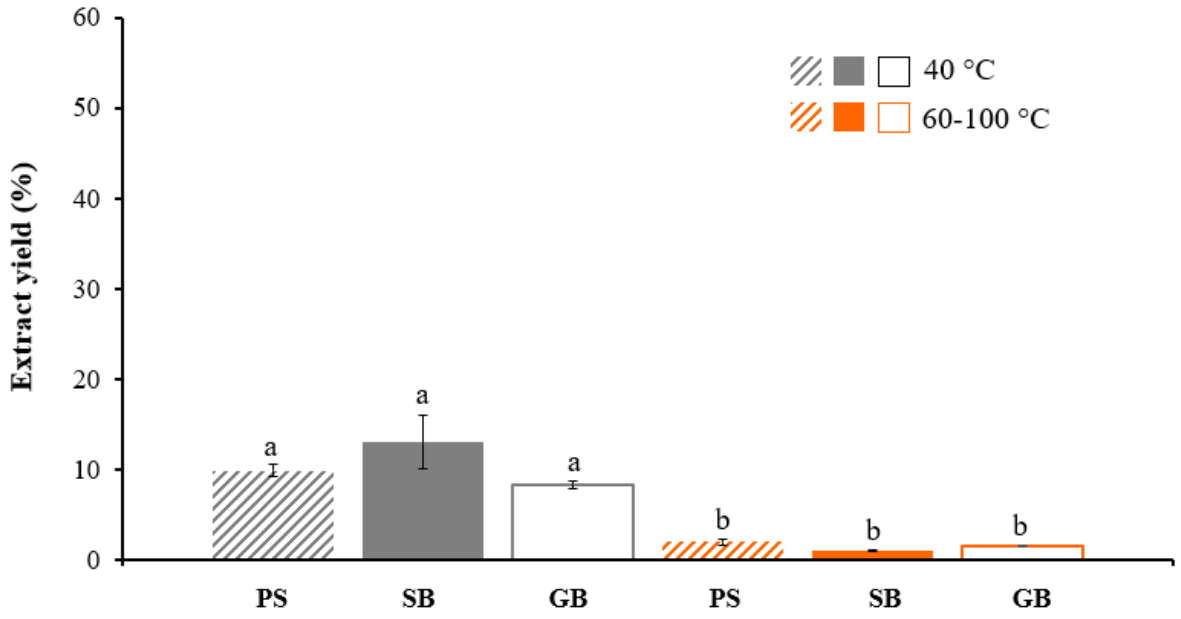

Figure 5. 4. Extract yield obtained at 16 MPa and 15 S/F ratio at different temperature profiles, isothermal (40 ºC, grey bars) and thermal gradient (60-100 ºC, orange bars), and different packings (PS perforated stainless steel, (hatched bar); SB stainless steel beads (solid bar); GB glass beads (blank bar)). [a,b] Bars with different letters are significantly different at $p < 0.05$ (Data presented in Appendix C, Table C.1).

The pressure effect on the extract yield was substantial because at higher pressures, the CO_2 density is higher as well as its solvent power, thus, there is more solubilization of lipids into the CO_2 phase and more lipids are collected in the extract stream. Furthermore, at the higher S/F ratio of 25, the extract yields were higher than those at the lower S/F ratio of 15, which was anticipated because at higher S/F ratio, there is a relatively larger amount of CO_2 available to solubilize lipids, resulting in a higher amount of lipid in the CO_2 phase and a higher amount of extract collected. Moreover, in relation to the same packing material with different geometry, there was less probability of lipid retention and more effective interfacial area for lipids to be solubilized into the CO_2 phase in the PS compared to SB, leading to higher extract amounts at S/F 25 and

(A)

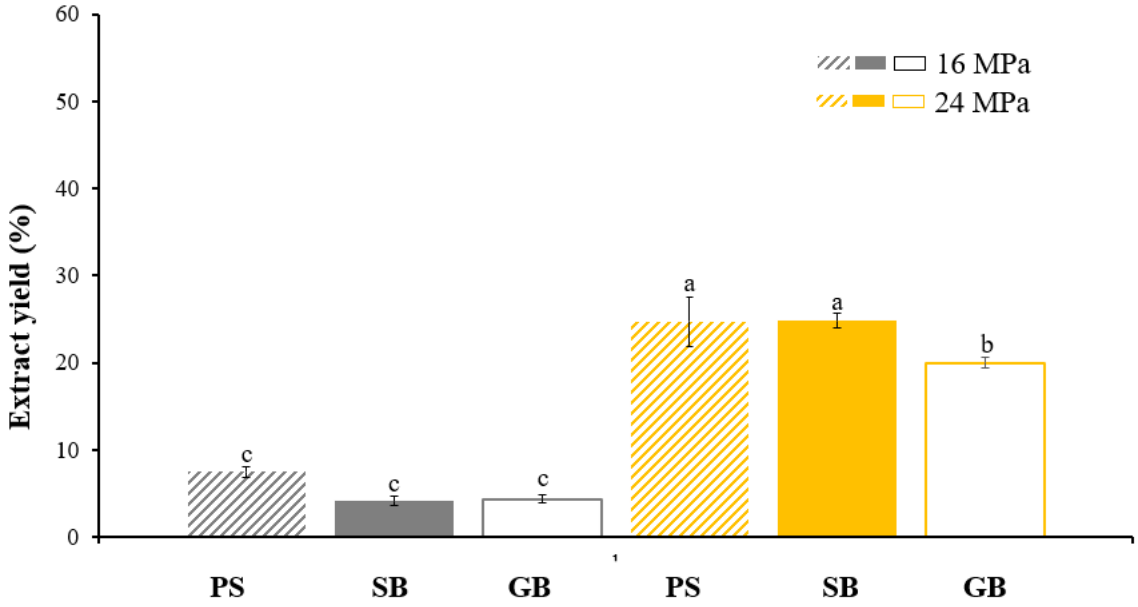

(B)

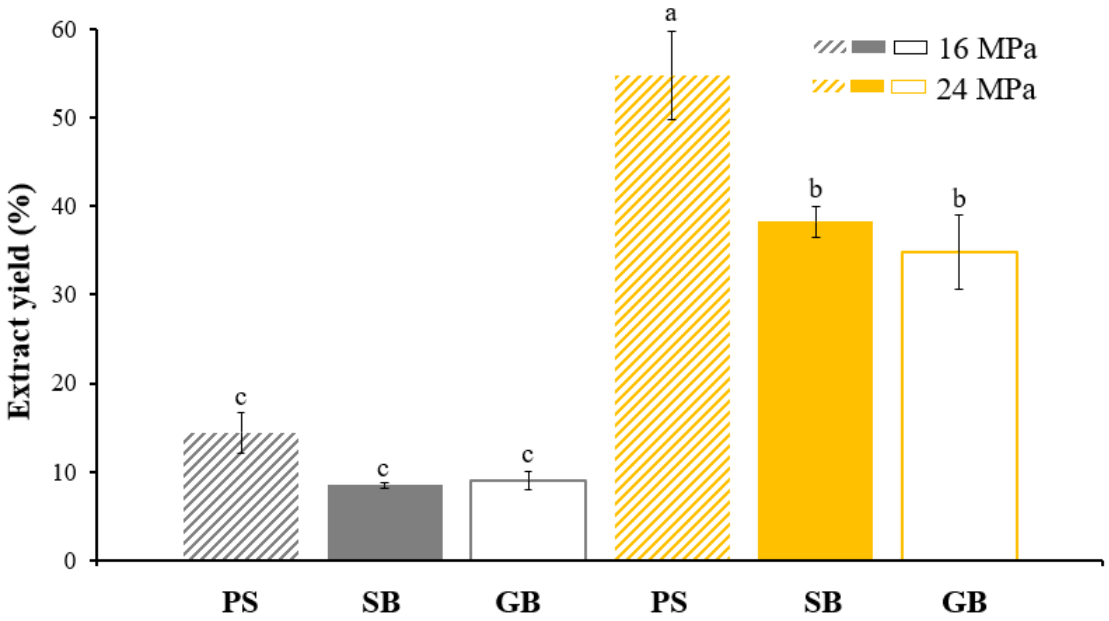

Figure 5. 5. Extract yield at 60 ºC: (A) 15 S/F, (B) 25 S/F ratio at different pressures of 16 MPa (grey bars) and 24 MPa (yellow bars), and types of packing (PS perforated stainless steel, (hatched bar); SB stainless steel beads (solid bar); GB glass beads (blank bar)). [a-c] Bars with different letters are significantly different at $p < 0.05$ (Data presented in Appendix C, Table C.1).

24 MPa. Therefore, it was expected that more lipids would be collected when PS was used compared to SB as a packing material, resulting in extract yield values at 25 S/F ratio of 14.4±2.3% and 8.5±0.2 % at 16 MPa and 54.8±5.0 % and 38.3±1.6 % at 24 MPa, respectively.

Regarding to the type of packing effect, at 25 S/F ratio and 24 MPa, the difference between packings of different geometries but the same material of stainless steel was remarkable, where perforated packing (PS) resulted in significantly higher amounts of extract compared to that obtained with beads (SB), which was mainly due to their characteristics (Table 5.1). At 24 MPa, there was no difference between SB and GB, demonstrating that there was no effect of the packing material with similar geometries on the extract amount at S/F 25 even though there was a difference at S/F 15. While PS was a 0.4 x 0.4 cm sheet and SB was a bead of 0.6 cm in diameter and both were made of SS, PS provided higher void volume (94%) and surface area (18.89 cm^{-1}) compared to SB (44% and 6.97 cm^{-1}, respectively).

5.3.3. Effect of process conditions on the free fatty acid separation efficiency

5.3.3.1. Effect of temperature configuration and type of packing

The effects of temperature profile and type of packing on the FFA-SE was shown in Figure 5.6 based on the experiments of Set 1, where only the effect of temperature was significant ($p < 0.05$), and there were no significant effects of packing and interaction. As explained in section 5.3.2.1, based on the higher CO_2 density and its solvent power at the isothermal condition of 40 °C, it was expected that a higher amount of lipids would be solubilized into the CO_2 phase and thus a higher FFA-SE was achieved compared to the thermal gradient condition, exhibiting FFA-SE values of 15.86 ±3.46% at 40 °C and 1.61±0.33% at 60-100 °C. Moreover, there is a relevant relationship between the solubility of lipids in CO_2 and the desired separation efficiency of a

specific lipid compound or class of compounds contained in a lipid mixture. Further discussion about the solubility of lipid classes in CO_2 is detailed in the next section.

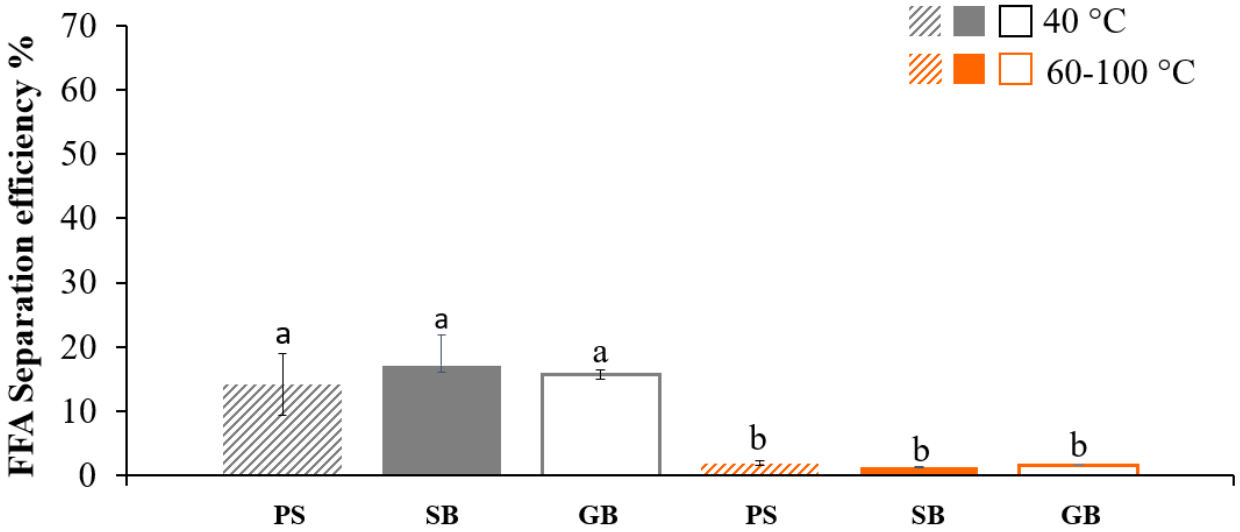

Figure 5. 6. FFA-SE at 16 MPa and15 S/F ratio as a function of the temperature profile, isothermal (40 ºC, grey bars) and thermal gradient (60-100 ºC, orange bars), and different packings (PS perforated stainless steel, (hatched bar); SB stainless steel beads (solid bar); GB glass beads (blank bar)). [a,b] Bars with different letters are significantly different at $p < 0.05$ (Data presented in Appendix C, Table C.2).

5.3.3.2. Effect of pressure, S/F ratio and type of packing

FFA-SE results of experiments from Set 2 evaluating the effects of pressure, S/F ratio and type of packing are presented in Figure 5.7 at S/F ratios of 15 and 25. At both S/F ratios, there were significant effects of pressure and the interaction of type of packing and pressure ($p < 0.05$) on FFA-SE. Even though the effect of packing on FFA-SE was not significant ($p > 0.05$) at 15 S/F ratio (Figure 5.7 (A)), it was significant ($p < 0.05$) at 25 S/F ratio (Figure 5.7 (B)). The pressure effect was significant on FFA-SE at 60 °C, using different types of packing, displaying overall values among the three packings of 10.73±3.5% and 45.00±11.54% at 16 and 24 MPa, respectively. As is well known and confirmed by the previous results, CO_2 has higher density and

(A)

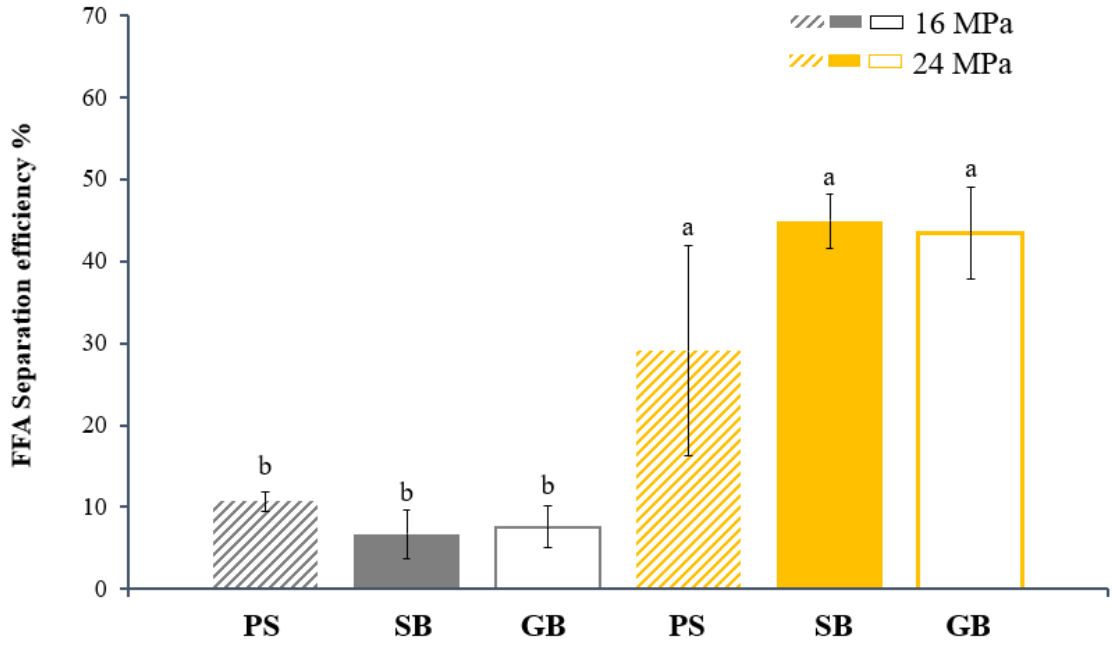

(B)

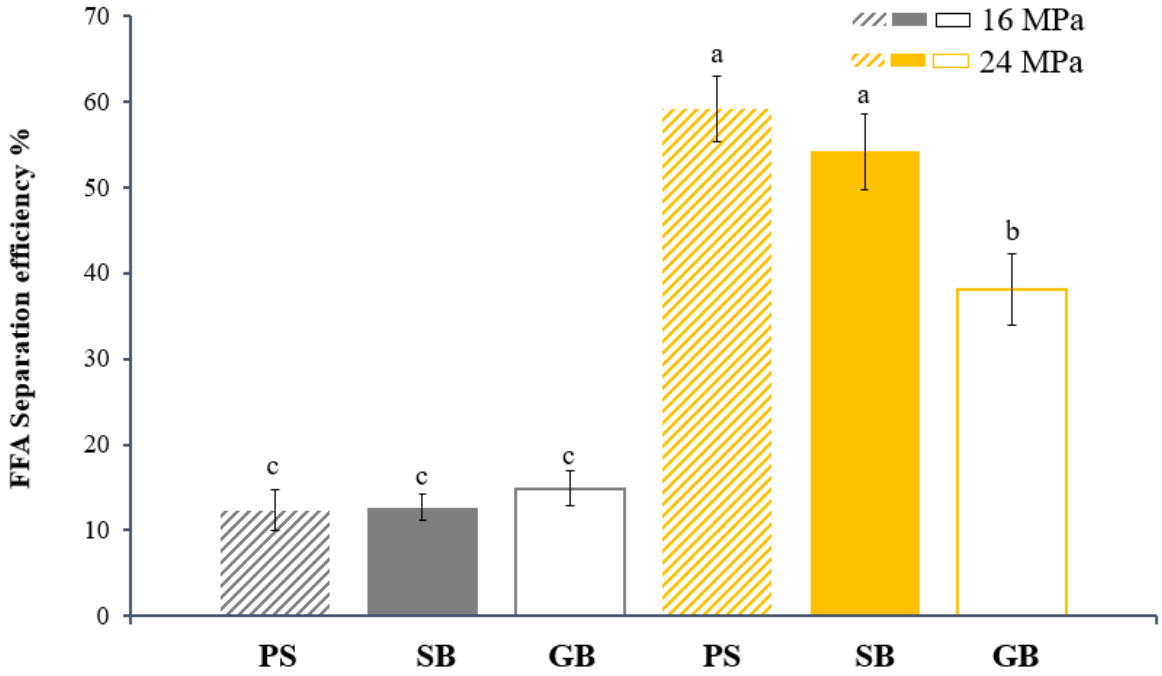

Figure 5. 7. FFA-SE at 60 ºC: (A) 15 S/F, and (B) 25 S/F at different pressures of 16 MPa (grey bars) and 24 MPa (yellow bars), and types of packing (PS perforated stainless steel, (hatched bar); SB stainless steel beads (solid bar); GB glass beads (blank bar)). [a-c] Bars with different letters are significantly different at $p < 0.05$ (Data presented in Appendix C, Table C.2).

thus higher solvent power at higher pressures, providing favorable conditions for lighter lipid compounds, such as FFA, to be solubilized into the CO_2 phase. However, it is important to consider that the separation efficiency of low molecular weight lipid compounds might be affected when they are isolated from complex lipid mixtures that contain higher molecular weight lipid compounds (for example, TAG), because at higher pressures, solubility of heavier compounds in CO_2 also increases.

Different feed lipid mixtures and packing materials have been studied under diverse experimental conditions to optimize the deacidification process of lipid mixtures or to isolate minor lipid compounds as reported in the literature (Table 2.1). In agreement with the previous studies, the separation efficiency of FFA and minor lipid compounds was positively impacted at higher pressures. For example, King et al. (1997) fractionated a glyceride mixture in a continuous countercurrent fractionation column with SC-CO_2, applying different pressures and temperatures. and obtained a higher top product yield, constituted by lower molecular weight glycerides (mono- and diacylglycerols), when the column pressure was increased from 17.2 to 34.4 MPa. Zacchi et al. (2006) continuously fractionated wheat germ oil in a countercurrent column with SC-CO_2, where the effects of temperature and pressure on the concentration of tocopherols were studied. They found that at 65 °C and 35 MPa, the FFA% was 16.6% in the extract fraction, concluding that the deacidification effect was enhanced when pressure was increased. Fang et al. (2007) studied the effect of several operating parameters on the enrichment of valuable compounds from an oil deodorizer distillate in a semi-continuous countercurrent fractionation column using SC-CO_2 and recovered tocopherols to a greater extent (>80%) with an increase in pressure from 14 to 20 MPa. Based on the previous studies and the present results, higher SC-CO_2 pressures increases the solubilization of lighter molecular weight lipids into CO_2, resulting in enhanced separation

efficiency. For example, the solubility of OA in SC-CO_2 was 4.0 ±0.32 x 10^{-2} g lipid/g CO_2 at 20 MPa and 40 °C, (Brunetti et al., 1989), whereas CanO solubility in SC-CO_2 at the same experimental conditions was 3 x 10^{-3} g lipid/g CO_2 (Fattori et al., 1988) confirming that there was more possibility for FFA to be solubilized into the CO_2 phase in contrast to TAG, resulting in higher FFA-SE at the conditions tested. This is due to the fact that FFA have smaller molecular weight and higher volatility compared to TAG, which are higher molecular weight and exhibits lower volatility, allowing higher solubilization of FFA into the CO_2 phase. However, with an increase in pressure, the separation efficiency of lighter compounds may be reduced in the presence of heavier lipids compounds, such as triacyglycerols, since the solubility of TAG also increases. For example, an increased solubility of CanO in SC-CO_2 was achieved when pressure was increased at 40 °C from 20 to 30 MPa, exhibiting values of 3 x 10^{-3} g lipid/g CO_2 to 8 x 10^{-3} g lipid/g CO_2 (Soares et al., 2007).

In this study, there was a significant effect of the type of packing on FFA-SE at 60 °C and 25 S/F ratio, whereas a lower S/F ratio of 15 did not exhibit such effect because of the enhanced possibility of lipid mixture accumulation inside the fractionation column regardless of the type of packing material since at 15 S/F ratio, there is less CO_2 available for lipid solubilization and a higher amount of lipid is pumped into the system. Whereas at 25 S/F ratio, there was enhanced availability of CO_2 for lipid solubilization inside the fractionation column, leading to increased FFA-SE reaching 59.33±3.79% at 24 MPa, 25 S/F ratio when PS was used as packing material. The S/F ratio effect on supercritical fluid fractionation of different lipid mixtures has been also addressed in other studies that were summarized in Chapter 2 (Table 2.1). For example, Ruivo et al. (2001) studied the effect of different process parameters on several output variables, including the extraction efficiency for methyl oleate. They defined it as the ratio between the amounts of

methyl oleate in the extract and in the feed for a given time, similar to the definition of FFA-SE employed in this study. When the S/F ratio was 20, the extraction efficiency of methyl oleate was maximized. In agreement with the results of the present study, higher S/F ratios provided a significant advantage on the separation efficiency of low molecular weight lipids.

5.3.4. Effect of process conditions on dynamic hold-up amounts and its free fatty acid content

5.3.4.1. Effect of temperature configuration and type of packing

The effects of temperature and type of packing on the dynamic hold-up (DH) amounts and its FFA% were assessed by the experiments in Set 1 and the results are shown in Figure 5.8. While the DH amount was significantly ($p < 0.05$) influenced by the temperature configuration, the type of packing, and their interaction, the FFA% in DH was not significantly ($p > 0.05$) affected by these variables. Temperature exhibited a significant effect on the DH amounts, where at thermal gradient and higher temperature (60-100 °C), the average DH was 57.37±17.11 g, while at isothermal condition (40 °C), DH was 35.83±36.38 g among the three different packing materials. As already mentioned in section 5.3.2.1, the extract yield was lower at the higher temperature (thermal gradient condition) due to lower CO_2 density, leading to overall higher DH amounts being retained inside the column.

The type of packing also had a significant ($p < 0.05$) effect on the DH amount, mainly because of the differences in their geometries and material, impacting their wettability by lipids in the CO_2 medium. The difference in void volume and surface area among the three packings (Table 5.1) has an intrinsic relationship with the DH amount. Lower void volume percentage corresponded to lower surface area, leading to higher DH amounts, as was the case when beads were used as the packing, independent of being made of SS or glass.

(A)

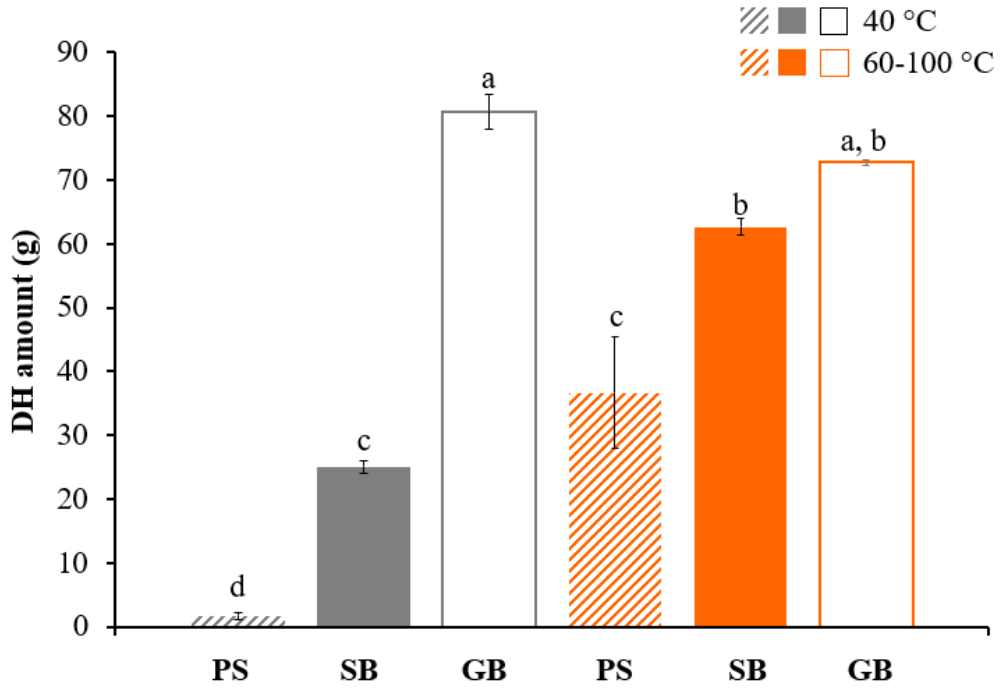

(B)

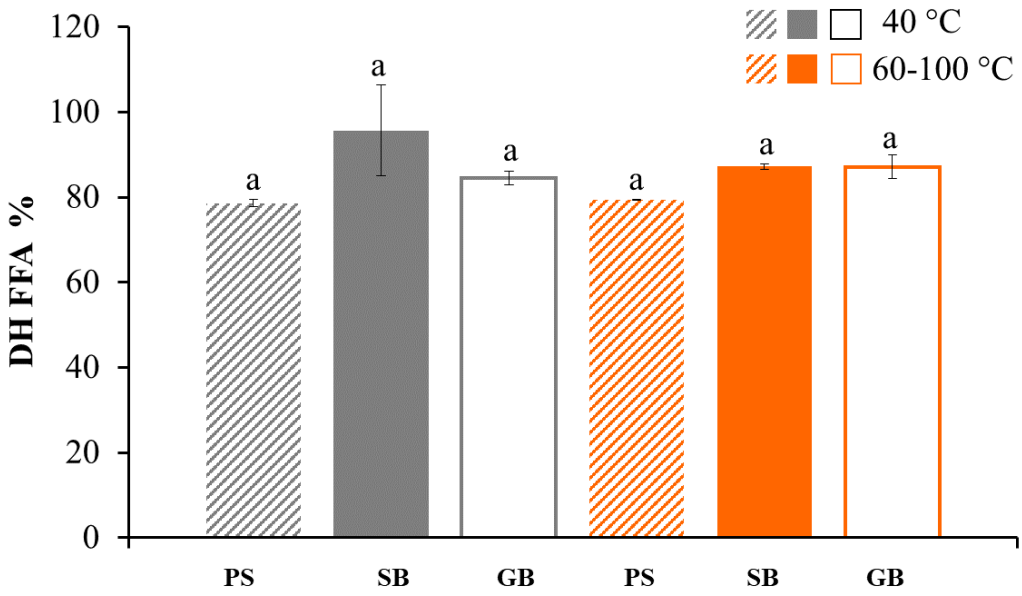

Figure 5. 8. (A) DH amount and (B) FFA% at 16 MPa, 15 S/F ratio as a function of the temperature profile, isothermal (40 ºC, grey bars) and thermal gradient (60-100 ºC, orange bars), and different packings (PS perforated stainless steel, (hatched bar); SB stainless steel beads (solid bar); GB glass beads (blank bar)). [a-d] Bars with different letters are significantly different at $p < 0.05$ (Data presented in Appendix C, Table C.3).

As a result, the use of beads as packing geometry might be challenging for CO_2-lipid mass transfer because the beads are more tightly packed, increasing the possibility for lipid entrapment in the small spaces between them, resulting in higher lipid accumulation and thus higher DH. DH amounts at 40 °C, 16 MPa and 15 S/F ratio for PS and SB were, 1.66±0.3 g and 25.058±1.03 g, respectively, which confirmed the trend that at higher void volume, lower was the DH amount collected (Figure 5.8(A)).

With respect to the material of the packing, the difference in the wettability of lipids on SS and glass surfaces was previously investigated in Chapters 3 and 4, respectively. The difference in the wettability behaviour of these materials was reflected in the differences in DH amounts collected; for example, 25.06±1 g and 80.77±2.71 g for SB and GB packings at 40 °C and 16 MPa, respectively (Figure 5.8 (A)). While lipid mixtures such as corn oil wetted the SS surface completely at 40 °C and 16 MPa with a contact angle (CA) value of 2.48° (Chapter 3), oleic acid (OA) only partially wetted the glass surface at the same conditions, exhibiting a CA value of 11.78° (Chapter 4). Even though the previous wettability results were not collected using the same model mixture of this study, the behaviour of the lipid mixture on these surfaces could be expected to be similar to that of OA at 40 °C and 16 MPa since 85% of the feed mixture was FFA. Based on the previous results obtained, the differences in wettability behaviour on diverse materials could be expected to follow a similar pattern for the behaviour of DH amount as GB > SB.

Regarding the FFA content of DH (Figure 5.8 (B)), there was no significant effect ($p > 0.05$) of temperature, type of packing or their interaction on the FFA% in DH. The higher FFA content of DH was 87.25±0.64 % at 60-100 ºC, whereas 95.65±10.68 % at 40 °C. During countercurrent continuous fractionation process, the raffinate is expected to contain a higher concentration of the components less soluble in SC-CO_2, which in this study is the triacylglycerols

and a reduced concentration of FFAs, which are removed in the extract. The DH composition is expected to be more similar to the raffinate composition. However, due to the challenges encountered during the raffinate collection and the relatively small amounts of extract removed, it is possible for the DH and raffinate samples to exhibit FFA% content similar to that in the feed composition.

5.3.4.2. Effect of pressure, S/F ratio and type of packing

The effects of pressure, S/F ratio and type of packing on the dynamic hold-up (DH) amounts were determined by performing Set 2 experiments and the results are presented in Figure 5.9. These effects were similar and consistent with the output variables presented previously, extract yield (section 5.3.2.2) and separation efficiency (section 5.3.3.2). When the extract yield increased with pressure (due to higher CO_2 density at elevated pressure) and S/F ratio (due to higher CO_2 amount available for lipid solubilization), there was a decrease in the DH amounts retained in the fractionation column and an enhancement in the FFA-SE as previously discussed in sections 5.3.2.2 and 5.3.3.2.

Regarding the effect of the type of packing, it showed consistent trends as displayed in Figure 5.9, which was in agreement with the effects on other process output variables (sections 5.3.2.2. and 5.3.3.2), mainly focusing on the differences among the three packings in terms of material (stainless steel vs glass) and geometries (perforated plate vs bead). For the packings of the same geometry but different material (SB vs GB), glass packing held more lipids than SS at all the conditions investigated. This variation was principally related to the difference in the wettability of lipids on these two types of materials in SC-CO_2 medium. For example, at 24 MPa and 15 S/F ratio, DH amounts for SB and GB were 36.28±3.18 g and 46.89±3.6 g, respectively,

(A)

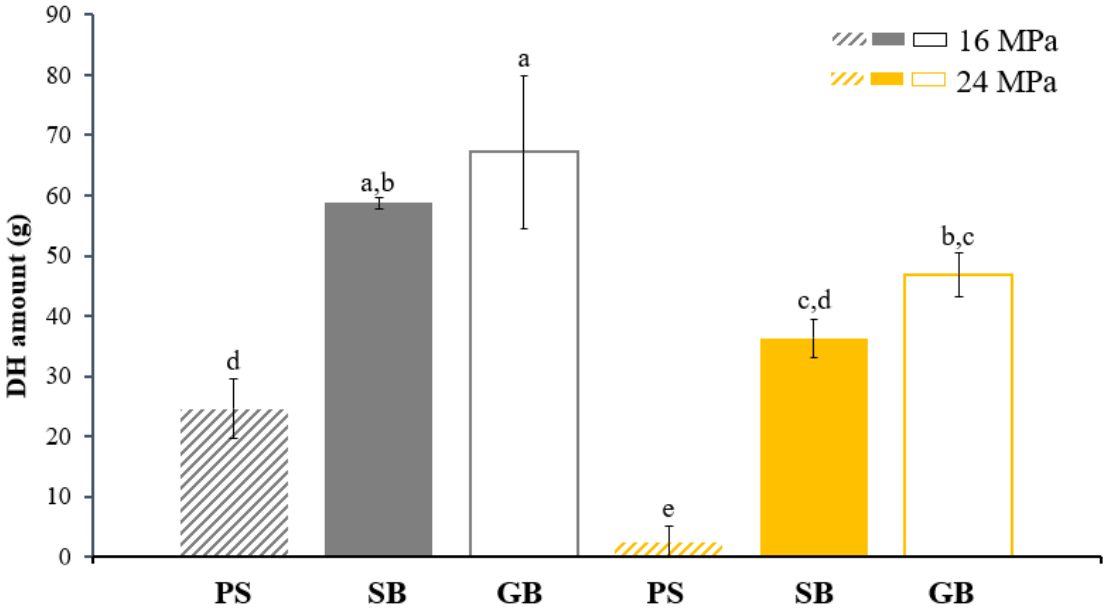

(B)

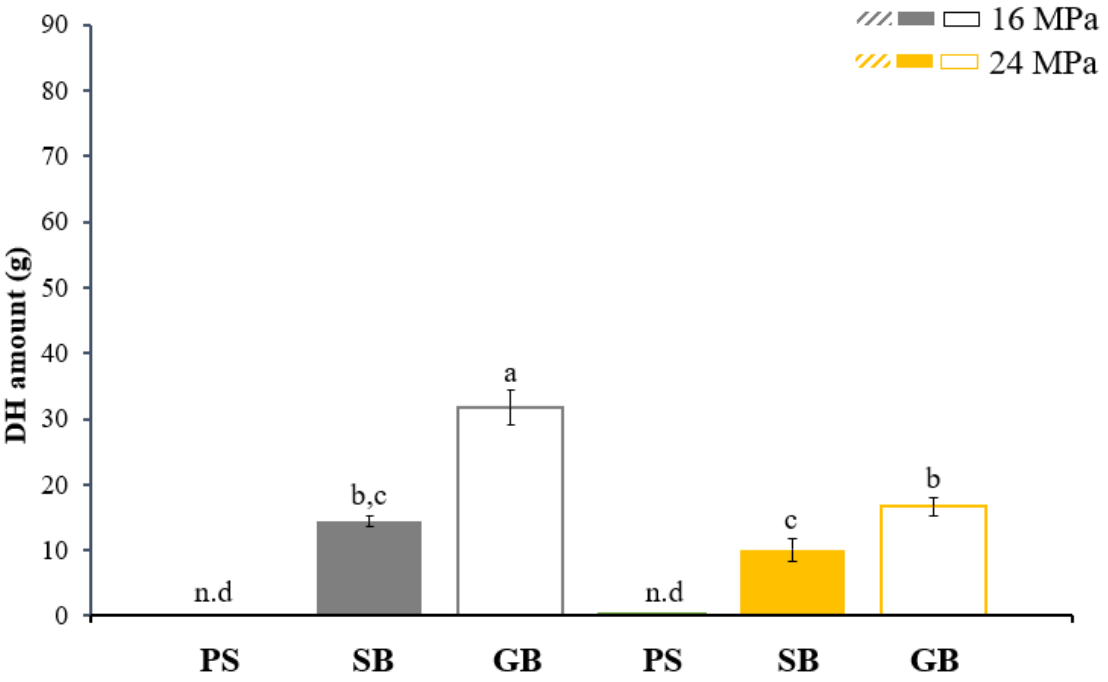

Figure 5. 9. DH amounts at 60 ºC: (A) 15 S/F, and (B) 25 S/F at different pressures of 16 MPa (grey bars) and 24 MPa (yellow bars), and types of packing (PS perforated stainless steel, (hatched bar); SB stainless steel beads (solid bar); GB glass beads (blank bar)). [a-e] Bars with different letters are significantly different at $p<0.05$ and [n.d.] indicates that the value was not determined (Data presented in Appendix C, Table C.3).

reflecting the difference due to the material even though those packings had the same geometry, linking this effect to the wettability of lipids on different materials. Moreover, the packing geometry also had an impact on the DH amount, similar to the previous experimental output variables, extract yield and FFA-SE (discussed in sections 5.3.2.2 and 5.3.3.2, respectively). For example, at 16 MPa and 15 S/F ratio, there was a significant difference ($p < 0.05$) in the DH amounts between PS and SB (24.59 ± 4.87 g and 58.74 ± 1.00 g, respectively) mainly due to their different void volumes and surface areas (Table 5.1), where higher void volume and larger mass transfer area for lipid solubilization into the CO_2 phase led to lower retention or adhesion of lipids on packings, resulting in lower DH amounts. For the case of SB, with a lower void volume (43.62%) and lower surface area (6.97 cm^2/cm^3), there was more lipid accumulation on the packing, filling the spaces between the beads, reducing the contact with CO_2 to solubilize lipids, resulting in higher DH amounts. As previously reported in Chapter 4, at 60 °C and 20 MPa, the wettability of canola oil on SS and glass surfaces varied from complete to partial wetting, with CA values of 2.3±0.30º to 17.0±1.67º, respectively. Even though the experimental conditions were not exactly the same, a similar behaviour of FFA under SC-CO_2 medium can be expected. As a result, a relation can be established between the wettability of packing and DH amount, as more wettable is the packing surface by the lipids in SC-CO_2 medium, enhancing the contact between the two phases, lower is the DH amount.

FFA concentration of the DH obtained at different conditions of Set 2 experiments was shown in Figure 5.10 Pressure had a significant effect on FFA% in the DH, at 25 S/F, but not at 15 S/F ($p > 0.05$). However, there were no significant ($p > 0.05$) effects of the type of packing and the interaction between packing and pressure on this variable. FFA% in the DH was expected to be close to the composition of the model mixture used as feed, as reflected in the results obtained.

(A)

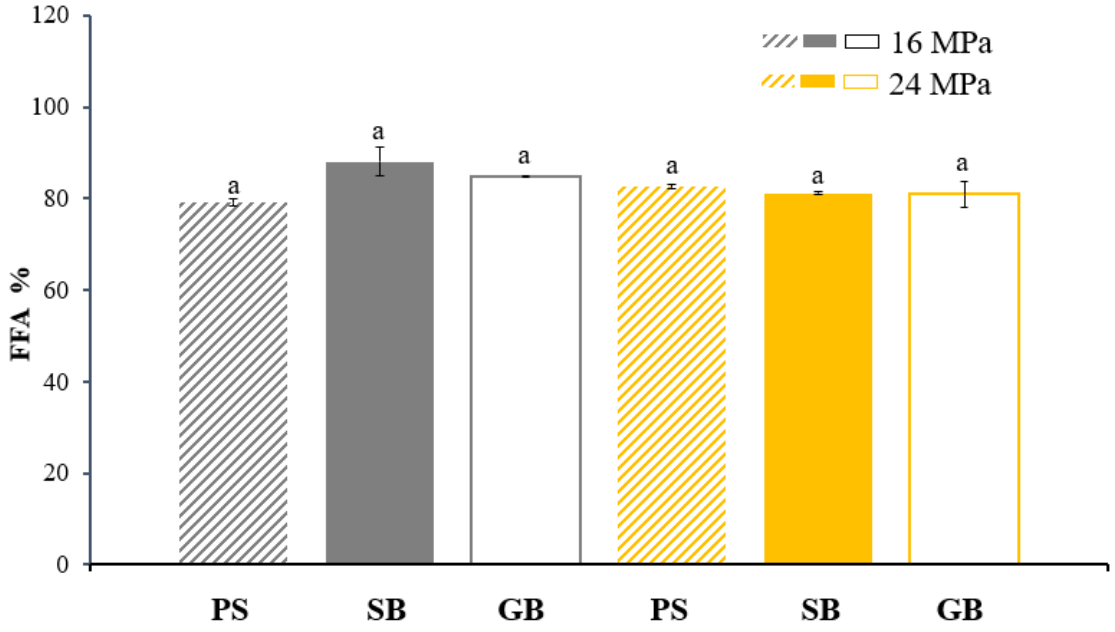

(B)

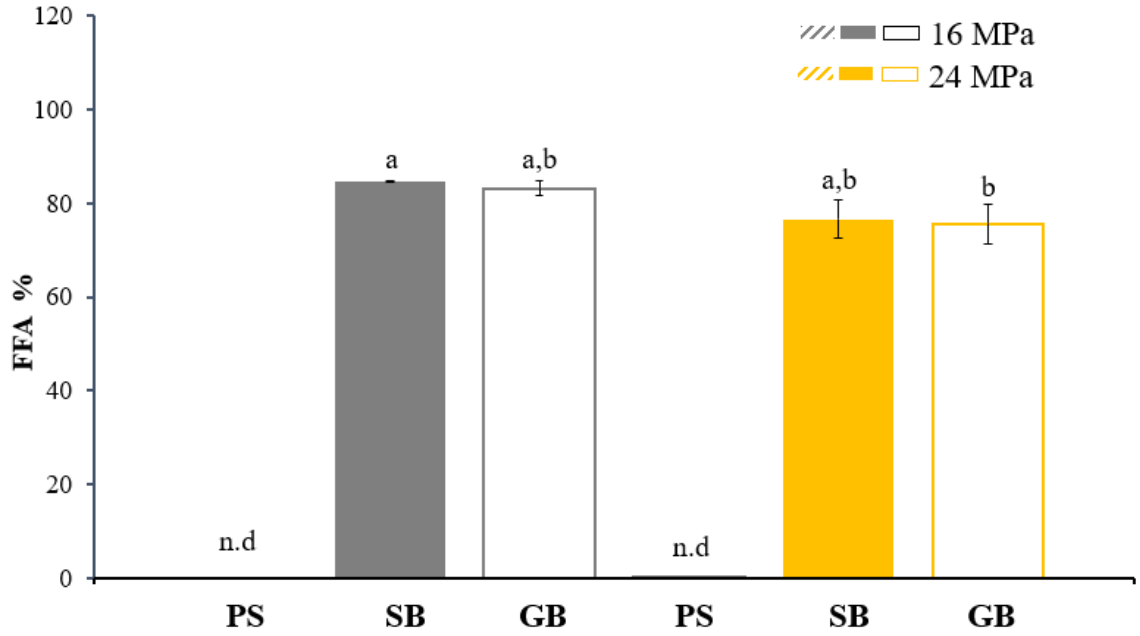

Figure 5. 10. FFA concentration in dynamic hold-up at 60 ºC: (A) 15 S/F, and (B) 25 S/F at different pressures of 16 MPa (grey bars) and 24 MPa (yellow bars), and types of packing (PS perforated stainless steel, (hatched bar); SB stainless steel beads (solid bar); GB glass beads (blank bar)). [a,b] Bars with different letters are significantly different at $p < 0.05$ and [n.d.] indicates that the value was not determined (Data presented in Appendix C, Table C.3).

In general, the average FFA concentration of DH at 60 °C was 83.98±3.30% and 79.14±3.79 % for 16 and 24 MPa, respectively, close to the FFA% in the feed mixture. However, the amounts of DH collected were very low (<0.04 g) (Figure 5.9) when PS was used at 25 S/F ratio and 16 and 24 MPa, making the FFA determination difficult. Low amounts of DH were obtained when PS packing was used at 25 S/F ratio because of the high surface area of the packing and higher amount of CO_2 available for lipid solubilization, contributing to better mass transfer, by enhancing the contact area for the lighter lipids (FFA) to be solubilized into the CO_2 phase, resulting in higher extract yield, FFA separation efficiencies and very low amounts of DH collected.

5.3.5. Relation between wettability and process outcomes

Several previous studies have investigated the effect of different types of packing on separation efficiency during the recovery of minor compounds from complex lipid mixtures (Table 2.1). For example, Catchpole et al. (1997) continuously fractionated squalene from shark liver oil, studying the effect of several operating parameters, including the type of packing. The authors used packings such as Rashing rings and Fenske rings made of glass, and wire wool and Rashing rings made of steel, finding that glass packings exhibited the lowest squalene separation efficiency, mainly because of the poor mass transfer and poor liquid distribution over the packing. Then, Catchpole, Grey, et al. (2000b) performed the countercurrent extract and fractionation of a variety of crude fish oils using SC-CO_2 and CO_2 + ethanol mixtures, studying the height of a transfer unit (HTU) and packed height needed to achieve efficient mass transfer between the mixture and CO_2 to reach the desired level of separation of minor lipid compounds, using glass Fenske spirals and stainless steel Pall rings in a demonstration scale fractionation column. However, the authors obtained low extraction efficiencies with both packings since the packing height was insufficient to achieve the desired degree of separation. Moreover, Stockfleth and Brunner (2001) examined

the effect of two random (Rashing rings and Berl saddles) and two structured (Sulzer CY and Sulzer EX) packings on the hydrodynamic behavior during the countercurrent fractionation of olive oil DOD/CO_2 and water/CO_2. They concluded that structured packings presented higher capacity compared to random packings. Furthermore, Ibáñez et al. (2002) concluded that during the fractionation of olive oil, the phytosterol enrichment factor was higher when glass Fenske rings were used in contrast to the other packings, regardless of the different S/F ratios considered. Additionally, the authors found that sterol recovery was higher at higher CO_2 flow rates when Dixon and Fenske rings were used, whereas at lower S/F ratios, sterol recovery was lower depending on the packing material. For the tocopherols, the recovery was up to 53.6% by using either Fenske or glass beads, confirming the selectivity of glass packings on tocopherol separation, while Rashing rings showed the lowest recovery of 16.5%. Also, they mentioned that the nature of glass packing enabled the formation of a uniform oil film on the packing, resulting in a higher specific surface area on these types of glass packings in comparison with the other packings used. In the previous study, Ibáñez et al. (2002) showed the importance of the packing material used in the countercurrent fractionation column; however, they evaluated selectivity, enrichment and recovery, whereas in this study, the process performance variables were extract yield, separation efficiency and dynamic hold-up amount.

On the other hand, Hurtado-Benavides et al. (2004) determined the number of transfer units (NTU) and HTU for different random packings under diverse experimental conditions using olive oil and CO_2. These parameters indicated the performance of the packed fractionation column at the mass transfer level. Fenske rings exhibited the best results in relation to the separation efficiency of minor compounds from olive oil. For example, the process efficiency expressed in terms of NTU was 11.20 and 4.27, while HTU was 0.16 m and 0.42 m for vitamin E and

phytosterols, respectively. They concluded that among the packings, there were differences linked to their different wettability and specific surface areas. Moreover, Torres et al. (2009) performed enzymatic esterification of soybean DOD and used the reaction product as the feed for the fractionation process to concentrate phytosterol esters using CO_2 and Fenske rings as packing material. Even though the authors did not mention the material used to make the Fenske rings, they obtained satisfactory results regarding concentration of tocopherols and sterol esters in the raffinate fraction. They enhanced the S/F ratio from 25 to 35, increasing the phytosterol ester concentration from 77.9 to 82.4 wt%, resulting in a 72% yield.

Despite the achievements of these extensive previous studies, there is still a lack of understanding about the effect of the lipid wettability on different packing materials under SC-CO_2 environment and its implications on the process performance during the isolation of minor lipid compounds from complex lipid mixtures using packed fractionation columns. Considering the principles of the separation process and the use of packing materials, the main focus is to wet thoroughly the packing material to enhance the separation efficiency of target compounds. Therefore, DH and FFA-SE obtained in this study were linked to the results of the previous wettability studies, as shown in Table 5.2. In the previous studies reported in Chapters 3 and 4, the contact angle (CA) for corn oil and oleic acid was determined on SS and glass surfaces at 40 and 60 °C and 16 to 24 MPa. Their wettability behaviour varied from partial to complete wettability, depending on the surface used and experimental conditions, and such wettability behaviour is intrinsically related to the DH and FFA-SE results obtained in this study. For the SS surface, complete wetting was achieved (CA < 10°), resulting in an increase in DH and a decrease in FFA-SE when temperature was elevated. However, for glass material, the results were different; when lipids partially wetted the glass surface, higher DH amounts and lower FFA-SE compared to those

for SS were obtained. Furthermore, based on the type of packing material, there were differences in DH amounts, intrinsically related to the wettability, while glass showed higher DH amounts, SS exhibited lower DH amounts under similar operating conditions.

The previous results have provided an initial approach to support the modeling and simulation of the SC-CO_2 fractionation of lipids using packed columns. This can involve computational fluid dynamics (CFD), where the flow of the phases in the presence of a solid surface can be simulated to understand the variation of flow pattern through the packed bed and the influence of the process conditions. Consequently, the flow pattern of lipids on surfaces in SC-CO_2 is intrinsically related to the mass transfer inside a packed column. As mentioned above, different studies have considered several experimental conditions to understand and characterize the mass transfer aspects. To be able to link IFT and CA data to the determination of mass transfer inside a packed column, it is essential to consider the following basic steps: 1) determination of the height of a transfer unit (HTU), which involves the stripping factor (ratio of the slope of equilibrium line to that of the operating line); and 2) determination of the mass transfer coefficient of each phase considering the stripping factor, velocities of the phases and effective interfacial area or wetted surface area. It is important to consider that the effective interfacial area in an irrigated packing by two phases must be called the wetted surface area. While the effective interfacial area involves surfaces of drops and jets, the wetted surface area reflects the surface areas in dead zones, which must be considered for the case of partial wettability of a liquid on packing in a given medium (Wang et al. 2005). In addition, surface properties and roughness of the packing also play an important role on the wettability behavior and should be considered in the determination of the wetted surface.

Jaeger (1998) attempted to link IFT and CA to the determination of the wetted surface area of an irrigated packing by lipids and CO_2 inside a countercurrent continuous packed column. The author determined the wetted surface area as the ratio of a liquid volume of a sessile drop (drop used to determine the CA of a liquid on a surface in a given medium) and the film thickness. The film thickness (δ) was determined relating the interfacial tension of liquid-vapour ($\sigma_{L/V}$), the density of the liquid (ρ_L), and CA (θ) ($\delta = \sqrt{\frac{2*\sigma_{L/V}}{\rho_L}} * (1 - cos\theta)$). Also, Jaeger (1998) calculated the minimum Reynolds number required to wet the surface of the packing, $Re_{min} = 2.94K_f^{0.2} * (1 - cos\theta)^{0.5}$, where K_f represents the Kapista number or fluid-film number. This number correlates surface tension forces to inertial forces as shown in the following expression: $K_f = \frac{\rho_L * \sigma_{L-f}^3}{g * \mu_L^4}$. Therefore, there are different terms that relate the wettability (as a function of IFT and CA) with mass transfer in packed columns during the fractionation of lipids using SC-CO_2, and it could be possible to avoid assuming complete wettability of lipids on packings in SC-CO_2 while performing modeling and simulation to provide a more realistic process design and simulation.

Additional preliminary experiments were performed, targeting the determination of CA of canola oil at 40 °C, 16 and 24 MPa on chemically and mechanically perforated SS sheets to simulate the perforated packing (PS) used in the column. The results presented in Appendix B, Figures B.3 – B6 showed diverse wetting patterns, such as no permeation, delayed and advanced permeation of lipid inside the perforations. These wetting patterns might be related with the advantage of using perforated SS packing instead of SS beads. Once the lipid drop is deposited on the perforated sheet, even though there is more surface area to hold more lipid, the uniformity of the lipid film may be more important since the film is disrupted by holes filled with CO_2. The CO_2 might exhibit a lubricant effect in these perforations, because once the lipid fills the holes, the CO_2

is available to solubilize the lipids, enhancing the contact and solubilization of lipids into CO_2, resulting in increased extract yield (Figures 5.3 and 5.4), while decreasing DH in PS packing. While the perforations offer those advantages, the possibility of lipid film renewal might continue offering greater possibilities to enhance mass transfer during the fractionation process.

Table 5. 2. Relationship between wettability studies and the present study on DH and FFA-SE

Material	System	P (MPa)	T (°C)	CA (°)	Wettability pattern	S/F (wt/wt)	DH amount	Separation Efficiency (%)
SS (Chapter 3 and this study)	Corn oil + SC-CO_2	16	40	2.48	complete	15	25.1	17.8
		16	60	4.21	complete	15	58.7	6.7
						25	14.3	12.7
		24		9.2	complete	15	36.3	44.9
						25	10.1	54.2
Glass (Chapter 4 and this study)	Oleic acid + SC-CO_2	16	40	11.78	partial	15	80.8	15.7
		16	60	12.95	partial	15	67.3	7.6
						25	31.8	14.9
		24		8.61	complete	15	46.9	43.6
						25	16.7	38.9

P: pressure; T: temperature; CA: contact angle; S/F: solvent to feed ratio; DH: dynamic hold-up

Additional attempts were made to determine the static hold-up (SH) by collecting residual lipids left in the column following drainage of DH. Preliminary results obtained at two conditions are presented in Appendix C, section C.2.2. Overall, the SH amount was higher for PS at 60 ºC, 24 MPa and 25 S/F, reflecting its higher surface area. However, further analysis must be performed to correlate this variable to the process conditions and other process performance parameters. Also, mass balance calculations for the experiments where SH was determined are exhibited in Appendix C, Table C.4. Despite the careful efforts while performing the experiments for this study, there were challenges in raffinate sample collection, which contributed to high material loss in some cases.

The findings of this study demonstrated that: a) there is a correlation between the FFA separation efficiency and DH amounts among the experimental conditions considered. FFA separation efficiency decreased with an increase in DH amount, which was confirmed by Pearson correlation analysis. Such analysis was performed between these two sets of results using Microsoft Excel, which resulted in a Pearson correlation coefficient of -0.5405 and b) the type of material used to increase mass transfer during the fractionation of lipid mixtures significantly influences the process separation efficiency. The results of this study were obtained using a model mixture while wettability studies were performed with individual lipid compounds/classes; therefore, there is need for more data about the wettability of the model mixture under the same process conditions to better understand the implications of packing wettability on process performance for lipid mixtures.

5.4. Conclusions

The effects of temperature, pressure, S/F ratio and type of packing were investigated on the process outcome variables of extract yield, FFA-SE and DH amount during the countercurrent continuous fractionation of a model mixture (85% FFA and 15% TAG) using SC- CO_2. In relation to the extract yield, at isobaric conditions and S/F ratio of 15, there was a significant effect of temperature mainly due to the temperature effect on CO_2 density, which dictates the solubility behaviour of lipids. At isothermal conditions, there were significant effects of packing material, pressure and S/F ratio on the extract yield. Higher extract yield was obtained when PS was used, because the PS packing offered less possibility of liquid retention and more effective interfacial area to allow better solubilization of lipids into CO_2 phase compared to SB. At higher pressures, CO_2 density and thus, solvent power is enhanced, and higher extract yield was obtained at 24 MPa

compared to 16 MPa. Higher S/F ratio of 25 provided more CO_2 for lipid solubilization, resulting in a higher amount of extract collected, resulting higher extract yield.

The FFA-SE was significantly affected by temperature, pressure, and S/F ratio. At 16 MPa and 15 S/F ratio, a higher FFA-SE was achieved at 40 °C compared to the thermal gradient condition. At isothermal conditions, S/F ratio and pressure exhibited remarkable effect on the FFA-SE. As expected, the FFA% of the DH was close to the composition of the model mixture used as feed. At isobaric conditions, pressure, S/F ratio and interaction between pressure and packing strongly affected the DH amount. DH amount collected was lower at higher S/F ratio. Those conditions that led to higher extract yield resulted in a reduction of DH amount, since less amount of lipids was retained inside the column. Glass packing held more lipids than SS, which is intrinsically related to the difference in the wettability of lipids on these two types of materials in SC-CO_2 medium.

Chapter 6. Conclusions and recommendations

6.1. Summary of key findings

With the intention to revalorize food waste and agri-food by-products, supercritical fluid technology offers possibilities for novel process development using CO_2 as a green solvent. Various fractionation processes have emerged over the years as an alternative to conventional processing of vegetable oil and oil refining-by-products to isolate minor compounds with health benefits, which might be used as value-added ingredients in human consumption products within different industries. Targeting fractionation of complex lipid mixtures inside a packed column using SC-CO_2, different studies have addressed process optimization based on multiple variables; however, there is a lack of understanding of the effect of the packing material and its wettability on the process outcomes such as extract yield, separation efficiency and dynamic hold-up. As a result, the overall goal of this Ph.D. thesis research was to address such lack of information considering a systematic approach, where first the wettability of lipids on different surfaces in dense gases was determined, then column fractionation of a model mixture was performed under different process conditions using different packings, and finally the effect of packing wettability on fractionation process outcomes was assessed.

In the first study (Chapter 3), corn oil-CO_2 and stainless steel (SS) material were used to determine contact angle, considering that 316 SS is the most common type of material used to manufacture packings for the vegetable oil refining industry. Also, the physicochemical properties of corn oil in SC-CO_2 were available in the literature to validate the experimental protocols for interfacial tension (IFT) and contact angle (CA) determination under different experimental conditions. The objective of this study was to determine the effect of pressure and temperature on

IFT and equilibrium contact angle (CA_{eq}) of corn oil in air, SC-CO_2 and SC-N_2 on polished stainless steel metal sheet under unsaturated and saturated surrounding phases at 40, 60, 80 °C and 0.1, 16, 20, 24 MPa. The results demonstrated that a) the IFT of corn oil/N_2 and corn oil/CO_2 showed a remarkable difference depending on pressure and temperature conditions of the N_2 or CO_2, which impacts their density values, b) IFT of corn oil in both gases decreased exponentially at isothermal condition when pressure was increased, but this decrease reached values below 5 mN/m when the oil was in contact with CO_2, whereas in N_2, the IFT reached a minimum of 20 mN/m, and c) the wetting behaviour of corn oil on polished SS surface under dense N_2 and CO_2 was characterized as complete wetting, showing values of CA_{eq} below 10°, mainly influenced by the saturation or unsaturation condition of the environment. This particular approach allowed the evaluation of the wetting properties of a liquid on a surface under saturated conditions where mass transfer is negligible. However, it is important to consider the effects of pressure, temperature and phase composition on the wettability determination.

Considering that glass was another material used in the fabrication of packings for packed columns, determination of the wettability behaviour of different lipid classes (oleic acid (OA) and canola oil (CanO)) on glass sheets was targeted in the second study (Chapter 4) under similar experimental conditions of the previous study (Chapter 3). The aim of this study was to determine the IFT and the CA_{eq} of OA and CanO on polished glass in SC-N_2 and SC-CO_2 environments at 40, 60, 80 ºC and 16, 20, 24 MPa. The results of this study demonstrated that a) the IFT of OA and CanO in SC-CO_2 determined at 60 ºC and pressures of up to 24 MPa showed a remarkable decrease with pressure due to the increase in CO_2 density and its solubility in the lipids; and b) the CA_{eq} of OA and CanO on glass surface showed a similar trend, with higher values in SC-N_2 compared to that in SC-CO_2 environment at 60 ºC and pressures of up to 24 MPa. While the OA/SC-CO_2 system

on glass exhibited partial to complete wettability at 40 ºC and 60 ºC, complete wettability was obtained at 80 ºC from 16 to 24 MPa. In contrast, the system of CanO/SC-CO_2 on glass surface exhibited three different wetting patterns with complete wettability at 40 ºC, partial wettability at 60 ºC and partial to complete wettability at 80 ºC with an increase in pressure. Therefore, the wettability of lipids on different surfaces in a supercritical fluid environment not only depends on the experimental conditions, but also on the composition of both phases, which remarkably influences the net effect on this property and surface phenomenon.

In relation to the spreading dynamics (Chapters 3 and 4), the differences in the spreading velocity (referring to the change in drop radius over time) of the different lipid droplets on SS and glass surfaces in SC-N_2 and SC-CO_2 environments were demonstrated. Based on the values of the power law exponent, the different lipid droplets on the surfaces evaluated reached a plateau, but the drop radius values of lipid droplets on these surfaces varied based on the surrounding fluid as well as the type of surface. For example, while on SS surface (Chapter 3), the radius of corn oil/N_2 and corn oil/CO_2 droplets were up to 4.5 and 3 mm, on glass surface (Chapter 4), the OA and CanO droplets in CO_2 were up to 15 and 11 mm, and those in N_2 were up to 5.5 mm (Appendix B, Figure B.1). These differences could be related to: a) the difference in the solubilization of lipids in the surrounding gas phase, which results in the formation or absence of a thin vapour film (which occurs in CO_2 but not in N_2) on top of the surface, allowing or avoiding faster contact between the oil droplet and the solid surface; b) the formation of a thin vapour film and its physicochemical properties could be different depending on the type of liquid droplet phase, type of supercritical fluid that forms the surrounding phase and its conditions (saturated or unsaturated), viscosity differences between phases and time scale of experiments. Therefore, it is recommended to

determine the early and intermediate stages of oil droplets under dense gases to better understand the fundamentals of events observed in this study.

It is relevant to mention that when the surface energy is high and IFT of the liquid is low, the liquid will wet the surface completely, whereas at low surface energies, the liquid will not wet the surface completely, as reflected in the CA values of CanO on SS and glass surfaces, respectively (Chapter 4). The overall variation in CA values in the systems studied emphasizes the delicate balance between the two phases in equilibrium: drop phase of lipid saturated with CO_2 and the surrounding phase of SC-CO_2 saturated with lipid, which also results in the formation of a thin film on the solid surface. Even though the physicochemical properties of the CO_2-saturated vapour film of OA and CanO are unknown, they play an important role in the wetting phenomena. In general, experimental conditions leading to higher solubility of SC-CO_2 in the lipid phase resulted in lower CA values, and in turn complete wetting of the glass surface.

The findings of the two studies focusing on wettability determination (Chapters 3 and 4) are novel in the field of the supercritical fluids in terms of the different wettability exhibited among lipid classes (OA, CanO and corn oil) on diverse types of surfaces of different materials (SS and glass) in SC-CO_2 as well as SC-N_2. Novel surface phenomenon was visualized for the first time for lipids on solid surfaces in SC-CO_2 medium, but not in SC-N_2 environment, such as bouncing of corn oil droplet on SS surface in SC-CO_2 as well as CanO and OA on glass in SC-CO_2, formation of SC fluid cavity during the lipid spreading as well as satellite droplet formation and sliding of CanO droplet on glass surface in SC-CO_2. The bouncing phenomena could be explained by the fact that the mass transfer phenomena based on the density difference between the phases could influence or momentarily modify the surface energy due to the formation of a thin vapour film (nanometric) with specific rheological behaviour to allow the bouncing of the corn oil droplet.

From the lipid droplet generation to spreading dynamics, based on the lipid/solid/dense gas system, various challenges and limitations were faced: a) the determination of the early and intermediate stages of oil droplet spreading under dense gases to be able to formulate and evaluate the fundamental understanding of the phenomena observed in Chapters 3 and 4, including the bouncing of the oil droplets prior to spreading under SC-CO_2 conditions, b) the characterization of the specific rheological behaviour and physicochemical properties of the thin vapour film that allowed the bouncing of the oil droplets in CO_2 medium, c) the interactions between solid/liquid systems in CO_2 as well as variation of surface energy of solid phase, d) changes in physicochemical properties (density, diffusion, IFT, viscosity) of the liquid and surrounding phases upon saturation with each other, e) the spreading dynamics of non-Newtonian fluids, and their practical applications in different fields of the industry; f) understanding the bouncing of lipid droplets on different materials in SC-CO_2, and its implications in process engineering. All of the above lead to variations in CA values, which have a major impact on the design and optimization of processes involving those systems, such as column fractionation, which must not be analyzed considering general approaches.

In the third study (Chapter 5), the main goal was to determine the effect of process parameters (temperature, pressure, S/F ratio and different type of packings) on the outcome variables such as extract yield, free fatty acid separation efficiency (FFA-SE) and dynamic hold-up (DH) amount. Continuous countercurrent fractionation of a model mixture (85% FFA and 15% TAG) was performed using three different types of packings (perforated stainless steel (PS), stainless steel beads (SB) and glass beads (GB)). The process parameters were solvent-to-feed (S/F) ratios of 15 and 25, pressures of 16 and 24 MPa and temperatures of 40 °C, 60 °C and thermal gradient of 60-100 °C. The extract yield and FFA-SE at isobaric conditions were significantly

affected by temperature, mainly due to the temperature effect on CO_2 density. At 40 °C, CO_2 density and its solvent power was higher than that at thermal gradient condition (60-100 °C), resulting in higher amount of lipids being solubilized into the CO_2 phase and thus enhanced extract yield and FFA-SE were achieved compared to the thermal gradient condition. Furthermore, at isothermal conditions, the extract yield and FFA-SE were intrinsically affected by the type of packing, pressure and S/F ratio, but pressure did not exhibit an effect on FAA-SE at 15 S/F. Regarding the effect of the packings, they were different not only in terms of the lipid wettability in CO_2 medium but also packing characteristics, regarding void volume and surface area. Low void volume percentage corresponded to low surface area, leading to higher DH amounts, as in the case of beads even though they were made of different materials. The perforated SS packing (PS) might have an advantage over the SS beads (SB), related to lubricant effect when CO_2 occupies the PS packing holes, allowing higher mass transfer between the phases. As a result, an induced film disruption mechanism could be produced by the PS packing, potentially generating an easier mechanism for lipid film renewal, enhancing mass transfer. The relationship between wettability and the process performance was established in this study. For example, as more wettable is the packing surface by the lipids in SC-CO_2 medium, enhancing the contact between the two phases, lower is the DH amount. Also, higher packing void volume and larger mass transfer area for lipid solubilization into the CO_2 phase led to lower retention or adhesion of lipids on packings, resulting in lower DH amounts and higher separation efficiencies. Both the material and geometry of the packing were important in terms of the effect on DH amounts.

With respect to the effect of pressure, as pressure increased, CO_2 density was enhanced, resulting in higher CO_2 solvent power to solubilize lipids into the CO_2 phase. However, the DH amounts at isobaric conditions were influenced not only by temperature, but also by the type of

packing. Moreover, in relation to the effect of S/F ratio, at the high S/F ratio of 25, the extract yield obtained was higher than at 15 S/F ratio, which was expected since there was a larger amount of CO_2 available to solubilize lipids, specifically low molecular weight compounds (FFA), allowing higher extract amounts to be collected and thus higher extract yield and FFA-SE values. Furthermore, Pearson correlation analysis was carried out to correlate the FFA separation efficiencies with the DH amounts at all experimental conditions, resulting in a negative value of -0.5405, demonstrating that as DH amount increases, the FFA separation efficiency decreases. Moreover, the selection of the different random packings (perforated Pro-Pak® SS, SS bead and glass beads) in Chapter 5 was considered based on the expensive cost to incorporate an in-line visual cell in the fractionation column used during the experiments to understand the wettability of lipid mixtures in contact with different packings used inside the column. The visual cell could provide a qualitative approach of the wettability of lipids in CO_2 on different surfaces, but not a comprehensive understanding of the wettability variation based on experimental conditions, which was the main reason for developing the studies detailed in Chapter 3 and 4. Despite the contributions of the results generated in the experiments performed in Chapter 5, there were challenges during the collection of the raffinate fractions (Appendix C, section C.2.3) mainly due to equipment limitations, which limited further analysis. As a result of the previously mentioned limitations, it is suggested to install in-line visual cells through the packed column as well as an improved set-up for raffinate collection.

Furthermore, the results obtained in the wettability and fractionation studies must be correlated using computational fluid dynamics (CFD) to understand how the wettability variation of lipids on different surfaces under SC-CO_2 environment affects the fluid dynamics inside the packed column as well as the mass transfer and the process outcomes. Despite the major

differences in the time scales of what was observed during contact angle measurements (Chapters 3 and 4) vs fractionation column experiments (Chapter 5), it is apparent that the differences in wettability behaviour have a major impact on process outcomes. Upon correlating these phenomena, there will be: a) fundamental knowledge generated that will lead to efficient scale up of the fractionation process for complex lipid mixtures; and b) reduction of engineering assumptions and more realistic modeling and simulations, which can positively influence economic feasibility studies and life cycle analysis (LCA).

These approaches would support the economic and environmental feasibility analysis for the vegetable oil industry to make better informed decisions during process selection targeting lipid separation or recovery of minor lipid components, and whether to incorporate it into an existing refining operation. The use of tools like CFD and LCA would offer the possibility to optimize the use of energy and solvent, in this case CO_2, during the continuous countercurrent fractionation using a packed column, since the S/F ratio, pressure and temperature dictate the amount of energy required to reach the desired process outcomes. Without fundamental understanding of the relationship between these variables, wettability and mass transfer, it is challenging to offer to different industries the possibility to use this process as an efficient alternative for lipid separations.

The findings of this Ph.D. research are significant for the supercritical fluid technology as well as for process engineering field, contributing to better understanding of how the wettability behaviour of lipids on surfaces in SC-CO_2 environment is inherently linked to the mass transfer inside packed columns and the fractionation process efficiency. Future directions of research must be considered in areas of surface science linked with supercritical fluids, due to the lack of understanding of specific spreading behaviour of fluids on surfaces in SC-CO_2 medium and their

implication in process engineering and industrial applications. The unique properties of each solid-fluid-SC fluid system must be taken into account because under different experimental conditions, variations in wettability behaviour may be expected, leading to significant effects on process design and optimization, which should not be performed under general design considerations.

6.2. Recommendations

Based on the extensive literature review, SC-CO_2 has been shown to have great versatility as a green solvent to fractionate targeted lipid components from complex lipid mixtures and to isolate minor compounds with health benefits. As a follow up to this Ph.D. thesis research, several complementary future investigations are suggested as follows:

- More research is needed to determine the physicochemical properties of phases involved in lipid + CO_2 + solid systems in equilibrium to facilitate the understanding of mass transfer and hydrodynamic behaviour during column fractionation operations.
- It is important to understand and determine the influence of the surface energy variations and interactions between phases of solid-lipid-CO_2 systems on the fluid dynamics behavior inside a packed fractionation column and their implications for designing more efficient chemical separation processes.
- More research is required to enhance the knowledge of lipid wettability (IFT and CA) on different surfaces during the fractionation of lipids under supercritical conditions to develop more realistic mass transfer models for packed columns based on variations of packing wettability (from wettable to non-wettable surfaces) and the interactions between solid-lipid-CO_2 phases.

- There is a need to develop correlations that relate lipid-CO_2 systems and their physicochemical properties (density, IFT, solubility, viscosity) with the packing material for optimal packing selection to maximize desired performance in the fractionation process.
- More research is required to determine the relation of static and dynamic hold-up during SC-CO_2 fractionation of lipid mixtures with the surface phenomena observed during this Ph.D. thesis research, including drop bouncing phenomena, satellite droplets, film formation on surfaces, and sliding of droplets.
- Additional research is required in relation to the IFT and CA of individual compounds of different lipid classes in CO_2 on different surfaces to properly determine their wettability and their correlation during the fractionation of complex lipid mixtures, for example, mono- and diacylglycerols, phospholipids, tocopherols, phytosterols, carotenes, and others.
- The formulation of a new dimensionless number that considers the interfacial rheology and dynamic viscosity of lipid mixtures in SC-CO_2 may be beneficial to properly describe the different hydrodynamic behavior, involving interactions between the different phases (liquid feed/CO_2/solid) inside a packed column.

References

Aguilera, J. M., & Del Valle, J. M. (1999). High pressure CO_2 extraction. Fundamentals and applications in the food industry. *Food Science and Technology International*, *5*(1), 1–24. https://doi.org/10.1177/10820132990050010

Ahmed, A., Qureshi, A. J., Fleck, B. A., & Waghmare, P. R. (2018). Effects of magnetic field on the
spreading dynamics of an impinging ferrofluid droplet. *Journal of Colloid and Interface Science*, *532*,
309–320. https://doi.org/10.1016/j.jcis.2018.07.110

Anastas, P. T., & Kirchhoff, M. M. (2002). Origins, current status, and future challenges of green chemistry. *Accounts of Chemical Research*, *35*(9), 686–694. https://doi.org/10.1021/ar010065m

Anastas, P. T., & Warner, J. C. (1998). *Green chemistry: Theory and practice*. Oxford University Press. (pp. 89)

Andreas, J. M., Hauser, E. A., & Tucker, W. B. (1938). Boundary tension by pendant drops. *Journal of Physical Chemistry*, *42*(8), 1001–1019. https://doi.org/10.1021/j100903a002

Arif, M., Barifcani, A., & Iglauer, S. (2016). Solid/CO_2 and solid/water interfacial tensions as a function of pressure, temperature, salinity and mineral type: Implications for CO_2-wettability and CO_2 geo-storage. *International Journal of Greenhouse Gas Control*, *53*, 263–273. https://doi.org/10.1016/j.ijggc.2016.08.020

Arif, M., Lebedev, M., Barifcani, A., & Iglauer, S. (2017). CO_2 storage in carbonates: Wettability of calcite. *International Journal of Greenhouse Gas Control*, *62*, 113–121. https://doi.org/10.1016/j.ijggc.2017.04.014

Ashokkumar, S., Adler-Nissen, J., & Moller, P. (2012). Factors affecting the wettability of different surface materials with vegetable oil at high temperatures and its relation to cleanability. *Applied Surface Science*, *263*, 86–94. https://doi.org/10.1016/j.apsusc.2012.09.002

ASTM International. (2017). *Standard test method for determination of free fatty acids contained in animal, marine, and vegetable fats and oils used in fat liquors and stuffing compounds*. https://www.astm.org/d5555-95r17.html

Aydar, A. Y., Rodriguez-Martinez, V., & Farkas, B. E. (2016). Determination and modeling of contact angle of Canola oil and olive oil on a PTFE surface at elevated temperatures using air or steam as surrounding media. *LWT- Food Science and Technology*, *65*, 304–310. https://doi.org/10.1016/j.lwt.2015.08.022

Banitabaei, S. A., & Amirfazli, A. (2016). Pneumatic drop generator: Liquid pinch-off and velocity of single droplets. *Colloids and Surfaces A: Physicochemical and Engineering Aspects*, *505*, 204–213. https://doi.org/10.1016/j.colsurfa.2016.05.061

Bateni, A., Susnar, S. S., Amirfazli, A., & Neumann, A. W. (2003). A high-accuracy polynomial fitting approach to determine contact angles. *Colloids and Surfaces A: Physicochemical and Engineering Aspects*, *219*(1–3), 215–231. https://doi.org/10.1016/S0927-7757(03)00053-0

Becker, S., Merz, R., Hasse, H., & Kopnarski, M. (2016). Solvent cleaning and wettability of technical steel and titanium surfaces. *Adsorption Science and Technology*, *34*(4–5), 261–274. https://doi.org/10.1177/0263617416645110

Bejarano, A., Simões, P. C., & Del Valle, J. M. (2016). Fractionation technologies for liquid mixtures using dense carbon dioxide. *Journal of Supercritical Fluids*, *107*, 321–348. https://doi.org/10.1016/j.supflu.2015.09.021

Ben-Othman, S., Jõudu, I., & Bhat, R. (2020). Bioactives from agri-food wastes: Present insights and future challenges. *Molecules*, *25*(3). https://doi.org/10.3390/molecules25030510

Bertola, V. (2009). An experimental study of bouncing Leidenfrost drops: Comparison between Newtonian and viscoelastic liquids. *International Journal of Heat and Mass Transfer*, *52*(7–8), 1786–1793. https://doi.org/10.1016/j.ijheatmasstransfer.2008.09.028

Bharath, R., Inomata, H., Adschiri, T., & Arai, K. (1992). Phase equilibrium study for the separation and fractionation of fatty oil components using supercritical carbon dioxide. *Fluid Phase Equilibria*, *81*, 307–320. https://doi.org/10.1016/0378-3812(92)85159-6

Blake, T. D., & Haynes, J. M. (1969). Kinetics of liquid/liquid displacement. *Journal of Colloid and Interface Science*, *30*(3), 421–423. https://doi.org/10.1016/0021-9797(69)90411-1

Brunetti, L., Daghetta, A., Fedeli, E., Kikic, I., & Zanderighi, L. (1989). Deacidification of olive oils by supercritical carbon dioxide. *Journal of the American Oil Chemists Society*, *66*(2), 209–211. https://doi.org/10.1007/BF02546062

Brunner, G., & Machado, N. T. (2012). Process design methodology for fractionation of fatty acids from palm fatty acid distillates in countercurrent packed columns with supercritical CO_2. *Journal of Supercritical Fluids*, *66*, 96–110. https://doi.org/10.1016/j.supflu.2012.02.012

Brunner, G., Malchow, T., Stiirken, K., & Gottschau, T. (1991). Separation of tocopherols from deodorizer condensates by countercurrent extraction with carbon dioxide. *Journal of Supercritical Fluids*, *4*(1), 72–80. https://doi.org/10.1016/0896-8446(91)90034-4

Cai, G., Katsumata, W., Okajima, I., Sako, T., Funazukuri, T., & Kong, C. Y. (2022). Determination of diffusivities of triolein in pressurized liquids and in supercritical CO_2. *Journal of Molecular Liquids*, *354*. https://doi.org/10.1016/j.molliq.2022.118860

Canola Council of Canada. *The oilseed processing industry*. https://www.canolacouncil.org/about-canola/processing-industry/ (Accessed on October 3rd,2023).

Carlson, A., Do-Quang, M., & Amberg, G. (2011). Dissipation in rapid dynamic wetting. *Journal of Fluid Mechanics*, *682*, 213–240. https://doi.org/10.1017/jfm.2011.211

Carré, A., & Eustache, F. (2000). Spreading kinetics of shear-thinning fluids in wetting and dewetting modes. *Langmuir*, *16*(6), 2936–2941. https://doi.org/10.1021/la991021d

Caswell, T. A. (2014). Dynamics of the vapor layer below a Leidenfrost drop. *Physical Review E - Statistical, Nonlinear, and Soft Matter Physics*, *90*(1) https://doi.org/10.1103/PhysRevE.90.013014

Catchpole, O. J., Grey, J. B., & Noermark, K. A. (2000a). Fractionation of fish oils using supercritical CO_2 and CO_2 + ethanol mixtures. *Journal of Supercritical Fluids*, *19*(1), 25–37. https://doi.org/10.1016/S0896-8446(00)00075-9

Catchpole, O. J., Simôes, P., Grey, J. B., Nogueiro, E. M. M., Carmelo, P. J., & Nunes da Ponte, M. (2000). Fractionation of lipids in a static mixer and packed column using supercritical carbon dioxide. *Industrial & Engineering Chemistry Research*, *39*(12), 4820–4827. https://doi.org/10.1021/ie0002529

Catchpole, O. J., Von Kamp, J. C., & Grey, J. B. (1997). Extraction of squalene from shark liver oil in a packed column using supercritical carbon dioxide. *Industrial and Engineering Chemistry Research*, *36*(10), 4318–4324. https://doi.org/10.1021/ie9702237

Chen, L., Li, L., Li, Z., & Zhang, K. (2017). Submillimeter-sized bubble entrapment and a high-speed jet emission during droplet impact on solid surfaces. *Langmuir*, *33*(29), 7225–7230. https://doi.org/10.1021/acs.langmuir.7b01506

Chen, L., & Li, Z. (2010). Bouncing droplets on nonsuperhydrophobic surfaces. *Physical Review E - Statistical, Nonlinear, and Soft Matter Physics*, *82*(1). https://doi.org/10.1103/PhysRevE.82.016308

Chen, S., & Bertola, V. (2016). The impact of viscoplastic drops on a heated surface in the Leidenfrost regime. *Soft Matter*, *12*(36), 7624–7631. https://doi.org/10.1039/c6sm00893c

Chrastil, J. (1982). Solubility of solids and liquids in supercritical gases. *Journal of Physical Chemistry*, *86*, 3016–3021. https://doi.org/10.1021/j100212a041

Christie, W. W. (2023a). The Lipid Web. Lipid essentials. Lipid Maps. https://lipidmaps.org/resources/lipid_web?page=lipids/lipids.html (Accessed September 20th, 2023)

Christie, W. W. (2023b). The Lipid Web. Sterols 3. Sterols and their conjugates from plants and lower organisms. *Journal of Lipid Research*. https://lipidmaps.org/resources/lipid_web?page=lipids/simple/plant-st/index.htm (Accessed September 20th, 2023)

Crinnion, W. J. (2010). The CDC fourth national report on human exposure to environmental chemicals: what it tells us about our toxic burden and how it assist environmental medicine physicians. *Alternative Medicine Review: A Journal of Clinical Therapeutic*, *15*(2), 101–109.

Damodaran, S., Fennema, O. R., & Parkin, K. L. (2008). Fennema's food chemistry (Fourth edition.). CRC Press/Taylor & Francis.

De Haan, A. B., & De Graauw, J. (1991). Mass transfer in supercritical extraction columns with structured packings for hydrocarbon processing. *Industrial & Engineering Chemistry Research*, *30* (11), 2463-2470 https://doi.org/10.1021/ie00059a016.

De Jesus, S. S., & Filho, R. M. (2020). Recent advances in lipid extraction using green solvents. *Renewable and Sustainable Energy Reviews*, *133*. https://doi.org/10.1016/j.rser.2020.110289

Dickson, J. L., Gupta, G., Horozov, T. S., Binks, B. P., & Johnston, K. P. (2006). Wetting phenomena at the CO_2/water/glass interface. *Langmuir*, *22*(5), 2161–2170. https://doi.org/10.1021/la0527238

Dittmar, D., Eggers, R., Kahl, H., & Enders, S. (2002). Measurement and modelling of the interfacial tension of triglyceride mixtures in contact with dense gases. *Chemical Engineering Science*, *57*, 355–363. https://doi.org/10.1016/S0009-2509(01)00388-8

Dunford, N. T., Teel, J. A., & King, J. W. (2003). A continuous countercurrent supercritical fluid deacidification process for phytosterol ester fortification in rice bran oil. *Food Research International*, *36*, 175–181. https://doi.org/10.1016/S0963-9969(02)00134-5

Eddi, A., Winkels, K. G., & Snoeijer, J. H. (2013). Short time dynamics of viscous drop spreading. *Physics of Fluids*, *25*(1) https://doi.org/10.1063/1.4788693

Fang, T., Goto, M., Wang, X., Ding, X., Geng, J., Sasaki, M., & Hirose, T. (2007). Separation of natural tocopherols from soybean oil byproduct with supercritical carbon dioxide. *Journal of Supercritical Fluids*, *40*(1), 50–58. https://doi.org/10.1016/j.supflu.2006.04.008

FAO. (2021). *The scourge of food loss and waste needs to be urgently tackled to achieve the world's 2030 target*. Https://www.fao.org/News/Story/En/Item/1441673/Icode/.

Fattori, M., Bulley, N. R., & Meisen, A. (1988). Carbon dioxide extraction of canola seed: oil solubility and effect of seed treatment. *Journal of the American Oil Chemists Society*, *65*(6), 968–974. https://doi.org/doi.org/10.1007/BF02544522

Feihrmann, A. C., Giufrida, W. M., Saldaña, M. D. A., de Carvalho Lima, J., Ferreira-Pinto, L., Botelho, J. R. S., Cabral, V. F., de Carvalho Junior, R. N., Corazza, M. L., & Cardozo-Filho, L. (2016). Phase behaviour of sesame (*Sesamum indicum* L.) seed oil using supercritical CO_2. *Canadian Journal of Chemical Engineering*, *94*(2), 310–314. https://doi.org/10.1002/cjce.22374

Fernández-Ronco, M. P., Cismondi, M., Gracia, I., De Lucas, A., & Rodríguez, J. F. (2010). High-pressure phase equilibria of binary and ternary mixtures of carbon dioxide, triglycerides and free fatty acids: Measurement and modeling with the GC-EOS. *Fluid Phase Equilibria*, *295*(1), 1–8. https://doi.org/10.1016/j.fluid.2010.03.016

Fine, F., Brochet, C., Gaud, M., Carre, P., Simon, N., Ramli, F., & Joffre, F. (2016). Micronutrients in vegetable oils: The impact of crushing and refining processes on vitamins and antioxidants in sunflower, rapeseed, and soybean oils. *European Journal of Lipid Science and Technology*, *118*(5), 680–697. https://doi.org/10.1002/ejlt.201400400

Fleck, U., Tiegs, C., & Brunner, G. (1998). Fractionation of fatty acid ethyl esters by supercritical CO_2: high separation efficiency using an automated countercurrent column. *Journal of Supercritical Fluids*, *14*(1), 67–74. https://doi.org/10.1016/S0896-8446(98)00100-4

Fornari, T., Vázquez, L., Torres, C. F., Ibáñez, E., Señoráns, F. J., & Reglero, G. (2008). Countercurrent supercritical fluid extraction of different lipid-type materials: Experimental and

thermodynamic modeling. *Journal of Supercritical Fluids*, *45*(2), 206–212. https://doi.org/10.1016/j.supflu.2008.03.001

Fowkes, F. M. (1962). Determination of interfacial tensions, contact angles and dispersion forces in surfaces by assuming additivity of intermolecular interactions in surfaces. *Journal of Physical Chemistry*, *66*(2), 232. https://doi.org/10.1021/j100808a524

Fowkes, F. M. (1963). Additivity of intermolecular forces at interfaces. I. Determination of the contribution to surface and interfacial tensions of dispersion forces in various liquids. *Journal of Physical Chemistry*, *67*(12), 2538–2541. https://doi.org/10.1021/j100806a008

Funazukuri, T., Hachisu, S., & Wakao, N. (1991). Measurements of binary diffusion coefficients of C16-C24 unsaturated fatty acid methyl esters in supercritical carbon dioxide. *Industrial and Engineering Chemistry Research*, *30*(6), 1323–1329. https://doi.org/10.1021/ie00054a038

Garmus, T. T., de Oliveira Giani, N. A., Rammazzina Filho, W. A., Queiroga, C. L., & Cabral, F. A. (2019). Solubility of oleic acid, triacylglycerol and their mixtures in supercritical carbon dioxide and thermodynamic modeling of phase equilibrium. *Journal of Supercritical Fluids*, *143*, 275–285. https://doi.org/10.1016/j.supflu.2018.08.018

Ghazani, S. M., & Marangoni, A. G. (2013). Minor components in canola oil and effects of refining on these constituents: A review. *Journal of the American Oil Chemists' Society*, *90*(7), 923–932. https://doi.org/10.1007/s11746-013-2254-8

Good, R. J., & Girifalco, L. A. (1960). A theory for estimation of surface and interfacial energies III. Estimation of surface energies of solids from contact angle data. *Journal of Physical Chemistry*, *64*, 561–565. https://doi.org/10.1021/j100834a012

Gracia, I., García, M. T., Rodríguez, J. F., Fernández, M. P., & de Lucas, A. (2009). Modelling of the phase behaviour for vegetable oils at supercritical conditions. *Journal of Supercritical Fluids*, *48*(3), 189–194. https://doi.org/10.1016/j.supflu.2008.11.006

Güçlü-Üstündağ, Ö., & Temelli, F. (2000). Correlating the solubility behavior of fatty acids, mono-, di-, and triglycerides, and fatty acid esters in supercritical carbon dioxide. *Industrial and Engineering Chemistry Research*, *39*(12), 4756–4766. https://doi.org/10.1021/ie0001523

Güçlü-Üstündag, Ö., & Temelli, F. (2004). Correlating the solubility behavior of minor lipid components in supercritical carbon dioxide. *Journal of Supercritical Fluids*, *31*(3), 235–253. https://doi.org/10.1016/j.supflu.2003.12.007

Güçlü-Üstündağ, Ö., & Temelli, F. (2007). Column fractionation of canola oil deodorizer distillate using supercritical carbon dioxide. *Journal of the American Oil Chemists' Society*, *84*(10), 953–961. https://doi.org/10.1007/s11746-007-1117-6

Hare, E. F., & Zisman, W. A. (1955). Autophobic liquids and the properties of their adsorbed films. *Journal of Physical Chemistry*, *59*(4), 335–340. https://doi.org/10.1021/j150526a014

Health Canada Food Directorate. (2010). *Summary of Health Canada's assessment of a health claim about plant sterols in foods and blood cholesterol lowering*. https://www.canada.ca/content/dam/hc-sc/migration/hc-sc/fn-an/alt_formats/pdf/label-

etiquet/claims-reclam/assess-evalu/phytosterols-claim-allegation-eng.pdf#:~:text=Health%20Canada%20has%20concluded%20that%20acceptable%20scientific%20evidence,sterol-enriched%20foods%20as%20foods%20and%20blood%20cholesterol%20lowering. (Accessed on September 14th, 2023)

Health Canada's Food Directorate. (2016, May). *Summary of Health Canada's assessment of a health claim about eicosapentaenoic acid, docosahexaenoic acid and triglyceride lowering*. https://www.canada.ca/en/health-canada/services/food-nutrition/food-labelling/health-claims/assessments/summary-assessment-health-claim-about-eicosapentaenoic-acid-docosahexaenoic-acid-triglyceride-lowering.html (Accessed on September 14th, 2023)

Hiller, N., Schiemann, H., Weidner, E., & Peter, S. (1993). Interfacial tension in systems with a supercritical component at high pressures. *Chemical Engineering & Technology*, *16*(3), 206–212. https://doi.org/10.1002/ceat.270160310

Hong, S. A., Kim, J. D., Kim, J., Kang, J. W., & Kang, I. J. (2010). Phase equilibria of palm oil, palm kernel oil, and oleic acid+supercritical carbon dioxide and modeling using Peng-Robinson EOS. *Journal of Industrial and Engineering Chemistry*, *16*(5), 859–865. https://doi.org/10.1016/j.jiec.2010.03.009

Hurtado-Benavides, A. M., Señoráns, F. J., Ibáñez, E., & Reglero, G. (2004). Countercurrent packed column supercritical CO_2 extraction of olive oil. Mass transfer evaluation. *Journal of Supercritical Fluids*, *28*(1), 29–35. https://doi.org/10.1016/S0896-8446(03)00004-4

Ibáñez, E., Hurtado Benavidez, A. M., Señoráns, F. J., & Reglero, G. (2002). Concentration of sterols and tocopherols from olive oil with supercritical carbon dioxide. *Journal of the American Oil Chemists Society 79*(2), 1255–1260. https://doi.org/10.1007/s11746-002-0636-x

Ilieva, P., Kilzer, A., & Weidner, E. (2016). Measurement of solubility, viscosity, density and interfacial tension of the systems tristearin and CO_2 and rapeseed oil and CO_2. *Journal of Supercritical Fluids*, *117*, 40–49. https://doi.org/10.1016/j.supflu.2016.07.014

Jaeger, P. (1998). *Grenzflächen und Stofftransport in verfahrenstechnischen Prozessenam Beispiel der Hochdruck- Gegenstromfaktionierung mitüberkritischemKohlendioxid*. Hamburg University of Technology (TUHH), Germany.

Jaeger, P., Schnitzler, J. V., & Eggers, R. (1996). Interfacial tension of fluid systems considering the nonstationary case with respect to mass transfer. *Chemical Engineering and Technology*, *19*(3), 197–202. https://doi.org/10.1002/ceat.270190302

James, E., Tangparitkul, S., Brooker, A., Amador, C., Graydon, A., Vaccaro, M., Cayre, O. J., Hunter, T. N., & Harbottle, D. (2018). Accelerated spreading of inviscid droplets prompted by the yielding of strongly elastic interfacial films. *Colloids and Surfaces A: Physicochemical and Engineering Aspects*, *554*, 326–333. https://doi.org/10.1016/j.colsurfa.2018.06.026

Jenab, E., & Temelli, F. (2011). Viscosity measurement and modeling of canola oil and its blend with canola stearin in equilibrium with high pressure carbon dioxide. *Journal of Supercritical Fluids*, *58*(1), 7–14. https://doi.org/10.1016/j.supflu.2011.05.001

Jenab, E., & Temelli, F. (2012). Density and volumetric expansion of carbon dioxide-expanded canola oil and its blend with fully-hydrogenated canola oil. *Journal of Supercritical Fluids*, *70*, 57–65. https://doi.org/10.1016/j.supflu.2012.03.018

Jesch, E. D., & Carr, T. P. (2017). Food ingredients that inhibit cholesterol absorption. *Preventive Nutrition and Food Science*, *22*(2), 67–80. https://doi.org/10.3746/pnf.2017.22.2.67

Kashulines, P., Rizvil, S. S. H., Harriott, P., & Zollweg, J. A. (1991). Viscosities of fatty acids and methylated fatty acids saturated with supercritical carbon dioxide. *Journal of the American Oil Chemists Society*, *68*, 912–921. https://doi.org/10.1007/BF02657535

Kaveh, N. S., Rudolph, E. S. J., Van Hemert, P., Rossen, W. R., & Wolf, K. H. (2014). Wettability evaluation of a CO_2/water/bentheimer sandstone system: Contact angle, dissolution, and bubble size. *Energy and Fuels*, *28*(6), 4002–4020. https://doi.org/10.1021/ef500034j

Kavehpour, P., Ovryn, B., & Mckinley, G. H. (2002). Evaporatively-driven Marangoni instabilities of volatile liquid films spreading on thermally conductive substrates. *Colloids and Surfaces A: Physicochemical and Engineering Aspects*, *206*, 409–423. https://doi.org/10.1016/S0927-7757(02)00064-X

King, J. W., Sable-Demessie, E., Temelli, F., & Tee1, J. A. (1997). Thermal gradient fractionation of glyceride mixtures under supercritical fluid conditions. *Journal of Supercritical Fluids*, *10*(2), 127–137. https://doi.org/10.1016/S0896-8446(97)00007-7

Kolinski, J. M., Mahadevan, L., & Rubinstein, S. M. (2014). Drops can bounce from perfectly hydrophilic surfaces. *Europhysics Letters*, *108*(2). https://doi.org/10.1209/0295-5075/108/24001

Lakdawala, A. M., Thaokar, R., & Sharma, A. (2015). DGLSM based study of temporal instability and formation of satellite drop in a capillary jet breakup. *Chemical Engineering Science*, *130*, 239–253. https://doi.org/10.1016/j.ces.2015.03.029

Law, K.-Y., & Zhao, H. (2016a). Wetting on flat and smooth surfaces. Surface wetting: In: Surface Wetting. Springer, Cham. https://doi-org.login.ezproxy.library.ualberta.ca/10.1007/978-3-319-25214-8_3 (pp. 35-54)

Law, K.-Y., & Zhao, H. (2016b). What do contact angles measure?. In: Surface Wetting. Springer, Cham. https://doi-org.login.ezproxy.library.ualberta.ca/10.1007/978-3-319-25214-8_5 (pp. 99–121).

Lockemann, C. A. (1994a). High-pressure phase equilibria and densities of the binary mixtures carbon dioxide—oleic acid, carbon dioxide—methyl myristate, and carbon dioxide—methyl palmitate and of the ternary mixture carbon dioxide—methyl myristate—methyl palmitate. *Chemical Engineering and Processing: Process Intensification*, *33*(3), 171–178. https://doi.org/10.1016/0255-2701(94)90007-8

Lockemann, C. A. (1994b). Interfacial tensions of the binary systems carbon dioxide-oleic acid, carbon dioxide-methyl myristate, and carbon dioxide-methyl palmitate and of the ternary system carbon dioxide-methyl myristate-methyl palmitate at high pressures. *Chemical Engineering and*

Processing: Process Intensification, *33*(4), 193–198. https://doi.org/10.1016/0255-2701(94)01000-5

Lockemann, C. A., & Schlünder, E.-U. (1995). Liquid-phase viscosities of the binary systems carbon dioxide-oleic acid, carbon dioxide-methyl myristate, and carbon dioxide-methyl palmitate at high pressures. *Chemical Engineering and Processing,* 34 (6), 487-493. https://doi.org/10.1016/0255-2701(94)00562-1

Lockemann', C. A., & Schlünder, E.-U. (1996). The effect of concentration on the liquid phase diffusivities in the binary systems carbon dioxide-oleic acid, carbon dioxide-methyl myristate and carbon dioxide-methyl palmitate at high pressures. *Chemical Engineering and Processing*, 35, 29–33. https://doi.org/doi.org/10.1016/0255-2701(95)04102-8

Mack, G. L., & Lee, D. A. (1963). The determination of contact angles from measurements of the dimensions of small bubbles and drops II. *Journal of Physical Chemistry*, *40*(2), 169–176. https://doi.org/10.1021/j150371a002

Maheshwari, P., Nikolov, Z. L., White, T. M., & Hartel, R. (1992). Solubility of fatty acids in supercritical carbon dioxide. *Journal of the American Oil Chemists Society*, *11*, 1069–1076. https://doi.org/10.1007/BF02541039

Moreau, R. A. (2005). 2.4 Corn oil. In J. & S. Wiley (Ed.), *Bailey's Industrial Oil and Fat Products* (6th Edition, Vols. 1–6, p. 156). John Wiley & Sons.

National Institute of Standards and Technology (NIST). (2005). NIST Chemisty WebBook. https://webbook.nist.gov/cgi/cbook.cgi?ID=C124389#

Nilsson, W. B., Gauglitz, E. J., & Hudson, J. K. (1991). Solubilities of methyl oleate, oleic acid, oleyl glycerols, glycerol mixtures in supercritical carbon dioxide. *Journal of the American Oil Chemists Society, 68*(2), 87–91. https://doi.org/10.1007/BF02662323

Osório, C., Machado, S., Peixoto, J., Bessada, S., Pimentel, F. B., Alves, R. C., & Oliveira, M. B. P. P. (2020). Pigments content (Chlorophylls, fucoxanthin and phycobiliproteins) of different commercial dried algae. *Separations*, *7*(2), 1–14. https://doi.org/10.3390/separations7020033

Penedo, P. L., Coelho, G. L. V, & Mendes, M. F. (2009). Phase equilibria of oleic acid, palmitic, stearic, linoleic and linolenic acids in supercritical CO_2. *Journal of Industrial and Engineering Chemistry*, *26*(01), 137–147. https://doi.org/10.1590/S0104-66322009000100013

Peter, S., & Jakob, H. (1991). The rheological behavior of coexisting phases in systems containing fatty acids and dense gases. *Journal of Supercritical Fluids*, *4*, 166–172. https://doi.org/10.1016/0896-8446(91)90004-P

Pieck, A., Crampon, C., Fabien, A., & Badens, E. (2021). A new correlation for predicting flooding point in supercritical fractionation packed columns. *Journal of Supercritical Fluids*, *179*, 105404. https://doi.org/10.1016/j.supflu.2021.105404

Pieck, C. A., Crampon, C., Charton, F., & Badens, E. (2017). A new model for the fractionation of fish oil FAEEs. *Journal of Supercritical Fluids*, *120*, 258–265. https://doi.org/10.1016/j.supflu.2016.05.024

Piironen, V., Lindsay, D. G., Miettinen, T. A., Toivo, J., & Lampi, A.-M. (2000). Review: Plant sterols: biosynthesis, biological function and their importance to human nutrition. *Journal of the Science of Food and Agriculture*, *80*, 939–966. https://doi.org/10.1002/(SICI)1097-0010(20000515)80:7<939::AID-JSFA644>3.0.CO;2-C

Prado, I. M., Giufrida, W. M., Alvarez, V. H., Cabral, V. F., Quispe-Condori, S., Saldaña, M. D. A., & Cardozo-Filho, L. (2011). Phase equilibrium measurements of sacha inchi oil (*Plukenetia volubilis*) and CO_2 at high pressures. *Journal of the American Oil Chemists Society*, *88*(8), 1263–1269. https://doi.org/10.1007/s11746-011-1786-z

Przybylski, R., Mag, T., Eskin, N. A. M., & McDonald, B. E. (2005). 2.2 Canola oil. In J. & S. Wiley (Ed.), *Bailey's Industrial Oil and Fat Products* (6th Edition, Vols. 1–6, p. 64). John Wiley & Sons.

Quéré, D. (2013). Leidenfrost dynamics. *Annual Review of Fluid Mechanics*, *45*, 197–215. https://doi.org/10.1146/annurev-fluid-011212-140709

Rahman, M. R., Mullagura, H. N., Kattemalalawadi, B., & Waghmare, P. R. (2018). Droplet spreading on liquid–fluid interface. *Colloids and Surfaces A: Physicochemical and Engineering Aspects*, *553*, 143–148. https://doi.org/10.1016/j.colsurfa.2018.05.042

Rangaswamy, S., Kumar, G. S., & Kuppusamy, C. (2021). Membrane technology for vegetable oil processing—Current status and future prospects. *Comprehensive Reviews in Food Science and Food Safety*, *20*(5), 5015–5042. https://doi.org/10.1111/1541-4337.12825

Regueira, T., Carvalho, P. J., Oliveira, M. B., Lugo, L., Coutinho, J. A. P., & Fernández, J. (2013). Experimental measurements and modeling of CO_2 solubility in sunflower, castor and rapeseed oils. *Journal of Supercritical Fluids*, *82*, 191–199. https://doi.org/10.1016/j.supflu.2013.07.010

Rezaei, K. A., & Temelli, F. (2000). Using supercritical fluid chromatography to determine diffusion coefficients of lipids in supercritical CO_2. *Journal of Supercritical Fluids*, *17*, 35–44. https://doi.org/10.1016/S0896-8446(99)00039-X

Ribeiro, A. M., Bemardo-Gil, M. G., Adachi, by, & Valle, D. (1995). Solubilities of triolein in supercritical CO_2. *Journal of Chemical & Engineering Data*, *40*, 1188–1192. https://doi.org/https://doi-org.login.ezproxy.library.ualberta.ca/10.1021/je00022a0

Riha, V., & Brunner, G. (2000). Separation of fish oil ethyl esters with supercritical carbon dioxide. *Journal of Supercritical Fluids*, *17*(1), 55–64. https://doi.org/10.1016/S0896-8446(99)00038-8

Ruivo, R., Cebola, M. J., Simões, P. C., & da Ponte, M. N. (2001). Fractionation of edible oil model mixtures by supercritical carbon dioxide in a packed column. Part I: Experimental results. *Industrial and Engineering Chemistry Research*, *40*(7), 1706–1711. https://doi.org/10.1021/ie000747y

Ruivo, R., Cebola, M. J., Simões, P. C., & Nunes da Ponte, M. (2002). Fractionation of edible oil model mixtures by supercritical carbon dioxide in a packed column. 2. A mass-transfer study. *Industrial and Engineering Chemistry Research*, *41*(9), 2305–2315. https://doi.org/10.1021/ie0106579

Sahasrabudhe, S. N., Rodriguez-Martinez, V., O'Meara, M., & Farkas, B. E. (2017). Density, viscosity, and surface tension of five vegetable oils at elevated temperatures: Measurement and modeling. *International Journal of Food Properties*, *20*, 1965–1981. https://doi.org/10.1080/10942912.2017.1360905

Sahena, F., Zaidul, I. S. M., Jinap, S., Karim, A. A., Abbas, K. A., Norulaini, N. A. N., & Omar, A. K. M. (2009). Application of supercritical CO_2 in lipid extraction - A review. *Journal of Food Engineering*, *95*(2), 240–253. https://doi.org/10.1016/j.jfoodeng.2009.06.026

Saini, R. K., Prasad, P., Shang, X., & Keum, Y. S. (2021). Advances in lipid extraction methods—a review. *International Journal of Molecular Sciences*, *22*(24) 13643 https://doi.org/10.3390/ijms222413643

Saldaña, M. D. A., dos Reis Coimbra, J. S., & Cardozo-Filho, L. (2015). Recovery, encapsulation and stabilization of bioactives from food residues using high pressure techniques. *Current Opinion in Food Science*, *5*, 76–85. https://doi.org/10.1016/j.cofs.2015.09.001

Seifried, B., & Temelli, F. (2010). Interfacial tension of marine lipids in contact with high pressure carbon dioxide. *Journal of Supercritical Fluids*, *52*(2), 203–214. https://doi.org/10.1016/j.supflu.2009.12.009

Seifried, B., & Temelli, F. (2011). Viscosity and rheological behaviour of carbon dioxide-expanded fish oil triglycerides: Measurement and modeling. *Journal of Supercritical Fluids*, *59*, 27–35. https://doi.org/10.1016/j.supflu.2011.07.010

Seifried, B., & Temelli, F. (2014). Viscosity and rheological behavior of carbon dioxide-expanded fish oil fatty acid ethyl esters: Measurement using a rotational viscometer and modeling. *Journal of Supercritical Fluids*, *95*, 519–524. https://doi.org/10.1016/j.supflu.2014.10.024

Senrayan, J., & Venkatachalam, S. (2019). A short extraction time of vegetable oil from *Carica papaya* L. seeds using continuous ultrasound acoustic cavitation: Analysis of fatty acid profile and thermal behavior. *Journal of Food Process Engineering*, *42*(1):e12950. https://doi.org/10.1111/jfpe.12950

Simões, P. C., Eggers, R., & Jaeger, P. T. (2000). Interfacial tension of edible oils in supercritical carbon dioxide. *European Journal of Lipid Science and Technology*, *102*(4), 263–265. https://doi.org/10.1002/(SICI)1438-9312(200004)102:4<263::AID-EJLT263>3.0.CO;2-D

Simões, P. C., Matos, H. A., Carmelo, P. J., de Azevedo, E. G., & da Ponte, M. N. (1995). Mass transfer in countercurrent packed columns: Application to supercritical CO_2 extraction of terpenes. *Industrial and Engineering Chemistry Research*, *34*(2), 613–618. https://doi.org/10.1021/ie00041a023

Soares, B. M. C., Gamarra, F. M. C., Paviani, L. C., Gonçalves, L. A. G., & Cabral, F. A. (2007). Solubility of triacylglycerols in supercritical carbon dioxide. *Journal of Supercritical Fluids*, *43*(1), 25–31. https://doi.org/10.1016/j.supflu.2007.03.013

Stockfleth, R., & Brunner, G. (1999). Hydrodynamics of a packed countercurrent column for the gas extraction. *Industrial and Engineering Chemistry Research*, *38*(10), 4000–4006. https://doi.org/10.1021/ie990251k

Stockfleth, R., & Brunner, G. (2001). Holdup, pressure drop, and flooding in packed countercurrent columns for the gas extraction. *Industrial and Engineering Chemistry Research*, *40*(1), 347–356. https://doi.org/10.1021/ie000466q

Sutjiadi-Sia, Y., Jaeger, P., & Eggers, R. (2008a). Interfacial phenomena of aqueous systems in dense carbon dioxide. *Journal of Supercritical Fluids*, *46*(3), 272–279. https://doi.org/10.1016/j.supflu.2008.06.001

Sutjiadi-Sia, Y., Jaeger, P., & Eggers, R. (2008b). Interfacial tension of solid materials against dense carbon dioxide. *Journal of Colloid and Interface Science*, *320*(1), 268–274. https://doi.org/10.1016/j.jcis.2007.12.021

Sutjiadi-Sia. (2008). *Interfacial phenomena of liquids in contact with dense CO_2* [PhD Thesis]. Hamburg University of Technology (TUHH), Germany.

Tegetmeier, A., Dittmar, D., Fredenhagen, A., & Eggers, R. (2000). Density and volume of water and triglyceride mixtures in contact with carbon dioxide. *Chemical Engineering and Processing*, *39*, 399–405. https://doi.org/10.1016/S0255-2701(99)00102-6

Tjahjadi, M., Stone, H. A., & Ottino, J. M. (1992). Satellite and subsatellite formation in capillary breakup. *Journal of Fluid Mechanics*, *243,* 297–317. https://doi.org/10.1017/S0022112092002738

Torres, C. F., Fornari, T., Torrelo, G., Señoráns, F. J., & Reglero, G. (2009). Production of phytosterol esters from soybean oil deodorizer distillates. *European Journal of Lipid Science and Technology*, *111*(5), 459–463. https://doi.org/10.1002/ejlt.200800141

Von Bahr, M., Tiberg, F., & Yaminsky, V. (2001). Spreading dynamics of liquids and surfactant solutions on partially wettable hydrophobic substrates. *Colloids and Surfaces A: Physicochemical and Engineering Aspects*, *193*, 85–96. https://doi.org/10.1016/S0927-7757(01)00756-7

Wang, G.Q., Yuan, X.G., Yu, K. T. (2005). Review of mass-transfer correlations for packed columns. *Industrial & Engineering Chemistry Research, 44*(23), 8715-8729. https://doi.org/10.1021/ie050017w

Yener, M. E., Kashulines, P., Rizvi, S. S. H., & Harriott, P. (1998). Viscosity measurement and modeling of lipid-supercritical carbon dioxide mixtures. *Journal of Supercritical Fluids*, *11*(3), 151–162. https://doi.org/10.1016/S0896-8446(97)00036-3

Yeo, J. Y. J., Soetaredjo, F. E., Ismadji, S., & Sunarso, J. (2021). Experimental measurement and correlation of phase equilibria of palmitic, stearic, oleic, linoleic, and linolenic acids in supercritical carbon dioxide. *Journal of Industrial and Engineering Chemistry*, *97*, 485–491. https://doi.org/10.1016/j.jiec.2021.03.002

Yu, Z., Rizvi, S., Zollweg, J. (1992) Phase equilibria of oleic acid, methyl oleate, and anhydrous milk fat in supercritical carbon dioxide. *Journal of Supercritical Fluids*, *5*(2), 114–122. https://doi.org/10.1016/0896-8446(92)90028-I

Zacchi, P., Bastida, S. C., Jaeger, P., Cocero, M. J., & Eggers, R. (2008). Countercurrent de-acidification of vegetable oils using supercritical CO_2: Holdup and RTD experiments. *Journal of Supercritical Fluids*, *45*(2), 238–244. https://doi.org/10.1016/j.supflu.2008.02.005

Zacchi, P., Daghero, J., Jaeger, P., & Eggers, R. (2006). Extraction/Fractionation and deacidification of wheat germ oil using supercritical carbon dioxide. *Brazilian Journal of Chemical Engineering*, *23*(01), 105–F

Appendix A. Supplementary material for Chapter 3

Data of interfacial tension (IFT) and contact angle of Chapter 3

Table A. 1. Interfacial tension (IFT) of corn oil in nitrogen at different pressures and temperatures

T (°C)	P (MPa)	IFT (mN/m)	
		Average	Std
40	0.1	32.0	0.3
	16	22.0	0.4
	20	20.0	0.4
	24	19.3	0.5
60	0.1	29.4	0.7
	16	21.6	0.7
	20	20.2	0.4
	24	18.8	0.8
80	0.1	29.2	0.4
	16	21.0	0.7
	20	18.6	1.2
	24	19.6	0.2

Average and standard deviation (Std) based on n=3

Table A. 2. Interfacial tension (IFT) of corn oil in saturated carbon dioxide at different temperatures and pressures

T (°C)	P (MPa)	IFT (mN/m)	
		Average	Std
40	0.1	32.0	0.3
	4	17.2	0.0
	8	7.4	0.1
	12	3.1	0.0
	16	2.5	0.1
	20	1.9	0.1
	24	1.9	0.1
60	0.1	29.4	0.7
	4	19.4	0.1
	8	10.5	0.8
	12	5.4	0.5
	16	4.0	0.1
	20	2.8	0.0
	24	2.2	0.1
80	0.1	29.2	0.4
	4	20.9	0.1
	8	14.4	0.3
	12	8.1	0.1
	16	6.0	0.3
	20	4.7	0.3
	24	3.7	0.3

Average and standard deviation (Std) based on n=3

Table A. 3. Interfacial tension (IFT) of corn oil in unsaturated and saturated CO_2 at 60 °C and different pressures

P (MPa)	IFT (mN/m)			
	Unsaturated		Saturated	
	Average	Std	Average	Std
16	4.0	0.1	3.6	0.3
20	2.8	0.0	2.6	0.1
24	2.2	0.1	2.2	0.2

Average and standard deviation (Std) based on n=3

Table A. 4. Contact angle of corn oil in unsaturated and saturated CO_2 at 60 °C and different pressures

P (MPa)	CA (°)			
	Unsaturated		Saturated	
	Average	Std	Average	Std
16	5.4	0.4	7.8	2.0
20	8.9	1.3	11.4	0.8
24	9.5	0.4	9.2	1.2

Average and standard deviation (Std) based on n=3

Table A. 5. Equilibrium contact angle (CA) of corn oil on stainless steel in different environments and experimental conditions

Environment	P (MPa)	T (°C)					
		40		60		80	
		Average CA (°)	Std (°)	Average CA (°)	Std (°)	Average CA (°)	Std (°)
N_2	0.1	6.2	2.2	4.7	0.1	5.8	1.4
	16	10.5	1.9	4.4	1.4	6.2	0.3
	20	6.8	0.8	4.2	0.7	3.2	1.2
	24	6.7	1.1	4.0	0.4	7.1	1.2
CO_2	0.1	6.2	2.2	4.7	0.1	5.8	1.4
	16	3.9	0.2	5.4	0.4	4.9	0.3
	20	5.0	0.4	8.9	1.3	4.1	1.0
	24	11.4	1.0	9.5	0.4	7.8	1.0

Average and standard deviation (Std) based on n=3

Appendix B. Supplementary material for Chapter 4

B.1. Data of interfacial tension (IFT) and contact angle of Chapter 4

Table B. 1. Interfacial tension of oleic acid and caola oil on glass in CO_2 at 60 °C and different pressures

Liquid phase	P (MPa)	IFT (mN/m)	
		Average	Std
OA	0.1	30.2	0.0
	4.0	21.7	0.1
	8.0	12.5	0.2
	10.0	7.4	0.2
	12.0	4.9	0.1
CanO	16	3.9	0.2
	20	5	0.4
	24	11.4	1

OA: oleic acid; CanO: canola oil; Average and standard deviation (Std) based on n=3

Table B. 2. Contact angle of oleic acid and canola oil on glass in N_2 at 60 °C and different pressures

Liquid phase	P (MPa)	CA (°)	
		Average	Std
OA	0.1	20.9	0.8
	16	20.9	0.4
	20	19.8	0.7
	24	19.7	1.5
CanO	0.1	18.6	1.1
	16	25.3	1.4
	20	24.6	0.9
	24	25.5	1.2

OA: oleic acid; CanO: canola oil; Average and standard deviation (Std) based on n=3

Table B. 3. Contact angle of oleic acid and canola oil on glass in CO_2 at different pressures and temperatures

T (°C)	P (MPa)	Oleic acid		Canola oil	
		CA (°)		CA (°)	
		Average	Std	Average	Std
40	0.1	23.3	2.3	23.3	2.3
	16.0	11.8	0.5	11.8	0.5
	20.0	8.9	0.3	8.9	0.3
	24.0	3.7	1.0	3.7	1.0
60	0.1	20.9	0.8	20.9	0.8
	16.0	13.0	0.5	13.0	0.5
	20.0	11.2	1.0	11.2	1.0
	24.0	8.6	0.5	8.6	0.5
80	0.1	20.1	0.3	20.1	0.3
	16.0	3.6	0.6	3.6	0.6
	20.0	4.0	1.4	4.0	1.4
	24.0	3.4	0.6	3.4	0.6

Average and standard deviation (Std) based on n=3

B.2. Spreading dynamics on oleic acid and canola oil in supercritical nitrogen

Spreading radius (Figure B.1) and log-log representation (Figure B.2) of the evolution of spreading radius over time for oleic acid (OA) and canola oil (CanO) in supercritical nitrogen (SC-N_2) are presented as supplementary information to the results of Chapter 4.

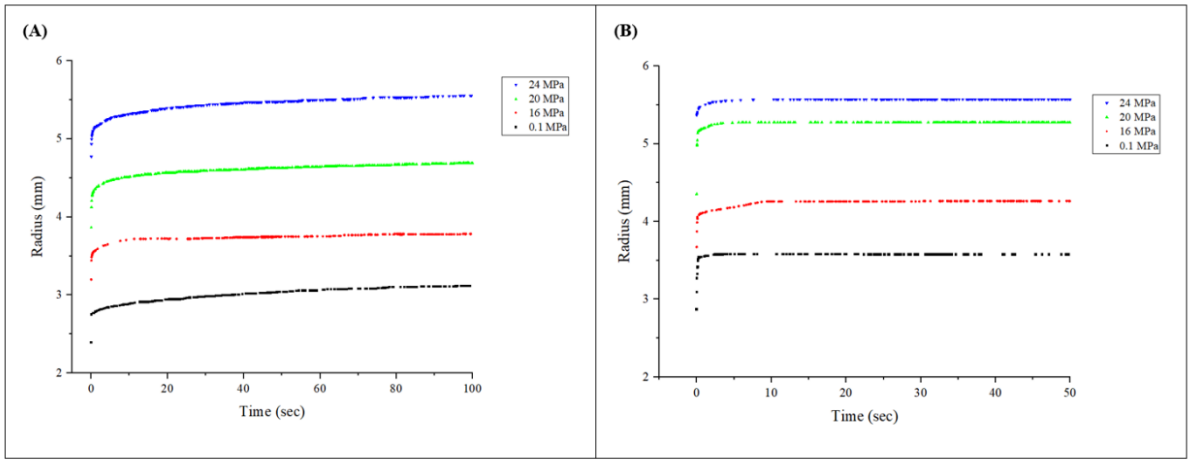

Figure B. 1. Spreading radius versus time of (A) oleic acid and (B) canola oil in SC-N_2 surrounding medium at 60 ºC as a function of pressure. (The curves are included to guide the eye)

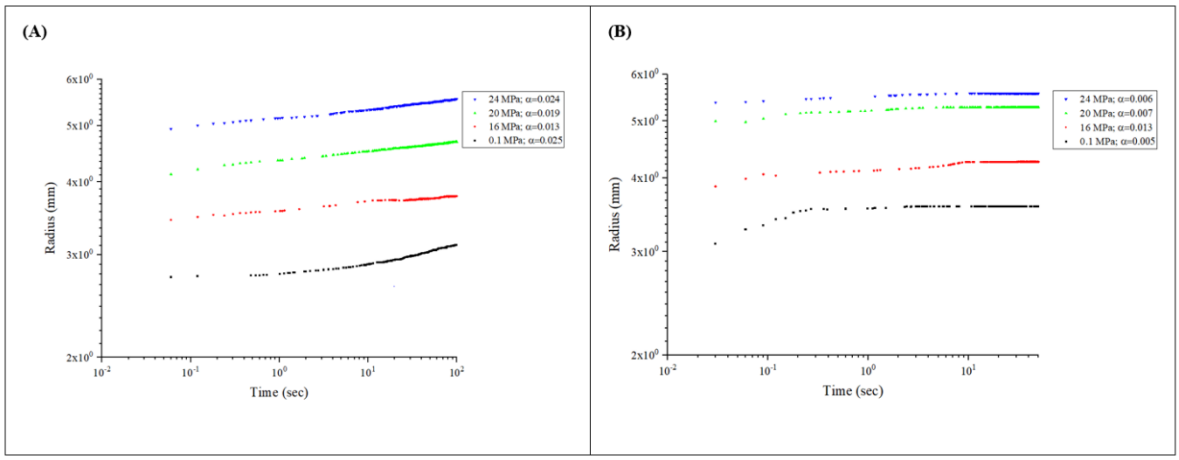

Figure B. 2. Log-log representation of the spreading radius versus of (A) oleic acid and (B) canola oil in SC-N_2 surrounding medium at 60 ºC as a function of pressure. (The curves are included to guide the eye)

B.3. Wettability behavior on perforated stainless steel plate

Wettability behaviour of chemically and mechanically perforated stainless steel (SS) surfaces was evaluated considering the differences in perforation method and its potential impact on wettability. The chemically perforated SS surface was obtained from McMaster-Carr (code:9215t32, Aurora, OH, USA), and the supplier information indicated that the perforation of the holes on this metal sheet was performed by the chemical etching process without any further details about this process. For mechanical perforations, the same polished SS surface used for contact angle (CA) determination of lipids in Chapters 3 and 4 was perforated using water jet cutting at the Machine Shop located in the Mechanical Engineering Building, University of Alberta. The determination of the surface roughness and hole roughness for each type of perforated SS sheet was performed following the roughness analysis protocol described in Chapter 3. These

experiments using chemically, and mechanically perforated SS sheets were completed following the CA determination protocols described in Chapters 3 and 4.

The spreading of corn oil droplet on chemically perforated SS surface in SC-N_2 and SC-CO_2 at 40 ºC and 16 MPa was presented in Figure B.3, while Figures B.4 to B.6 present the spreading behavior of CanO in SC-CO_2 at 40 °C, and pressures of 16 and 20 MPa.

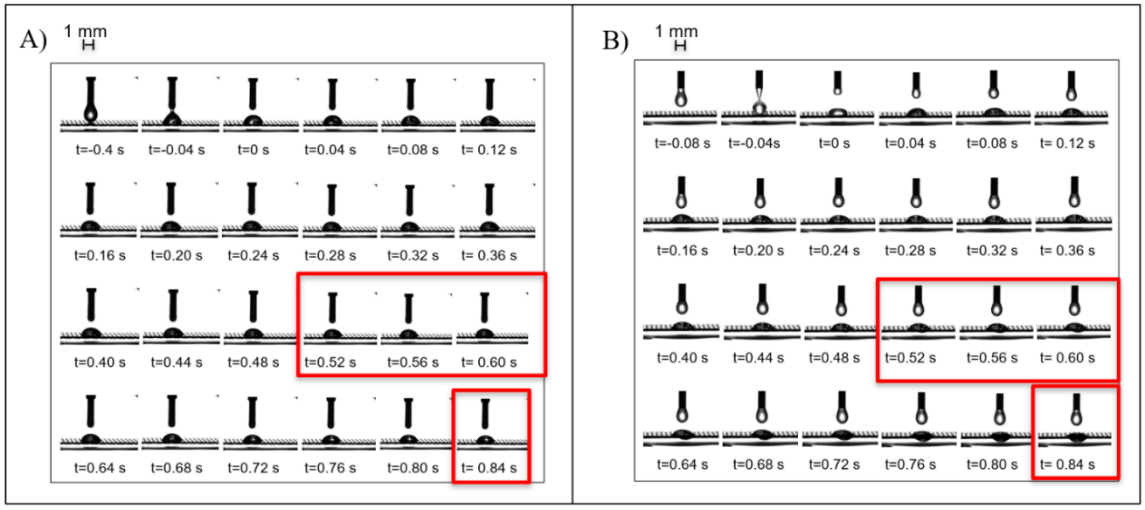

Figure B. 3. Wetting phenomena of corn oil drop on chemically perforated stainless steel under dense gases (A) nitrogen and (B) carbon dioxide at 40 ºC and 16 MPa.

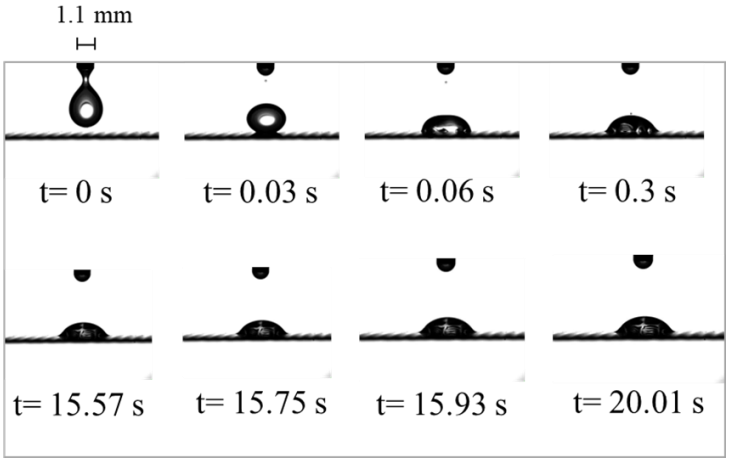

Figure B. 4. Wetting phenomena of canola oil in SC-CO_2 medium on chemically perforated SS surface at 40 °C and 20 MPa (no lipid permeation).

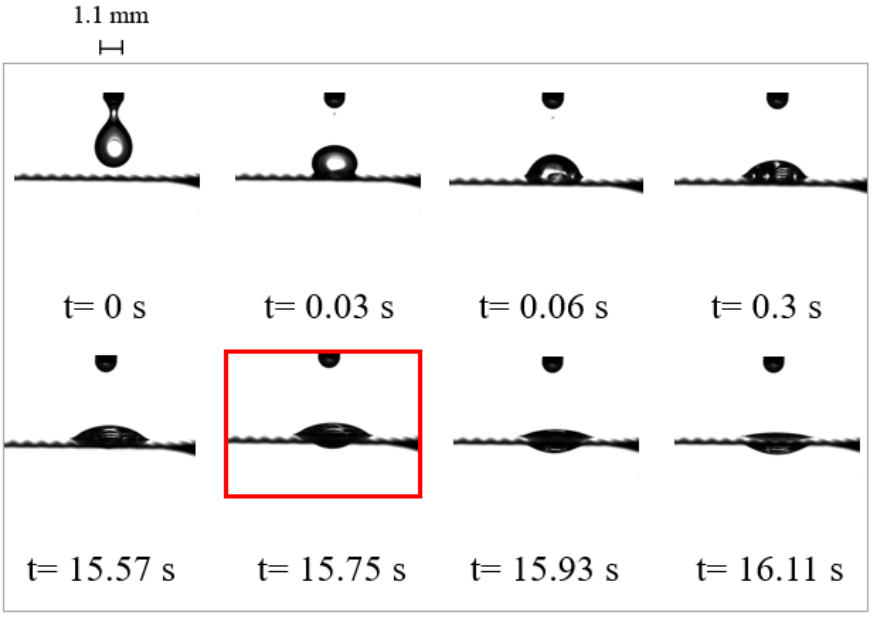

Figure B. 5. Wetting phenomena of canola oil in SC-CO_2 medium on chemically perforated SS surface at 40 °C and 16 MPa (delayed lipid permeation).

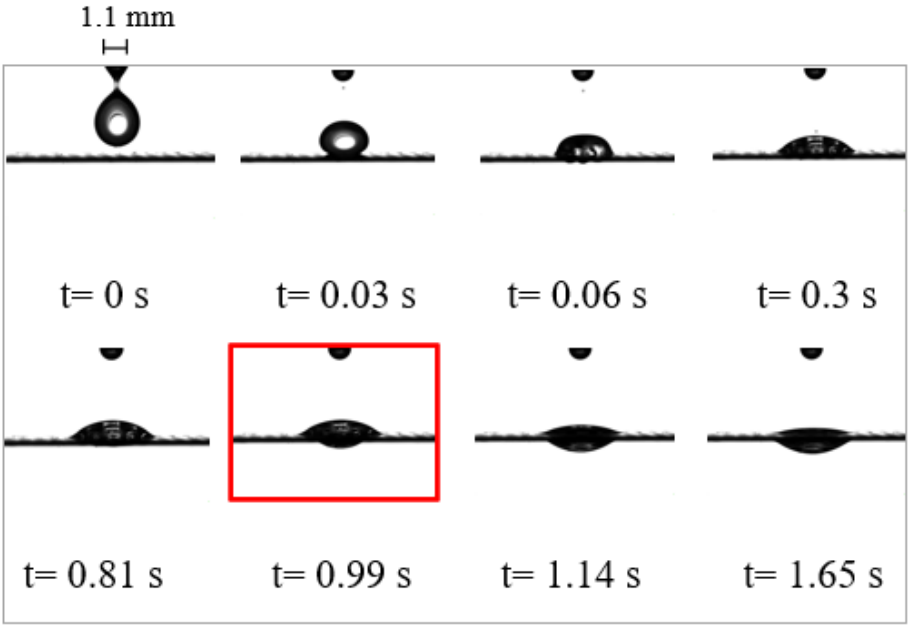

Figure B. 6. Wetting phenomena of canola oil in SC-CO_2 medium on chemically perforated SS surface at 40 °C and 20 MPa (advanced lipid permeation).

There were challenges to obtain consistent wetting patterns due to the difficulties in maintaining constant lipid drop dosing velocity (Figures B.3 – B.6). However, all experiments were completed in triplicate and Table B.4 summarizes the results related to the different permeation patterns of lipids in dense gases on different perforated plates. Based on roughness analysis results (Table B.5), the perforated SS sheets had relevant proportion differences in roughness between the hole and surface for each type of SS sheet. For example, the surface roughness proportion ratio between mechanical and chemically perforated plates was 32:1, whereas that for the hole roughness was 1:22.

Table B. 4. Wetting phenomena results related to permeation of canola oil on perforations of mechanically and chemically perforated SS sheets under dense gases of N_2 and CO_2 at 40 °C and different pressures.

Type of perforated sheet	Surrounding fluid	Pressure MPa	Findings
Mechanical	N_2	0.1	Fast falling, fast permeation
		16	Slow falling, fast permeation
		20	Fast falling, slow/fast permeation
		24	Slow/fast falling, slow/fast/no permeation
	CO_2	0.1	Slow falling, fast/no permeation, sliding droplet to sides
		16	Slow/fast falling, fast/no permeation
		20	Sliding to sides, permeation
		24	Fast permeation/drop on top + permeation
Chemical	N_2	16	Slow falling, slow/fast permeation
		20	Slow/fast falling, slow/fast permeation
		24	Slow falling, slow permeation
	CO_2	16	Delayed lipid permeation
		20	No lipid permeation, advanced lipid permeation
		24	Fast falling, slow permeation

Table B. 5. Roughness results for mechanical and chemical perforated SS sheets

Type of perforation method	Section of surface	Roughness (nm)	Std
Mechanical	surface	7480	912.34
	hole	630	34.67
Chemical	surface	233	38.11
	hole	14020	546.01

Average and standard deviation (Std) based on n=3

Appendix C. Supplementary material for Chapter 5.

C.1. Data of extract amount, extract yield, separation efficiency, dynamic and static hold-up and FFA% in DH and SH of Chapter 5

Table C. 1. Extract amount, extract yield and raffinate amounts obtained with different types of packing under different experimental conditions.

Packing	Variable	Experimental conditions											
		40 °C 16 MPa, 15 S/F		60-100 °C, 16 MPa, 15 S/F		60 °C, 16 MPa, 15 S/F		60 °C, 16 MPa, 25 S/F		60 °C, 24 MPa, 15 S/F		60 °C, 24 MPa, 25 S/F	
		Average	Std	Average	Std	Average	Std	Average	Std	Average	Std	Average	Std
PS	Extract amount (g)	11.9	0.8	2.4	0.4	9.0	0.8	10.4	1.6	29.8	3.5	39.4	3.6
	Extract yield (%)	9.9	0.7	2.0	0.3	7.4	0.7	14.4	2.3	24.7	2.9	54.8	5.0
	Raffinate amount (g)	27.5	3.3	51.1	11.6	54.1	2.1	35.9	4.5	48.3	1.4	0.3	0.2
SB	Extract amount (g)	15.7	3.6	1.2	0.2	5.0	0.6	6.1	0.2	29.9	1.0	27.6	1.2
	Extract yield (%)	13.0	3.0	1.0	0.2	4.1	0.5	8.5	0.2	24.8	0.8	38.3	1.7
	Raffinate amount (g)	55.2	1.7	17.0	4.6	24.7	1.9	26.4	1.0	17.2	1.1	6.8	1.5
GB	Extract amount (g)	10.0	0.5	1.9	0.1	5.2	0.6	6.5	0.7	24.1	0.8	25.0	3.0
	Extract yield (%)	8.3	0.4	1.5	0.0	4.3	0.5	9.0	1.0	20.0	0.6	34.8	4.2
	Raffinate amount (g)	8.4	1.1	9.8	2.1	8.8	0.2	8.3	0.6	7.4	0.5	4.9	1.0

PS: perforated stainless steel packing; SB: stainless steel beads; GB: glass beads; S/F: solvent- to-feed ratio
Average and standard deviation (Std) based on n=2 for 40 °C and 60-100°C, and n=3 for 60 °C.

Table C. 2. Separation efficiency under different experimental conditions

PACKING	Experimental conditions											
	40 °C, 16 MPa, 15 S/F		60-100 °C, 16 MPa, 15 S/F		60 °C, 16 MPa, 15 S/F		60 °C, 16 MPa, 25 S/F		60 °C, 24 MPa, 15 S/F		60 °C, 24 MPa, 25 S/F	
	Average	Std	Average	Std	Average	Std	Average	Std	Average	Std	Average	Std
PS	14.1	4.79	1.93	0.33	10.71	1.2	12.36	2.44	29.08	12.82	59.08	3.8
SB	17.8	4.8	1.3	0.1	6.7	3	12.7	1.6	44.9	3.3	54.2	4.4
GB	15.7	0.7	1.6	0.1	7.6	2.5	14.9	2.1	43.5	5.6	38.09	4.2

PS: perforated stainless steel packing; SB: stainless steel beads; GB: glass beads; S/F: solvent- to-feed ratio
Average and standard deviation (Std) based on n=2 for 40 °C and 60-100°C, and n=3 for 60 °C.

Table C. 3. Dynamic hold-up (DH) amounts, free fatty acid (FFA) concentration in DH, static hold-up amount, SH FFA concentration obtained using different types of packing under different experimental conditions.

Variable	Packing	Experimental conditions											
		40 °C, 16 MPa, 15 S/F		60-100 °C, 16 MPa, 15 S/F		60 °C, 16 MPa, 15 S/F		60 °C, 16 MPa, 25 S/F		60 °C, 24 MPa, 15 S/F		60 °C, 24 MPa, 25 S/F	
		Average	Std	Average	Std	Average	Std	Average	Std	Average	Std	Average	Std
	PS	1.66	0.63	36.69	8.66	24.59	4.87	0.01	0.01	2.35	2.80	0.01	0.00
DH FFA (%)		78.60	0.85	79.45	0.07	79.07	0.72	0.01	0.00	82.5	0.42	0.01	0.00
SH amount (g)		0.51	0.71									16.80	3.54
SH FFA (%)		78.95	0.92									78.95	0.919
DH amount (g)	SB	25.06	1.03	62.64	1.25	58.74	1.00	14.34	0.83	36.28	3.18	10.06	1.67
DH FFA (%)		95.65	10.68	87.25	0.64	88.07	3.12	84.63	0.15	81.13	0.32	76.67	4.22
SH amount (g)		3.88	0.57									3.26	1.17
SH FFA (%)		87.50	5.52									86.23	7.39
DH amount (g)	GB	80.78	2.71	72.79	0.46	67.28	12.69	31.80	2.70	46.89	3.60	16.69	1.36
DH FFA (%)		84.55	1.63	87.20	2.69	84.90	0.10	83.27	1.42	80.90	2.95	75.63	4.19
SH amount (g)		4.04	0.54									2.30	0.37
SH FFA (%)		89.25	3.46									85.40	1.27

PS: perforated stainless steel packing; SB: stainless steel beads; GB: glass beads; S/F: solvent- to-feed ratio
Average and standard deviation (Std) based on n=2 for 40 °C and 60-100°C, and n=3 for 60 °C.

C.2.1. Static hold-up definition and determination

As defined in Chapter 5, there are two different types of liquid hold-up during the fractionation of lipid mixtures in countercurrent mode using supercritical carbon dioxide (SC-CO_2), static (SH) and dynamic hold-up (DH). SH refers to the liquid attached to the packing material by adhesive forces; thus, it does not drain from the packing, and it must be removed by other means; whereas DH refers to the liquid that drains out of the column once the gas and liquid pumps are stopped (Stockfleth & Brunner, 2001).

During the fractionation column operation, SH was determined for two sets of experiments in duplicates: a) 40 °C, 16 MPa, 15 S/F, and b) 60°C, 24 MPa, 25 S/F. After the collection of DH, the column was pressurized again with CO_2 at the same experimental conditions, and the lipids remaining on the packing material were allowed to solubilize into the CO_2 phase over 60 min in a batch mode operation. After this time, CO_2 inlet valve was closed and the SH fraction was collected by means of the on/off valve located at the exit of the calming section, similar to how DH was collected.

C.2.2. Results

The experimental static hold-up amount and its FFA% are shown in Figure C.1 under two conditions selected to represent mild and harsh conditions. Based on the experimental design of those conditions, it is not possible to determine the effect of temperature, pressure and S/F ratios on SH for the three different packings. However, at 25 S/F ratio, the SH amount was higher for PS than for the bead packings, mainly due to the higher surface area of PS for the lipids to get entrapped inside the perforated holes. Moreover, similar lipid solubility in CO_2 could be expected based on the similar CO_2 density at the experimental conditions, 794.90 kg/m^3 and 776.07 kg/m^3 at 40 °C/16 MPa and 60 °C/24 MPa, respectively (NIST, 2005).

(A)

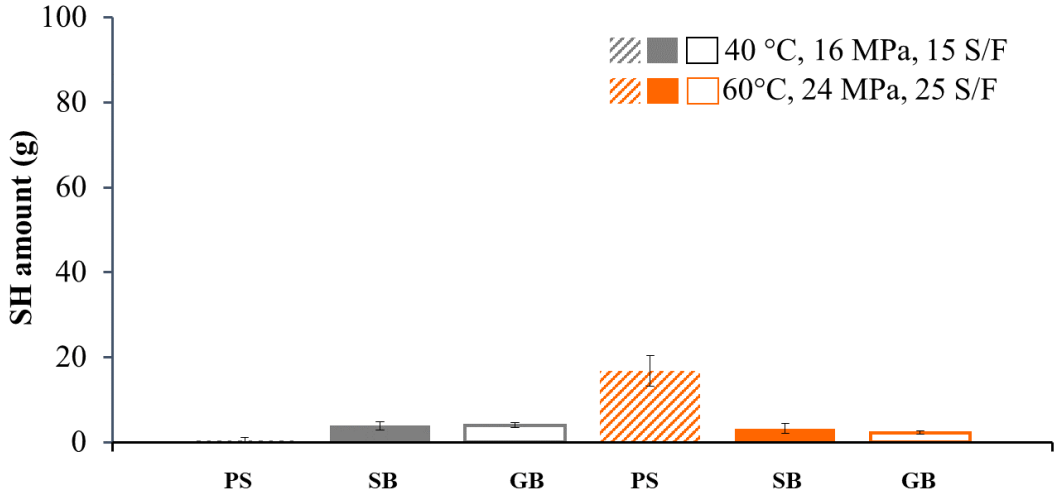

B)

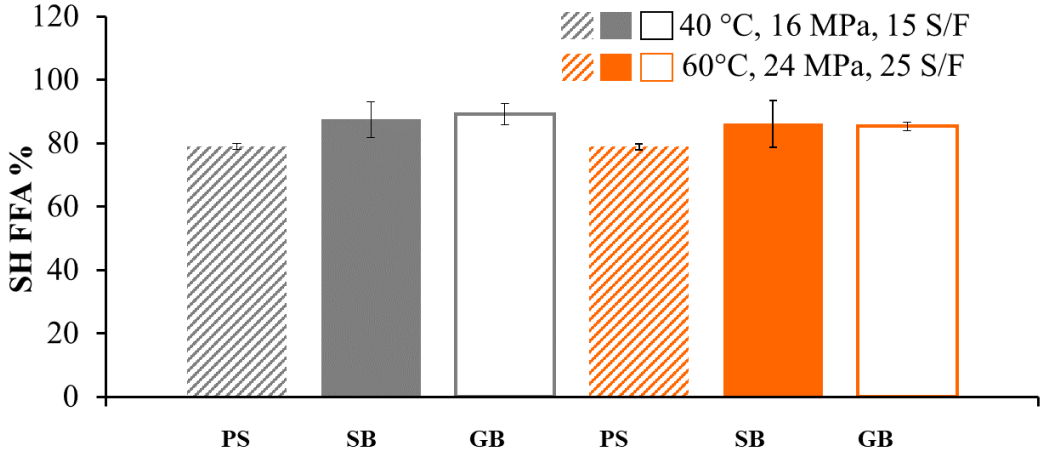

Figure C. 1. (A) SH amounts and (B) SH FFA concentration at 40 ºC, 16 MPa, 15 S/F ratio (mild condition, grey bars) and 60 ºC, 24 MPa and 25 S/F ratio (severe condition, orange bars), and different packings (PS perforated stainless steel, (hatched bar); SB stainless steel beads (solid bar); GB glass beads (blank bar)) (Data presented in Table C.2., Appendix C).

C.2.3. Mass balance of experiments considered for the determination of static hold-up.

The mass balance of the experiments where static hold-up (SH) was determined experimentally is presented in Table C.3. There were challenges faced during raffinate collection.

The collection of the raffinate from the calming section was performed by means of an on/off valve manipulated manually while avoiding depressurization of the column at each sample collection. Despite the effort to consistently collect the raffinate fraction every 30 min for 40 s, it was not possible to have consistent values for each condition.

Table C. 4. Mass balance of experiments where static hold-up was experimentally determined.

Packing	Temperature (°C)	Pressure (MPa)	S/F (wt/wt)	Mass flow rate (g/min)	Total feed in 3 h (g)	Amount in feeding tubing (g)	Total extract (g)	Total Raffinate (g)	DH (g)	SH (g)	Loss (g)	Loss %
PS	40	16	15	0.67	120.6	11.5	11.9	27.5	1.66	13.6	54.5	49.9
SB				0.67	120.6	11.5	15.7	55.2	25.1	3.9	9.3	8.5
GB				0.67	120.6	11.5	10.1	8.4	80.8	4.0	5.8	5.4
PS	60	24	25	0.4	72	11.5	41.5	0.4	0.00	16.8	1.8	3.1
SB				0.4	72	11.5	28.3	6.3	9.5	3.3	13.1	21.7
GS				0.4	72	11.5	24.1	5.2	17.4	2.3	11.4	18.9

PS: perforated packing; SB: stainless steel beads; GB: glass beads; S/F: solvent-to-feed ratio; DH: dynamic hold-up; SH: static hod-up; n=1.